Fakultät für Medizin

Essential role for premature senescence of myofibroblasts in myocardial fibrosis

Kathleen Meyer

Vollständiger Abdruck der von der Fakultät für Medizin der Technischen Universität München zur Erlangung des akademischen Grades eines

Doktors der Naturwissenschaften (Dr. rer. nat.)

genehmigten Dissertation.

Vorsitzender: Prof. Dr. Percy A. Knolle

Prüfer der Dissertation:

1. Prof. Dr. Dr. Stefan Engelhardt

2. Prof. Dr. Martin Klingenspor

3. Prof. Dr. Martin Biel

Die Dissertation wurde am 13.09.2016 bei der Technischen Universität München eingereicht und durch die Fakultät für Medizin am 12.04.2017 angenommen.

Acknowledgements

This work was performed at the Institute of Pharmacology and Toxicology (IPT) at the Technical University in Munich. At this point I would like to thank Prof. Dr. Dr. Stefan Engelhardt as my first supervisor for all his support and supervision during my studies. Especially, I am very grateful for the critical and fruitful inputs during the seminars, which remarkably contributed to the progress of my work. Moreover, I would like to thank him for the opportunity to use all the well-established *in vitro* and *in vivo* techniques and the exceptional equipment available in his laboratory.

I would like to thank PD Dr. Antonio Sarikas as my mentor. I am particularly very thankful for supervising and guiding my work. Especially, I am very thankful for the chances I had to improve myself as a scientist and also as a person during the last years in his laboratory. Also, I am very grateful for many opportunities to represent my work during significant meetings in the field, where I deeply appreciated his advises and excellent remarks in presenting the project and myself to the scientific community.

I thank Prof. Dr. Martin Klingenspor very much for the fruitful discussions and precious inputs during the seminars. Moreover, I want to thank him for the straightforward cooperation and collaboration.

Additionally, I am very happy that I had the chance to work together with many great people and scientists of the IPT. In general, I thank everybody of the institute, but especially Sabine Brummer, Urzula Kremser, Selahattin Sahiner, Mehmet Durmaz and Stanislas Werfel for their support, help and kindness. Also, I thank Melanie Anger for being such a kind person, which really made things easier. Additionally, I would like to say thank you to Andrea Ahles, Laura Hinz and Lucia Koblitz, to whom I keep a special and hopefully long lasting relationship. Particulary, I would profoundly like to thank Deepak Ramanujam, Isabell Flohrschütz, Kornelija Sakac and Bettina Hodwin for establishing exceptional friendships during the last years.

I would deeply like to thank my family, especially my parents, grandparents and my sister for their unlimited understanding and support during the last years.

I would also like to thank Sabine Gibas for her very special support and the close friendship during the last years. I particularly thank her for understanding me on a very unique level.

I say thanks to Charly and his friends for giving me some “lab-independent” happiness in my life.

A very special thanks goes to Yassine Sassi for all his care, help and support during the last years.

An exceptional thanks goes also to Dr. rer. nat. Sandro Eichler to whom I hold the highest respect. I am incredibly grateful that I had the opportunity to meet such a brilliant mind and an even more brilliant heart. His words and actions continue to guide me as they always did.

Abbreviations

AAV9 - adeno-associated virus of serotype 9

α-SMA - α-smooth muscle actin

AngII - angiotensin II

AMCM - adult mouse cardiac myocytes

AMCF - adult mouse cardiac fibroblasts

ARF - alternative reading frame

ASF1a - anti-silencing function A

ATM - ataxia telangiectasia mutated

ATR - ataxia telangiectasia rad 3 related

BAK - Bcl2-antagonist/killer

BAX - Bcl-2 associated protein X

BRCA1 - breast cancer 1

CCL - CC chemokine ligand

CDK - cyclin-dependent kinases

CDKN1A - cyclin-dependent kinase 1A

CDKN2A - cyclin-dependent kinase 2A

CF - cardiac fibroblasts

CHK1 - checkpoint kinase 1

CHK2 - checkpoint kinase 2

CIP - cyclin-dependent kinase inhibitor

CM - cardiac myocyte

CSF - colony stimulating factor

CTGF - connective tissue growth factor

CUL7 - cullin7

CVD - cardiovascular disease

CXCL - CXC-motif ligand

CXCR - CXC chemokine receptors receptors

DAPI - 4', 6-diamidino-2-phenylindole

DcR2 - decoy receptor 2

DDR - DNA damage response

DAPI - 4', 6-diamidino-2-phenylindole

DcR2 - decoy receptor 2

ED-A - extra domain A (ED-A)-fibronectin

EMT - epithelial-to-mesenchymal transition

ERK - extracellular signal-related kinase

ET-1 - endothelin-1

ETS - E26 transformation specific

FasL - fas ligand

GADD45α - growth arrest and DNA damage inducible gene

GPCRs - G protein-coupled receptors

Hif1α - hypoxia-inducible factor 1 α

HIRA - histone repressor A

HMGA - high mobility group protein1

HP1- histone protein 1

HSCs - hepatic stellate cells

HSPGs - heparin sulfate proteoglycans

H3/K9me3 - histone 3/lysine 9 trimethylation

H3/K27me3 - histone 3 /lysine 27 trimethylation

H3/K27me3 - histone 3 /lysine 27 trimethylation

IGBP - insulin-like growth factor binding protein

IGF - insulin-like growth factor

IL - interleukin

KIP - kinase inhibitor proteins

MacroH2a - histone H2A

MAPK - mitogen-activated kinase

MDM2/HMDM2 - mouse double 2 homolog

MI - myocardial infarction

MMP - matrix metalloproteases

MyoCF - myofibroblasts

MRN - Mre11-Rad50-Nbs1

MRTF- myocardin-related transcription factor

NF1- neurofibromatosis-related protein 1

NOV- nephroblastoma overexpressed

NRCF - neonatal rat cardiofibroblasts

NRCM - neonatal rat cardiomyocytes

pAd - adenovirus

53BP - p53 binding protein

PI3K - phosphatidylinositol-3-kinase

PML bodies - promyelocytic leukemia nuclear bodies

PTEN - phosphatase and tensin homolog

PUMA - p53 unregulated modulator of apoptosis

RAAS - renin-angiotensin-aldosterone system

RFC - replication factor C

RhoA - ras homolog gene family member

ROS - reactive oxygen species

RPA - replication protein A

SA-ß-gal - senescence-associated ß-galactosidase

SAHF - senescence-associated heterochromatin foci

SASP - senescence-associated secretory phenotype

SRF - serum response factor

TAC - transverse aortic constriction

TGF-ß - transforming growth factor ß

TIF - telomere dysfunction induced foci

TIS - therapy-induced senescence

TIMP - tissue inhibitor of metalloproteases

TNF α - tumor necrosis factor α

TSIC - tumor suppressor loss-induced senescence

VHL - von Hippel-Lindau

Index

1 Introduction

Cardiovascular disease (CVD) remains the leading cause of mortality worldwide accounting for approximately 30% of all global deaths (Mozaffarian et al. 2015). Moreover, it displays a remarkable economic burden with estimated costs of more than 918 billion dollars alone within the US in 2030 (Mozaffarian et al. 2015). Importantly, nearly all etiologies of cardiac diseases are associated to and exacerbated by pathological cardiac remodeling and the excessive deposition of extracellular matrix (ECM) proteins, namely fibrosis (Kong et al. 2014). Despite a significant involvement of cardiac fibrosis in heart failure, its limited understanding delays the development of efficient therapies. Thus, it is not possible to prevent or reverse cardiac fibrosis during heart failure.

1.1 Cardiac fibrosis

An increase or alterations in the realignment of collagens modulate the development of cardiac fibrosis resulting in ECM accumulation. Although fibrosis is an essential part of the wound healing process with short-term adaptive features, its progression over a prolonged time period leads to cellular and finally to organic dysfunction (Longo et al. 2015). Cardiac fibrotic scars, consisting of fibrillar collagen I and III, lead to organ stiffness, thus to diastolic dysfunction, aberrant left ventricular filling, reduced left ventricular (LV) compliance and increased diastolic pressure. This in turn results in an overall decrease in conduction performance and contraction flexibility (Díez et al. 2001). Even though multiple primary diseases and thereby many different pathophysiologies initiate fibrotic remodeling, molecular signaling networks are very common. In general, there are 4 stages of fibrogenesis (Longo et al. 2015) (**Figure I-1**). The initiation by an insult to the heart (e.g. myocardial infarction (MI) or pressure overload) leads to cardiomyocyte (CM) hypertrophy or apoptosis (1st phase). This activates effector cells of mesenchymal origin, determined as the 2nd phase. Effector cells are fibroblasts, fibrocytes, tissue specific pericytes and fibroblasts derived through epithelial-to-mesenchymal (EMT) or endothelial-to-mesenchymal transition (EndoMT). A key event is the transdifferentiation of activated fibroblasts into proto- and later mature synthetic myofibroblasts. During the 3rd phase, these cells produce a variety of ECM proteins leading to an expansion of ECM. In addition, effector cells secrete cytokines and growth factors, which stimulate further effector cells to transdifferentiate into fibroblasts and finally myofibroblasts. The 4th phase represents the dynamic deposition of the ECM by myofibroblasts, which leads to the progression of fibrosis promoting the cycle to advance

fibrogenesis. Within the heart, two types of fibrosis are distinguished (Weber 2000): Replacement or reparative fibrosis and reactive fibrosis. Both types are initiated through different types of cardiac insult. Replacement fibrosis occurs mainly after acute cardiomyocyte loss and appears within the interstitium. It is characterized by ECM degradation products, which lead to chemoattracting immune signaling, thereby promoting inflammation, which in turn induces myofibroblast transdifferentiation and fibrosis (e.g. after MI or chronic α-adrenergic stimulation). Reactive fibrosis arises upon increased mechanical load e.g. hypertension and subsequent increase of neurohormonal stimuli (Sutton MG and Sharpe N 2000, Lorell & Carabello 2000). Reactive fibrosis spreads from perivascular regions into the myocardium (Díez et al. 2001, Krenning et al. 2010).

Hypertensive heart failure and pressure overload are primarily associated to reactive perivascular and interstitial fibrosis initially in the absence of CM apoptosis or necrosis. However, consistent catecholamine or angiotensin II (AngII) signaling leads to cardiomyocyte loss, resulting in both, reactive and replacement fibrosis within the heart (Leask 2015). Neurohormonal stimuli, the renin angiotensin system (RAAS) and high salt concentrations play fundamental roles within hypertension initiated remodeling and the maladaptive accumulation of extracellular matrix (Tsukamoto et al. 2013).

Despite the initiatial type of cardiac injury, cardiac fibroblasts are fundamental key players within the myocardium during the pathophysiology of fibrosis.

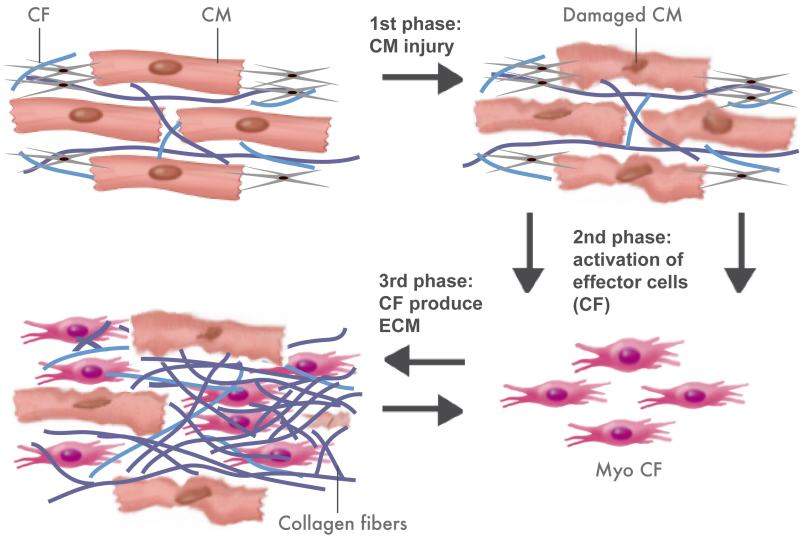

Figure I-1: Stages of cardiac fibrosis. An inciting stimulus resulting in cardiac myocyte damage (1st phase) leads to an activation of fibrogenic effector cells (2nd phase), which in turn proliferate and produce a variety of extracellular matrix proteins (3rd phase). Para- and autocrine signaling increase effector cell activity, which finally becomes auto-regulatory and maladaptive. CF: Cardiac fibroblasts, CM: Cardiac myocytes, Myo CF: Cardiac myofibroblasts. (Modified after Longo et al. 2015)

1.2 Cardiac fibroblasts

A main part of the cardiac cell population consists of cardiac non-myocytes. However, the exact composition and amount of cardiac fibroblasts (CF) within this cell fraction remains controversial. Although many reports suggested CF as the major cell population, recent findings propose that CF account for less than 20% of non-myocytes (Porter & Turner 2009, Snider et al. 2010, Pinto et al. 2016). CF essentially contribute to ECM homeostasis, myocardial development and sense as well as react to changes in their microenvironment (Porter & Turner 2009, Snider et al. 2010, Pinto et al. 2016). Thus, they are actively involved in maintaining the ECM turnover at physiological and pathophysiological conditions.

1.2.1 Cardiac fibroblasts during physiology

CF are the primary source of biosynthesizing, deposing and degrading ECM proteins. Hence, they produce and secrete a plethora of bioactive molecules, matrix building and degrading enzymes and respective inhibitors such as matrix metalloproteases (MMPs) and tissue inhibitors of metalloproteases (TIMPs) (Spinale & Wilbur 2009, Porter & Turner 2009, Moore et al. 2012). CF produce bioactive molecules with self-regulating auto- and paracrine functions and manifold activities on cardiac cells, e.g. modulation of cardiomyocyte hypertrophy, apoptosis or endothelial cell proliferation (Porter & Turner 2009a). Thus, they significantly contribute to mechanical, structural, and biochemical cardiac functions. Cardiac fibroblasts are a heterogeneous cell population with many different origins and functions depending on their developmental stage and (patho)physiologic condition (Zeisberg & Kalluri 2010). Morphologically, they are flat and spindle shaped and not attached to the basement membrane (Krenning et al. 2010). Under non-pathological conditions, CF are quiescent. In disease, a molecular key event is the transdifferentiation and accumulation of myofibroblasts from of many different precursor cells (**Figure I-2**).

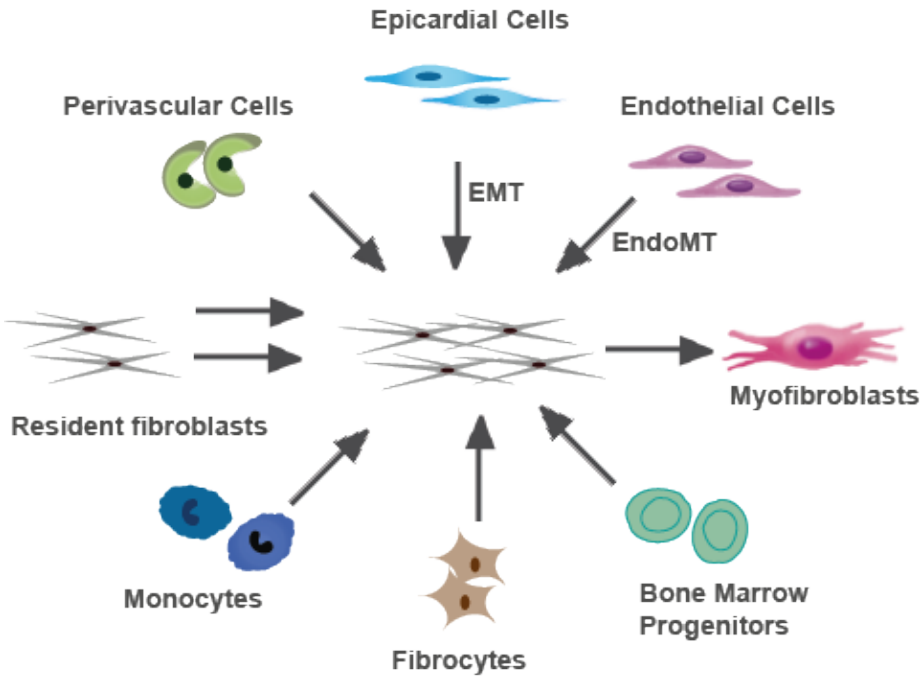

Figure I-2: Sources of cardiac fibroblasts: During development, cardiac fibroblasts originate from proepicardial epithelial cells through epithelilal-mesenchymal transition (EMT). Valvular fibroblasts derive from endocardial cells through endothelial-mesenchymal transition (EndoMT). In fibrotic mammalian hearts, fibroblasts and finally myofibroblasts arise from resident cardiac fibroblasts, monocytes, fibrocytes, bone marrow progenitor cells, fibrocytes as perivascular cells. Additionally, EMT and EndoMT are sources of myofibroblast generation. (Modified after Krenning et al. 2010 and Kong et al. 2014)

1.2.2 Cardiac fibroblasts during pathophysiology

Upon myocardial injury, CF undergo structural and functional changes while transdifferentiating into proto- and later into mature and synthetic myofibroblasts.

The cardiac proto-myofibroblast. Under stress conditions CF differentiate first into an intermediate cellular phenotype, namely proto-myofibroblasts. They are typically synthesizing stress fibers and focal adhesion sites. Additionally, they produce a special splice variant of fibronectin, called extra domain A (ED-A)-fibronectin to form a complex network at their cell surface. Protomyofibroblasts can produce contractile force, are proliferative and migrate to the site of tissue damage producing a collagen and fibronection rich ECM to promote wound healing (Figure I-3) (Gabbiani 2003). Mechanical tension is a main inducer for the phenotype conversion, but growth factors, like platelet-derived growth factor α (PDGF-A) also have been shown to play crucial roles (Boström et al. 1996).

The cardiac myofibroblast (MyoCF). Protomyofibroblasts further convert into mature myofibroblasts. Myofibroblasts are not present in the healthy myocardium except for the valve leaflets. However, during cardiac insult, they accumulate at sites of injury or globally

throughout the whole heart at sites of fibrogenesis. Myofibroblasts are hypoproliferative and less migratory than their precursors and highly synthetically active (Turner & Porter 2013). They express the contractile protein α-smooth muscle actin (α-SMA), produce complex stress fibers and many mature focal adhesion structures **(Figure I-3)**.

The origin of MyoCF is heterogeneous. Recent studies showed that activated fibroblasts mainly derive from resident fibroblasts by proliferation (Krenning et al. 2010, Moore-Morris et al. 2014). Resident fibroblasts are sensitive to circulating proliferative signals, which occur during cardiac injury (Camelliti et al. 2005). Moreover, activated fibroblasts can be recruited from different sources, like epithelial cells (by EMT), endothelial cells (by EndoMT), bone marrow progenitors, monocytes and perivascular cells (**Figure I-2**) (Krenning et al. 2010, Hung et al. 2013, Travers et al. 2016).

Many factors induce the phenoconversion to myofibroblasts, like Ang II, Endothelin-1 (ET-1), or connective tissue growth factor (CTGF) and transforming growth factor ß (TGF-ß) (Travers et al. 2016)

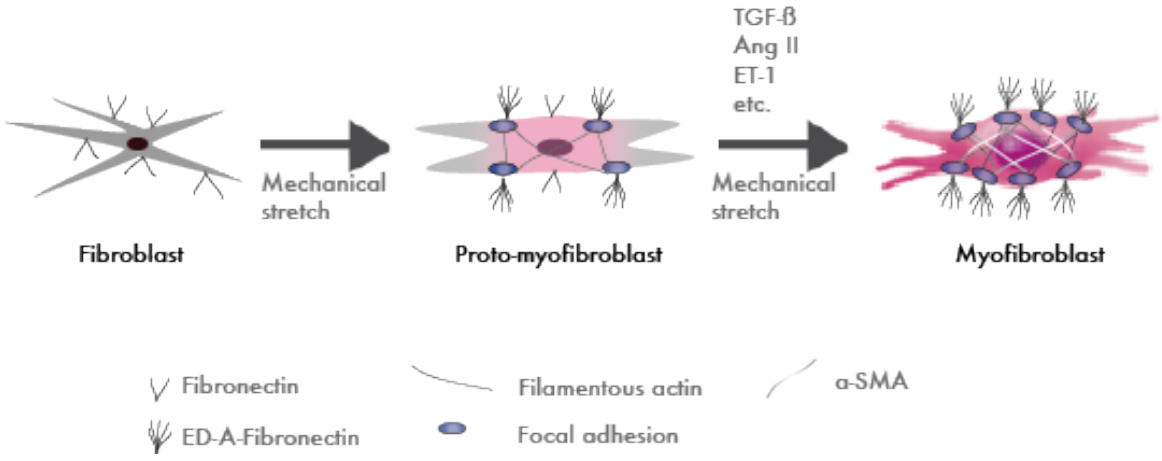

Figure I-3: Differentiation steps of fibroblasts into (proto)myofibrobalsts. Interstitial resident fibroblasts produce fibronectin and lack the generation of filamentous actin, α-smooth muscle actin (α-SMA) and ED-A-fibronectin. Upon mechanical stretch, fibroblasts transdifferentiate into protomyofiboblasts establishing the expression of filamentous actin, ED-A-fibronectin and focal adhesion sites. Myofibroblasts derive after TGF-ß-, Ang II or ET-1 stimulation and develop complex stress fibers incorporating α-SMA. (Modified after Falke et al. 2015)

Upon cardiac injury, coordinated and overlapping biochemical and mechanical signaling pathways modulate myofibroblast transdifferentiation and fibrogenesis. Canonical and non-canonical TGF-ß signaling, Ang II and ET-1 as well as the serum response factor (SRF)-myocardin-related transcription factor (MRTF)-Ras homolog gene family member SRF-MRTF-RhoA-GTPase pathway are central signaling pathways for myofibroblast

transdifferentiation. Moreover, transient receptor potential (TRP)-channel activation and mechanotransduction have been shown to play crucial roles in CF activation (Leask 2007, Davis & Molkentin 2014, Leask 2015, Travers et al. 2016).

1.3 Cellular senescence

Cellular senescence was recently described as an essential key modulator of tissue fibrosis in different organ systems.

Originally described in 1961 as a phenotype of human diploid fibroblasts undergoing replicative exhaustion under cell culture conditions, cellular senescence can be induced by a variety of cellular damage or stresses leading to different types of cellular senescence (Hayflick & Moorhead 1961, Serrano et al. 1997, Rodier & Campisi 2011, Muñoz-Espín & Serrano 2014).

1.3.1 Types of cellular senescence

Replicative Senescence. The Hayflick limit is characterized as the restricted proliferation capacity of replicating primary cells. This phenomenon is based on the progressive shortening of telomeres. Telomeres are protective chromosomal repetitive DNA segments associated to numerous proteins (Stewart & Weinberg 2002). Due to the end-replication problem - the incapability of the DNA polymerase to replicate the complete 5'-3' directed DNA strand - cells lose 50-200 base pairs (bp) each cell cycle (Harley et al. 1990). Upon a critical minimal telomere length and subsequent structural changes, chromosomal ends become dysfunctional and activate a DNA damage response (DDR) (Herbig et al. 2004, di Fagagna et al. 2003, Takai et al. 2003). The DDR involves many proteins like apical kinases, which in turn activate DNA damage mediators and downstream kinases as well as effectors such as Trp53 (referred to as p53). Depending on the magnitude of damage, the DDR leads to apoptosis or cellular replicative senescence. Although replicative senescence might be the basis of the ageing process in some regenerative tissues (i.e. due to stem cell pool exhaustion), the abundance of replication capable cells in the adult organism is comparatively rare. However, post-mitotic (non-replicating) cells also undergo senescence through different stimuli in the absence of replication and telomere shortening, but upon exposure to particular stress situations.

Developmentally programmed senescence. Cellular senescence occurs physiologically during embryonic development, referred to as "developmentally programmed senescence"

(Muñoz-Espín et al. 2013, Storer et al. 2013, Serrano, 2014). During embryogenesis, several developmental structures were found to become senescent, like the mesonephros or the endolypmhatic sac, in order to remove transient embryonic structures or to balance cellularity. In general, TGF-ß and phosphatidylinositol-3-kinase (PI3K) signaling with p21 $^{CIP1/WAF1}$ as a common mediator and an inflammatory phenotype are key events upon developmental cues (Muñoz-Espín et al. 2013, Storer et al. 2013).

Stress induced senescence.

DNA damage induced senescence. Besides replication, also ionizing radiation, chemotherapeutic drugs, or reactive oxygen species (ROS) can induce senescence upon activation of the DNA damage response. DNA single strand breaks or double strand breaks are recognized by sensor molecules such as replication protein A (RPA) and replication factor C (RFC), which in turn recruit the 911 (Rad9-Hus1-Rad1) - or the MRN (Mre11-Rad50-Nbs1) complex. This activates proteins like ataxia telangiectasia mutated (ATM) and ataxia telangiectasia rad 3 related (ATR) that in turn phosphorylates mediator molecules such as p53 binding protein (53BP), breast cancer 1 (BRCA1), which then activate the downstream kinases checkpoint kinase 1 and 2 (CHK1 and CHK2, respectively). The latter ones transduce the signal to effectors such as p53 that finally induces senescence. The DNA damage response can also lead to apoptosis, depending on the nature of DNA damage and dosage as well as on the cell type (Kurz & Lees-Miller 2004, Chen et al. 2007).

Reactive oxygen species (ROS)-induced senescence. ROS accumulate during many situations, i.e. oncogene activation, chemotherapy or within fibrogenesis (Passos et al. 2010, Nelson et al. 2012, Macip et al. 2002, Jones & Cichowski 2008). ROS react with DNA molecules and induce double or single strand breaks thereby activating the DDR and subsequently senescence (Cooke et al. 2003, Guachalla & Rudolph 2010).

Oncogene induced senescence (OIS). Upon overexpression of oncogenes, i.e. oncogenic Ras or Raf, cells will become senescent rather than transformed. It has been well established that this type of cellular senescence, referred to as “oncogene induced senescence” (OIS), is an important tumor barrier *in vivo* (Serrano et al. 1997, Collado & Serrano 2010, Serrano 2007). Oncogene activation leads to Cyclin-dependent kinase 2A (CDKN2A) derepression as well as to DDR due to aberrant replication fork formation and ROS generation (Jones & Cichowski 2008, Mooi & Peeper 2006, d’Adda di Fagagna 2008, Bartkova et al. 2006, Di Micco et al. 2006). Similar to oncogene overactivation, loss of tumor suppressors can also lead to senescence as it was described for phosphatase and tensin homolog (PTEN) and neurofibromatosis-related protein 1 (NF1) or von Hippel-Lindau (VHL),

termed as “tumor suppressor loss-induced senescence” (TSIC) (Kuilman et al. 2010, Chen et al. 2005, Courtois-Cox et al. 2006, Young et al. 2008).

Tissue damage induced senescence. Recent findings pointed out a role for cellular senescence during tissue damage, particularly fibrosis (Krizhanovsky et al. 2008, Jun & Lau 2010a, Jun & Lau 2010b, Demaria et al. 2014, Kim et al. 2013, Kong et al. 2012, Serrano 2014). Senescent cells accumulate within cutaneous wounds and at sites of liver damage in order to limit fibrogenesis in a p53- and p16 ^{INK4a} -dependent manner.

1.3.2 Mechanisms of senescence induction

The ARF/p53/p21 $^{CIP1/WAF1}$ and the p16 ^{INK4a}/pRB signaling are crucial to induce and maintain the senescence program, independently of which senescence type has been activated (Serrano et al. 1997, van Deursen 2014, Childs et al. 2014)

The p16 ^{INK4a}/ARF signaling. The INK4A/ARF (also referred to as CDKN2A) locus is placed on human chromosome 9p21 and is one of the most frequently mutated DNA loci in cancer (Serrano et al. 1993, Serrano et al. 1996, Serrano 1997, Serrano 2000). The polycistronic arrangement is unique in the mammalian genome and encodes two distinct gene products. First, the inhibitory protein of cyclin-dependent kinases 4 and 6 (CDK4 and CDK6, respectively), p16 ^{INK4} and second, the alternative reading frame (ARF19 in mouse and ARF14 in human). The two gene products share two exons in alternate reading frames and have distinct first exons (**Figure I-4**) (Sherr 2001).

The p16 ^{INK4a}- signaling. Many stress stimuli primarily induce the p16 ^{INK4a} pathway, i.e. oncogenic RAS via the mitogen-activated kinase (MAPK) (Lin et al. 1998). Additionally ROS, DNA damage or suboptimal culture conditions induce p16 ^{INK4a}- signaling (Satyanarayana & Rudolph 2004, LaPak & Burd 2014, Kim & Sharpless 2006). E26 transformation specific (ETS) transcription factors and Polycomb repressor proteins, such as Bmi and CBX7 are involved in p16 ^{INK4a}- induced senescence, however detailed activation is not yet known (Bracken et al. 2007, Martin et al. 2013). p16 ^{INK4a} is a CDK4/6 inhibitory protein, thereby leading to the hypophosphorylation of the retinoblastoma-related protein (Rb). Hypo phosphorylated Rb sequesters transcription factors of the E2F family to the cytoplasm and prevents the transcription of cell cycle progression genes (Henley & Dick 2012). Additionally, the p16 ^{INK4a} -Rb signaling is essential for inducing senescence-associated heterochromatin foci (SAHF). SAHF are a special form of facultative heterochromatin that silence genes necessary for proliferation (Narita et al. 2003). Many chromatin modifications are involved in SAHF generation. Histone3/lysine acetylation is reversed and changed to histone 3/lysine 9

trimethylation (H3/K9me3) and histone 3 /lysine 27 trimethylation (H3/K27me3) by SUV39H1 methyltransferases (Narita et al. 2003, Braig et al. 2005). This in turn attracts histone protein 1 (HP1) or histone H2A (MacroH2a) and chromatin modifying proteins like histone repressor A (HIRA) (Zhang et al. 2005). A key event of SAHF initiation is the HIRA translocation to subcellular organelles namely promyelocytic leukemia nuclear bodies (PML bodies), which serve as a basis for the complex association of HIRA and the anti silencing function A (ASF1a) (Zhang et al. 2005). Also non-histone chromatin proteins are increasingly present during SAHF formation as high mobility group proteins HMGA1 and HMGA2 (Narita et al. 2006). After SAHF formation p16 ^{INK4a} is not longer needed for heterochromatin maintenance.

The ARF signaling. The alternative reading frame of the INK4A locus builds stable complexes to mouse double 2 homolog MDM2 (HDM2). ARF inhibits the MDM2 ubiquitin ligase which facilitates the proteosomal degradation of p53, thereby connecting the p53 to the p16 ^{INK4a} pathway (**Figure I-5**) (Sherr & McCormick 2002).

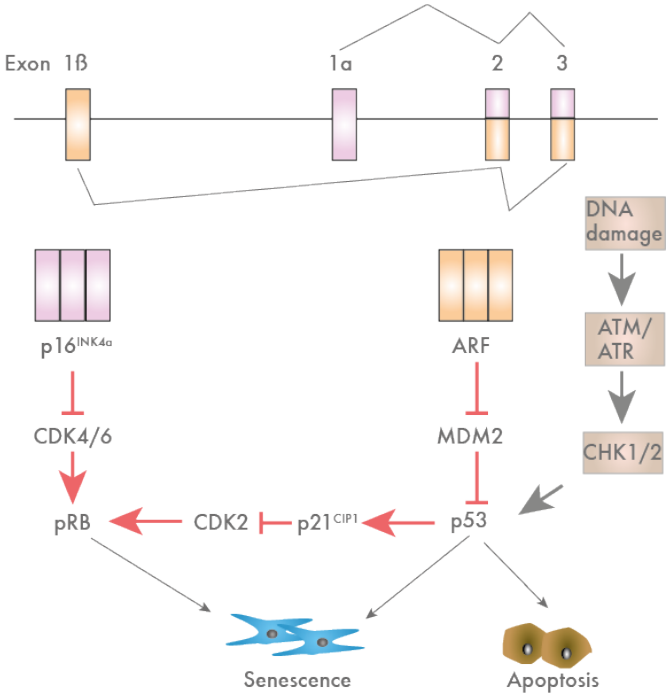

Figure I-4: *CDKN2A* locus and signaling. The *CDKN2A* locus encodes two tumor suppressor genes, namely p16 ^{INK4a} and alternative reading frame (ARF). p16 ^{INK4a} inhibits cyclin dependent kinases 4 and 6, which leads to the hypophosphorylated variant of the retinoblastoma protein (RB). This in turn sequesters transcription factors from the E2F family in the cytoplasm and prevents the expression of cell cycle progression genes. ARF stabilizes p53 by inhibiting the ubiquitin ligase MDM2, promotes p21 $^{CIP1/WAF1}$ expression and thereby cyclin dependent kinase 2 inhibition. Both gene products of the *CDKN2A* locus result in cell cycle inhibition and senescence. (Modified after Sharpless & Sherr 2015)

The p53 signaling. The *Trp53* gene is located on exon 17p13 in humans, spans eleven exons and transcribes a tetrameric transcription factor. p53 is an essential key player in response to cellular and DNA damage subsequently inducing apoptosis or senescence. It is mutated in more than ¾ of all human cancers, highlighting it as the most important tumor suppressor and the “guardian of the genome” (Muller & Vousden 2014). The (telomere-

dependent or- independent) DDR primarily activates senescence via the p53 pathway, which is mainly controlled post transcriptionally at many points. Two main classes of transcriptional p53 targets are known. First, the negative cell cycle regulators, cyclin-dependent kinase 1A (CDKN1A, here referred to as p21 $^{CIP1/WAF1}$), 14-3-3 and growth arrest, and DNA damage inducible gene (GADD45α). The second class are apoptosis inducing genes, such as p53 upregulated modulator of apoptosis (PUMA) and the BH domain proteins Bcl-2 associated protein X (BAX) and Bcl2- antagonist/killer (BAK) (Vogelstein et al. 2000). Thus, p53 decides between the two cell fates apoptosis and senescence. Following senescence induction, p21 $^{CIP1/WAF1}$ is the main p53 downstream target, since it represses CDKs, leads to hypophosphorylated Rb, and prevents the transcription of cell cycle progression genes. Upon DDR, p53 becomes phosphorylated at serine 20 by CHK1 or CHK2 leading to the dissociation of the ubiquitin ligase HDM2/Mdm2 (Figure I-4) (Herbig et al. 2004).

CCN1 signaling. Cysteine rich protein 61 (CYR61, synonymous to CCN1), mapped to the human chromosome 1p, has been shown to induce senescence by inducing both, the p53 signaling and the p16 ^{INK4a} axis (Jay et al. 1997, Jun & Lau 2010a, Jun & Lau 2010b, Kim et al. 2013, Jim Leu et al. 2013, Du et al. 2014).

CCN1 protein. CCN1 is a member of the CCN protein family, which consists of six proteins. The acronym is derived from the first three members identified, namely, CYR61, connective tissue growth factor (CTGF) and nephroblastoma overexpressed (NOV) (Brigstock et al. 2003). CCN1 is a matricellular protein, thus having more regulative rather than structural functions (Bornstein & Sage 2002). The protein structure is highly conserved and consists of 38 cysteines distributed over four domains, which share sequence homologies to several proteins. The first is the Insulin-like growth factor binding protein domain (IGBP domain), then the von-Willebrand factor type c repeat (vWC), the thrombospondin type 1 repeat (TSR) and finally the carboxyl terminus with a cysteine knot. CCN1 transcription is regulated by a variety of factors, including TGF-ß, Ang II, hypoxia, agonists of G-protein coupled receptors (GPCRs) and cyclic AMP (cAMP) (C.C. Chen & Lau 2009, Hilfiker et al. 2002, Hilfiker-Kleiner et al. 2004, Lau 2011). Transcriptional activation is also mediated by serum response factor (SRF) or stretch, involving Rho-GTPase activated cytoskeleton remodeling and subsequent recruitment of the myocardin related transcriptional activator (MRTF-A), which in turn binds the serum responsive element (SRE) in the CCN1 promoter (Han et al. 2003, Chen & Du 2007, Hinkel et al. 2014). CCN1 has many functions, which are strongly context dependent. It can promote cell survival as well as induce apoptosis. Further it was shown to induce proliferation, and yet triggers senescence, it is a well-described tumor suppressor, in the same way it can enhance tumor growth. Moreover, CCN1 is known to be a potent pro-

angiogenic factor (Fataccioli et al. 2002, C. C. Chen & Lau 2009, Jun & Lau 2010b, Jun & Lau 2010b, Du et al. 2014, C.C. Chen et al. 2007, Chen et al. 2004, Juric et al. 2009 Leask 2011, Haseley et al. 2012, Chen et al. 2015). This multifunctionality is based on the binding to many different surface receptors, especially integrins and their co-receptors (Lau 2016). Depending on which subtypes of integrins are present and which cell is affected, certain physiological consequences take place. Moreover, CCN1 is not acting independently, but rather acts synergically with other molecules, i.e. during apoptosis induction, such as tumor necrosis factor α (TNF α), fas ligand (FasL) and tumor necrosis factor-related apoptosis inducing ligand (TRAIL) (C.-C. Chen et al. 2007, Franzen et al. 2009, Jun & Lau 2011).

CCN1-induced senescence activation. The key integrins for inducing fibroblast senescence is $\alpha_6\beta_1$ and the cell-surface heparan sulfate proteoglycans (Jun & Lau 2010a, Jun & Lau 2010b, Kim et al. 2013, Jim Leu et al. 2013). Upon CCN1 binding, the NADPH oxidase/RAC1 complex is activated and produces ROS leading to a stable DDR. The DNA damage in turn induces p53 phosphorylation and stabilization, thereby triggering senescence, in part by transcriptionally inducing p21 $^{CIP1/WAF1}$. p21 $^{CIP1/WAF1}$ subsequently inhibits the CDK2 complex, which results in the hypophosphorylation and activation of the tumor suppressor Rb and its senescence inducing downstream signaling (see above). In parallel, ROS activate the extracellular signal-related kinase (ERK) and p38 MAPK pathway, which is a known inducer of p16 ^{INK4a} expression and consequently senescence (Jun & Lau 2010a, Jun & Lau 2010) (**Figure I-5**).

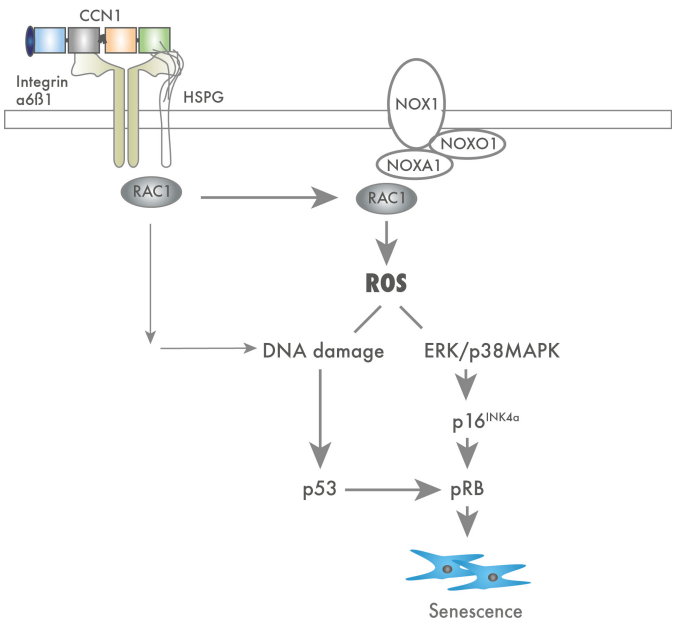

Figure I-5: CCN1 signaling. CCN1 binds to its fibroblast receptor $\alpha_6\beta_1$ and heparansulfate proteoglycans (HSPG), thereby activating RAC and RAC dependent NADPH oxidase, which generates a robust accumulation of ROS. ROS induce DNA damage, p53 stabilization and p21$^{CIP1/WAF1}$ expression. Additionally, ROS lead to the activation of the ERK/p38 MAPK pathway that results in p16 ^{INK4a} expression. Both, p21 $^{CIP1/WAF1}$ and p16 ^{INK4a} induce senescence. (Modified after (J.-I. Jun & Lau 2010)

1.3.3 Phenotype of cellular senescence

The senescent phenotype can be mainly distinguished by the initiating stimulus or the signaling routes. Hence, the phenotype of senescent cells varies in its extent, partially depending on the time of stimulation and the DDR/SASP involvement. There are some characteristic features that define senescent cells, although none of them alone can determine senescence. For this reason, a panel of senescence markers is commonly used for investigation.

Cell cycle arrest. The only common feature of cellular senescence is the essentially irreversible proliferation arrest induced by the upregulation of tumor suppressor networks, mainly p53 and p16 ^{INK4a} (Serrano et al. 1997, Campisi & d'Adda di Fagagna 2007, Childs et al. 2014).

The upregulation of tumor suppressors. Depending on the stimuli and senescence induction, the p53 and p16 ^{INK4a} networks are upregulated and components of the pathway measureable (Collado & Serrano 2006, Lee et al. 2011). Under normal, non-stressed conditions, tumor suppressors are at low, almost undetectable level present (Christophorou et al. 2006, Ressler et al. 2006). For the p53 pathway, p53 itself or p21 $^{CIP1/WAF1}$ are common markers (Serrano et al. 1997). Less commonly used are the transactivational p53 targets deleted in esophageal cancer (DEC1) and decoy receptor 2 (DcR2) (Collado et al. 2005). For the p16 ^{INK4a} signaling, p16 ^{INK4a}, p19 ^{ARF} or the hypophosphorylated Rb as well as SAHF components are characteristic measurable features (Serrano et al. 1997, Campisi 2005). Other tumor suppressors from the INK4A family, like p15 ^{INK4B}, p18 ^{INK4C}, p19 ^{INK4D} or the cyclin-dependent kinase inhibitor (CIP) family, like p27 ^{KIP1} and p57 ^{KIP2} are upregulated in some senescence conditions, but are not as frequently used (Besson et al. 2008).

SA-ß-galactosidase. Senescence-associated ß-galactosidase (SA-ß-gal) is one of the most commonly used senescence markers (Dimri et al. 1995). Encoded by the *GLB1* gene, endogenous ß-D galactosidase is a metabolic enzyme, responsible for the hydrolization of ß-galactosides into monosaccharides. Senescent cells accumulate SA-ß-gal due to their increase in lysosomal mass. However, its expression is not necessary for senescence induction (Kurz et al. 2000, Lee et al. 2006). Senescent cells experience a functional reprograming including hypermetabolism, which might explain the increase in lysosomes in order to maintain the energy homeostasis. Moreover, inhibition of the metabolism is able to specifically target and eliminate senescent cells upon therapy-induced senescence (TIS) (Dörr et al. 2013).

Senescence-associated heterochromatin foci (SAHF). Altered chromatin structures can be an essential part of senescence induction. Condensed heterochromatin can be detected with 4',6-diamidino-2-phenylindole (DAPI) staining, showing nuclear focal condensed DNA aggregates. More specifically, trimethylated histone 3 at lysine 9 or 27, HP1 isoforms HP1α, β or γ and Macro H2A chromatin proteins can be detected. Moreover HIRA or HMGA proteins define SAHF in senescent cells (Narita et al. 2003).

DNA damage foci and DNA SCARS. Upon DNA damage, the DDR is activated and parts of the signaling cascade are used to identify senescent cells. Upon DNA damage, proteins like apical kinases ATM, ATR, and DNA damage mediators p53BP and yH2AX accumulate. Subsequent downstream kinases CHK1 and CHK2 and effector molecules as p53 and cdc25 can be measured (d'Adda di Fagagna 2008, Rossiello et al. 2014). When DNA damage occurs at the sites of telomeres due to replicative senescence, the foci can be detected as described and are named telomere dysfunction induced foci (TIF), whereas short telomeres can also be detected at the same time (Herbig & Sedivy 2006). If DNA damage can be repaired, the foci are transient, accumulate DNA repair proteins such as replication protein A (RPA) and RAD51, and resolve within 24 hours. In case of an irreparable DNA damage, the foci are persistent and are called DNA segments with chromatin alterations reinforcing senescence (DNA SCARS). The latter one is responsible for senescence induction and enforces chronic DDR signaling activation (di Fagagna et al. 2003, Beausejour 2003, Rodier et al. 2011).

The senescence associated secretory phenotype (SASP). Depending on the cell type and cellular stress responsible for the senescence activation, the SASP composition varies, although some key factors are equal in almost all senescence phenotypes and cell types (Kuilman & Peeper 2009, Young & Narita 2009, Coppé et al. 2010, Shivshankar et al. 2012). Another conserved feature of the secretory phenotype is the dynamic induction of the SASP, which leads to a gradual release of different SASP factors (Coppé et al. 2008, Rodier et al. 2009).

The SASP consists of three types of molecules. First, soluble signaling molecules like interleukins, chemokines, and growth factors. Second, the SASP contains proteases as well as ECM modulating enzymes. Third, senescent cells secrete non-proteins belonging to the ROS family.

Soluble molecules. The most prominent soluble factor is interleukin 6 (IL-6), a pro-inflammatory and pleiotropic cytokine involved in DNA damage, oncogene and stressed induced senescence (Kuilman et al. 2008, Coppé et al. 2008). IL-6 is directly activated by p53 independent of chronic DDR signaling (Rodier et al. 2009). Additionally, both interleukin

1 (IL-1) forms, IL-1α and IL1-ß, are secreted by senescent cells. IL-1α plays a key role in SASP activation and enforcing senescence in neighboring cells (Acosta et al. 2013, Laberge et al. 2015). Amongst others, chemokines from the chemokine CXC-motif ligand 1 (CXCL) and CC chemokine ligand (CCL) families are upregulated and released by senescent cells, and CXCL-1 and 2 (synonymous to GROα and GROß, respectively), as well as CXCL8 (synonymous to IL-8) are most abundant. Moreover, IL-1α acts upstream of IL-6 and IL-8 in senescent cells (Orjalo et al. 2009). CXCL8 binding to CXC chemokine receptors CXCR1 and especially CXCR2 reinforces senescence by initiating the DNA damage signaling in an autocrine and paracrine manner (Acosta et al. 2008, Acosta et al. 2013). CCL-1 (eotaxin-3), CCL-20, CCL-3 (macrophage inflammatory protein MIP3α and MIP1α) and CCL-1 are increased among the CCL members. Insulin-like growth factor (IGF) signaling may also be important in senescence induction by secretion of IGF binding proteins (IGFBP) (Coppé et al. 2008, Kim et al. 2007, Tran et al. 2014). Colony stimulating factors (CSF) like GM-CSF and G-CSF are also highly upregulated by senescent cells.

Proteases. Primarily matrix metalloproteases (MMPs) are highly released by senescent cells. Generally, these calcium-dependent endopeptidases are cleaving all ECM proteins as well as bioactive molecules (Moore & Crocker 2012). Depending on the subclass there are some varieties in the substrate spectrum. Especially MMP-1,-3,-7 and-9 are upregulated in senescent cells and process collagen and also chemokines of the CXC and CC family to become potent receptor agonists (Rodríguez et al. 2010, Morrison et al. 2009). MMPs are inhibited by the protease family of tissue inhibitors of MMPs (TIMP). Also serine proteases play a role in senescence, like modulators of the plasminogen activation pathway, including urokinase-or tissue-type plasminogen activators (uPA or tPA) and their inhibitors PAI-1 and PAI-2) (Visse & Nagase 2003, Moore et al. 2012).

Non protein factors. To date, there is nothing known about non-protein contribution to the secretory phenotype of senescent cells, like nucleotides, bradikinins and others. Reactive oxygen species and nitric oxide were shown to be released by senescent cells, but their contribution to the SASP has not yet been determined (Lee AC et al. 1999)

1.3.4 Senescence during pathophysiology

Beside tumor suppression as one of the most important functions, many studies have demonstrated a beneficial role for cellular senescence in other pathologic conditions, such as atherosclerosis and pulmonary hypertension (Visel et al. 2010, Samani & Schunkert 2008, Mercer et al. 2005, Khanna 2009, Guevara et al. 1999, Mizuno et al. 2011, Mouraret et al.

2013, Yu et al. 2005). Importantly, a body of evidence has uncovered senescence as a key regulator of fibrosis in different organ systems (Muñoz-Espín & Serrano 2014).

Senescence limits liver fibrosis. In humans, senescent cells can be detected along the fibrotic scar within the liver (Wiemann et al. 2002). Senescent cells also accumulate in the liver in animal models, which underwent chemical treatment or bile duct ligation (Krizhanovsky et al. 2008, Kim et al. 2013, Borkham-Kamphorst et al. 2014). These studies show that predominantly hepatic stellate cells (HSCs), the ECM producing cells of the liver, undergo senescence upon upregulation of p16 ^{INK4a}, p53 and p21 $^{CIP1/WAF1}$ after an initial phase of hyperproliferation. In senescence deficient *Trp53* and or *p16* ^{INK4a} KO mice, fibrosis increases after liver damage. That identifies senescence as a fibrosis limiting mechanism in the liver (Krizhanovsky et al. 2008). The matricellular protein CCN1 has been shown to be produced and secreted by hepatocytes upon liver damage, inducing senescence of hepatic stellate cells (HSCs) and subsequently restricting liver fibrosis (Kim et al. 2013, Borkham-Kamphorst et al. 2014). IL-22 was also shown to induce senescence of HSCs and reduce liver fibrosis (Kong et al. 2012). Moreover, recombinant CCN1 or adenoviral overexpression of CCN1, as well as IL-22 treatment could revert established scars (Kong et al. 2012, Kim et al. 2013, Borkham-Kamphorst et al. 2014).

Senescence limits skin fibrosis. Initially, Jun and Lau. identified senescence as a key event during cutaneous wound healing. CCN1 signaling plays a crucial role, since CCN1 deficient mice have a slower wound closure and exacerbated skin fibrosis (Jun & Lau 2010a, Jun & Lau 2010b). The study shows that senescent cells produce and secrete anti-fibrotic MMPs. Moreover, treatment of wounds with CCN1 restricts cutaneous fibrosis. More recent investigations by Demaria et al. supported the fact that senescent fibroblasts are crucial for optimal wound closure kinetics. The depletion of p16 ^{INK4a}- positive, senescent endothelial cells and fibroblasts results in a slower wound healing process (Demaria et al. 2014). Similar results were obtained by an investigation showing that depletion of p16 ^{INK4a}- positive cells during ageing is beneficial, but has detrimental effects on wound closure (Baker et al. 2016).

Senescence limits renal fibrosis. Senescence was associated in humans and many animal models with renal damage or kidney ageing (Naesens 2011, Verzola et al. 2008, Melk et al. 2004, Westhoff et al. 2008, Clements et al. 2013). Ureteral obstruction induced renal fibrosis was increased in *CDKN2A* null and SA-ß-gal deficient mice (Wolstein et al. 2010). p16 ^{INK4a} -mimicking by treatment with a CDK4 inhibitor resulted in a decreased fibrotic response after ischemia (DiRocco et al. 2014). However, it has also been shown that CDK4 inhibition can be detrimental for renal fibrogenesis upon ischemic kidney injury (Braun et al. 2012).

Senescence and cardiac fibrosis. Senescent cells have been shown to accumulate during cardiac fibrosis upon myocardial infarction in a p53, p16 ^{INK4a} and p21 $^{CIP1/WAF1}$- dependent manner (Zhu et al. 2013). However, the pathophysiological role of cellular senescence during cardiac fibrogenesis has not yet been fully addressed.

1.4 Aim and objectives

The aim of this study was to investigate the pathophysiological role of premature cellular senescence in cardiac fibrosis.

The first objective was to find out if senescent cells accumulate during cardiac fibrogenesis in different cardiac injury models and fibrosis types. For this, two established mouse models of cardiac fibrosis as well as human heart biopsies were investigated for fibrosis and cellular senescence.

The second objective was to identify the cell type becoming senescent in the course of fibrogenesis. For this, cardiac cells were isolated and analysed for senescence markers. Moreover, heart sections of different fibrosis models were investigated for several markers of cardiac cell types and cellular senescence.

Finally, the third objective was to rule out the biological relevance of cellular senescence within cardiac fibrosis. Therefore, genetic and viral senescence-gain-of-function and senescence-loss-of-function mouse models were subjected to cardiac injury. Cardiac fibrogenesis, cellular senescence and heart function was analysed to causally link the cellular senescence program to the modulation of fibrogenesis in the heart.

2 Materials

2.1 Chemicals

Acetone	BASF (Ludwigshafen, Germany)
Acetic acid glacial	Roth (Karlsruhe, Germany)
Agar	AppliChem (Darmstadt, Germany)
Agarose	Roth (Karlsruhe, Germany)
Ammonia solution 32%	Roth (Karlsruhe, Germany)
Ampicillin	Roth (Karlsruhe, Germany)
Antipain	Sigma Aldrich (Taufkirchen, Germany)
Ampicillin sodium salt	Roth (Karlsruhe, Germany)
2,3-Butanedione monoxime (BDM)	Sigma Aldrich (Taufkirchen, Germany)
Bromphenol blue	Roth (Karlsruhe, Germany)
Bromodeoxyuridine (BrdU)	Sigma Aldrich (Taufkirchen, Germany)
Bovine Serum Albumin (BSA) fraction V	AppliChem (Darmstadt, Germany)
Chloramphenicol	Roth (Karlsruhe, Germany)
Citric acid	Roth (Karlsruhe, Germany)
Complete Mini, Proteinase inhibitores	Roche (Mannheim, Germany)
Dimethylsulfoxid (DMSO)	AppliChem (Darmstadt, Germany)
Direct Red 80	Sigma Aldrich (Taufkirchen, Germany)
D-(+)-Glucose	Sigma Aldrich (Taufkirchen, Germany)
Dithiothreitol (DTT)	Roth (Karlsruhe, Germany)
Ethanol	Roth (Karlsruhe, Germany)
Ethylene glycol-bis (2-amino-ethylether)-N,N,N',N'-Tetra acetic acid	Sigma Aldrich (Taufkirchen, Germany)
Ethylenediamine-tetraaceticacid	Roth (Karlsruhe, Germany)
Isopropanol	BASF (Ludwigshafen, Germany)
Kanamycin sulfate	Roth (Karlsruhe, Germany)
Leupeptin	Sigma Aldrich (Taufkirchen, Germany)
Magnesium chloride	Sigma Aldrich(Taufkirchen, Germany)
Magnesium sulfate ($MgSO_4$)	Sigma Aldrich (Taufkirchen, Germany)
Methanol	Roth (Karlsruhe, Germany)
Monopotassium phosphate (KH_2PO_4)	Sigma Aldrich (Taufkirchen, Germany)
N,N-Dimethylformamide (DMF)	Sigma Aldrich (Taufkirchen, Germany)
Nonfat dried milk powder	AppliChem (Darmstadt, Germany)

Paraformaldehyde (PFA)	Sigma Aldrich (Taufkirchen, Germany)
Parablast	Sigma Aldrich (Taufkirchen, Germany)
Phenylarsine oxide (PAO)	Sigma Aldrich (Taufkirchen, Germany)
Phenylmethanesufonyl fluoride **(**PMSF)	Sigma Aldrich (Taufkirchen, Germany)
Picric Acid-Saturated Solution 1.3%	Sigma Aldrich (Taufkirchen, Germany)
Potassium ferricyanide ($K_3[Fe(CN)_6]$)	Roth (Karlsruhe, Germany)
Potassium ferrocyanide ($K_4[Fe(CN)_6]$)	Roth (Karlsruhe, Germany)
Saccharose	Roth (Karlsruhe, Germany)
Sodium bicarbonate (NaHCO3)	Sigma Aldrich (Taufkirchen, Germany)
Sodium chloride (NaCl)	Sigma Aldrich (Taufkirchen, Germany)
Sodium fluoride (NaF)	Sigma Aldrich (Taufkirchen, Germany)
Sodiumdodecylsulfate (SDS)	Roth (Karlsruhe, Germany)
Sodium hydroxide (NaOH)	Roth (Karlsruhe, Germany)
Sodium hydrogen phosphate dibasic (Na_2HPO_4)	Roth (Karlsruhe, Germany)
Sodiumdihydrogen phosphate dihydrate (NaH_2PO_4)	Roth (Karlsruhe, Germany)
Sodium orthovanadate (Na_3VO_4)	Sigma Aldrich (Taufkirchen, Germany)
Taurine	Sigma Aldrich (Taufkirchen, Germany)
Toluene	Staub & Co (Nürnberg, Germany)
Tris base	Roth (Karlsruhe, Germany)
Tri-sodium-citrate (dihydrate)	Roth (Karlsruhe, Germany)
Tryptone-Peptone	AppliChem (Darmstadt, Germany)
Paraplast X-TRA	Sigma Aldrich (Taufkirchen, Germany)
Phenol red	Sigma Aldrich (Taufkirchen, Germany)
Potassium Acetate	Roth (Karlsruhe, Germany)
Potassium chloride (KCl)	Sigma Aldrich (Taufkirchen, Germany)
SOB Medium powder	Roth (Karlsruhe, Germany)
Sodium dodecyl phosphate (SDS)	Roth (Karlsruhe, Germany)
Yeast extract	AppliChem (Darmstadt, Germany)
5-bromo-4-chloro-3-indolyl-β-D-galactopyranoside (X-Gal)	Roth (Karlsruhe, Germany)

2.2 Reagents and solutions

Acrylamide 30%	BioRad (München, Germany)
Aqua ad inectabilia Braun (Apo water)	Braun (Melsungen, Germany)
Aquatex	Merck (Darmstadt, Germany)
Ketone hydrochloride	Pfizer (New York; USA)
Bouin's Solution	Sigma Aldrich (Taufkirchen, Germany)
Bradford dye reagent (5x)	BioRad (München, Germany)
Chloroform (Trichlormethane, $CHCl_3$)	Roth (Karlsruhe, Germany)
Cryomatrix (Shandon^{tm})	ThermoFisher Scientific (Surrey, United Kingdom)
Eosin Y Solution Aqueous	Sigma Aldrich (Taufkirchen, Germany)
DEPEX	Merck (Darmstadt, Germany)
Deoxynucleoside triphosphates (dNTPs)	Thermo Fisher Scientific (Surrey, United Kingdom)
Deoxy-thymine nucleotides (oligodTs)	Roth (Karlsruhe, Germany)
Dimethylsulfoxide (DMSO)	Sigma Aldrich (Taufkirchen, Germany)
4`,6-Diamidin-2-phenylindol (DAPI)	Sigma-Aldrich (Deisenhofen, Germany)
DNA loading (GelPilot) dye 5x	Qiagen (Hilden, Germany)
Dulbecco's Modified Eagle Medium DMEM	GIBCO (Karlsruhe, Germany)
DMFO	Roth (Karlsruhe, Germany)
Dimethylsulfoxid (DMSO)	Roth (Karlsruhe, Germany)
Eosin Y	Sigma-Aldrich
Ethidium bromide	Roth (Karlsruhe, Germany)
Fast Green FCF	Sigma Aldrich (Taufkirchen, Germany)
FastStart Universal SYBR Green Master	Roche (Mannheim, Germany)
Fetal calf serum (FCS)	PAN (Aidenbach, Germany)
Fluorescin Avidin D	Vector Laboratories (Burlingame, USA)
Goat serum	Thermo Fisher Scientific (Surrey, United Kingdom)
Glutaraldehyde 50%	Applichem (Darmstadt, Germany)
Glycerol	AppliChem (Darmstadt, Germany)
Goat serum	
Hematoxyline 2	Thermo Fisher Scientific (Surrey, United Kingdom)
Heparin-natrium 25000 I.U	Ratiopharm
Hydrochloride acid	Roth (Karlsruhe, Germany)

Hydrochloric acid 37% (HCl)	Roth (Karlsruhe, Germany)
Hydrogen peroxide 30% (H_2O_2)	Roth (Karlsruhe, Germany)
Iodixanol (60% in water)	ProgenBiotech
Isofluran	Abbott (Wiesbaden, Germany)
Laminin	BD Biosciences (Heidelberg, Germany)
Lipofectamine™ 2000	Thermo Fisher Scientific (Surrey, United Kingdom)
2-Mercaptoethanol	AppliChem (Darmstadt, Germany)
Mounting medium for fluorescence with DAPI	Vector Laboratories (Burlingame, USA)
Minimum Essential Eagle (MEM)	Gibco (Karlsruhe, Germany)
Murine RNAse Inhibitor	Thermo Fisher Scientific (Surrey, United Kingdom)
Nonident P40 (MP-40)	AppliChem (Darmstadt, Germany)
Opti-MEM® I	Gibco (Karlsruhe, Germany)
Polyethylenimin (PEI)	Sigma Aldrich (Taufkirchen, Germany)
Penicillin/Streptavidin	Thermo Fisher Scientific (Surrey, United Kingdom)
PeqGold RNAPure 200ml	Peqlab (Erlangen, Germany)
Phenol/Chloroform/Isoamyl alcohol	Roth (Karlsruhe, Germany)
Phosphate buffered sailne	Thermo Fisher Scientific (Surrey, United Kingdom)
Picric Acid-Saturated Solution 1.3%	Roth (Karlsruhe, Germany)
RNase Zap	
Sodium chloride (NaCl 0.9%)	Braun (Bethlehem, USA)
Tetramethylethylendiamine (TEMED)	Sigma-Aldrich (Deisenhofen, Germany)
Texas Red Avidin D	Vector Laboratories (Burlingame, USA)
Triton X-100	Sigma Aldrich (Taufkirchen, Germany)
TriFast, peqGold	Peqlab (Erlangen, Germany)
Tween 20	Roth (Karlsruhe, Germany)

2.3 Buffers and media

2.3.1 Common buffers

Hepes Buffer, 1M	Sigma Aldrich (Taufkirchen, Germany)
TE buffer	Thermo Fisher (United Kingdom)
Phosphate buffer(0.1M, pH 7.3)	
NaH2PO4	15.6 g
Na2HPO4	10.35 g
H2O	1000 ml
Phosphate buffer with Tween 20 (PBST, 0.05%)	
1 X PBS	1000 ml
Tween 20	0.5 ml
Adeno-associated virus (AAV) lysis Buffer	
50 mM Tris-base	6.06 g
150 mM NaCl	8.77 g
5 mM MgCl2 6xH20	1.02 g
Gibco water	900 ml
adjust pH to 8.5	
add up to 1 l	

2.3.2 Bacterial growth media and solutions

LB Agar	
Tryptone-Peptone	40 g
Yeast extract	20 g
NaCl	20 g
1M NaOH	4 ml
Agar	60 g
H2O	ad 4l
LB Medium	
Tryptone-Peptone	50 g
Yeast extract	25 g
NaCl	25 g
1M NaOH	5 ml
H2O	ad 5l
Ampicillin stock solution 1000x	

5g Ampicillin	5g
H2O	
ad 50 ml	
(100 mg/ml)	
Kanamycin stock solution 300x	
Kanamycin	500 mg
H2O	ad 50 ml
(10 mg/ml)	
Chloramphenicol stock solution 1500x	
Chloramphenicol	150 mg
100% high grade Ethanol	ad 5 ml
(30 mg/ml)	

2.3.3 Cell culture media

HEK293T culture medium	
DMEM	
(+4.5g/l D-Glucose, L-Glutamine, Pyruvate)	450 ml
10% FCS	50 ml
Penicillin/Streptomycin	5 ml
Neonatal rat cardiomyocyte (NRCM) culture medium incomplete	
MEM	10,8 g
Vitamin B12	1 ml
NaHCO3	350 mg
H2O	ad 1 l
NRCM culture medium 5% FCS	
NRCM medium incomplete containing	
FCS	25 ml
Penicillin/Streptomycin	5 ml
BrdU	5 ml
NRCM medium incomplete	ad 500 ml
NRCF culture medium 5% FCS	
NRCM medium incomplete containing	
FCS 10%	
Penicillin/Streptomycin 1%	
AMCM Plating Medium	

MEM	45.5 ml
FCS	2.5 ml
500mM BDM	1 ml
Penicillin/Streptomycin	0.5 ml
200mM L-Glutamine	

AMCM culture medium 5% FCS

Equal to NRCM culture medium 5%

AMCF culture medium 5% FCS

Equal to NRCF culture medium 5%

2.3.4 Adult mouse cell isolation buffer, media and solutions

Stock Perfusion buffer

Sodium chloride (NaCl)	6.6 g
KCl	0.35 g
KH2PO4	0.082 g
Na2HPO4	0.085 g
MgSO4-7H2O	0.3 g
Phenol Red	0.012 g
NaHCO3	1.01 g
KHCO3	1.01 g
Taurine	3.75 g

Perfusion buffer

490 ml Stock Buffer	490 ml
500 mM BDM	10 ml
5% Glucose	10 ml

Digestion buffer

Collagenase Typ2 II	46 mg
100 mM $CaCl_2$	15 µl
Perfusion Buffer	20 ml

Buffer P1

9 ml perfusion buffer

1 ml FCS PAN 3302-P282905

12.5 µl $CaCl_2$ (10mM)

Buffer P2

Perfusion buffer	47.5 ml
FCS	2.5 ml

10 mM$CaCl_2$	62.5 µl
BrdU	
BrdU	230 mg
H2O	74,8 ml

sterile filtering, 2ml aliquots store at -20°C

2.3.5 Buffers for protein work

1x Bradford solution

dilution of 5x Bradford stock BioRad (Hercules, USA) 1:5.

Protein lysis buffer

20 mM Tris pH7.5

150 mM NaCl 1

1 mM EDTA

1 mM EGTA

Triton-X-100 1% (V/V)

2.5 mM sodiumpyrophosphate

1mM Na3VO4

add 1 tablet Complete Mini per 10ml

LAEMMLI loading buffer 4x (DTT based)

Final concentration	mix (7.5ml total)
200 mM TrisCl (pH 6.8)	1.5 ml 1M TrisCl (pH 6.8)
400 mM DTT	3 ml 1M DTT (-20°C)
8% SDS	0.6 g SDS powder
0.4% Bromophenol blue	0.03 g
50% glycerol	3 ml (100% Glycerol, prewarm!)

Tris-Glycine SDS 10x Buffer (Running buffer)

Tris/Cl	30 g
Glycine	144 g
SDS	15 g
H2O	ad 1000 ml

10x transfer buffer

1 M Tris/Cl pH 8,3	225 ml
Glycine	101,34 g
H2O	ad 1000 ml

1x transfer buffer:

1 M Tris/Cl pH 8,3	25 ml
Glycine	11,26 g
Methanol	100 ml
H2O	ad 1000 ml

2.3.6 Buffers for DNA work

Phenol-/Chloroform Lysis buffer	
Tris	12.1 g
EDTA	1.87 g
NaCl	11.7 g
TAE buffer	
Tris	242 g
Acetic acid	57.1 ml
EDTA	37.2 g
H_2O	1000 ml
Loading buffer (5x)	
0,5 M EDTA pH 8,0	1,4 ml
Glycerol	3,6 ml
Bromphenol blue	0,01 g
H_2O	7 ml
10x Accuprime buffer	
PEI “MAX” 50 mg	
Add 45 ml pharmaceutical Water,	
Adjust pH to 1.9	

2.3.7 Buffers for RNA work

5x Protoscript II Reaction buffer

2.3.8 Buffers for (immuno)histochemical stainings

Sirius Red Solution	
Direct Red 80	0.125 g
ddWater	15 ml
take it through the filter, then add	
Picric Acid-Saturated Solution 1.3%	235 ml
32% Ammonia Solution	500 µl

dd Water	160 ml
Eosin Y Solution aqueous	
ddWater	80 ml
Acetic acid glacial	1 drop
0.1% Fast Green	
FastGreen FCF	500 mg
ddWater	500 ml
0.01% Sirius Red	
Direct Red 80	50 mg
dd Water	15 ml
take it through the filter, then add	
Picric acid-saturated solution 1.3%	85 ml
X-Gal Fixation buffer	
Phosphate buffer	250 ml
0.1M EGTA	12.5 ml
1M $MgCl_2$	0.5 ml
50% glutaraldehyde	1 ml
X-Gal staining buffer	
Phosphate buffer	250 ml
1M $MgCl_2$	0.5 ml
0.5M K4[Fe(CN)6]	2.5 ml
0.5M K3[Fe(CN)6]	2.5 ml
X-Gal	2,5 ml (1:100)
X-Gal Stock solution	
X-gal	100 mg
add Diemthylformamide	1 ml
(store at -20°C)	
1 M $MgCl_2$ (250ml)	
$MgCl_2$	23,8 g
add H2O	250 ml
0.1M EGTA (2Litre), pH – 7.3	
EGTA	76 g
add H2O	2 l
K4[Fe(CN)6] (0.5M) Solution	
K4[Fe(CN)6]	10.5 g
H2O	50 ml

K3[Fe(CN)6] (0.5M) Solution	
K3[Fe(CN)8]	8.2 g
H2O	50 ml
$MgCl_2$ (1M)	
$MgCl_2$	23.8 g
H2O	250 ml
Tri-sodium-citrate (dihydrate) buffer (pH 6.0)	
Tri-sodium-citrate (dihydrate)	2.94 g
H2O	1000 ml
adjust pH 6.0 (HCl)	
Tween 20	0.5 ml
EDTA buffer (pH 8.0)	
EDTA	0.37 g
H2O	1000 ml
adjust pH 8.0 (NaOH)	
Tween 20	0.5 ml

2.4 Enzymes

AccuPrime Pfx DNA Polymerase	Invitrogen (Karlsruhe, Germany)
Benzonase	Merck (Darmstadt, Germany)
BP Clonase	ThermoFisher Scientific (Surrey, United Kingdom)
Collagenase type II	Worthington (Lakewood, USA)
LR Clonase	ThermoFisher Scientific (Surrey, United Kingdom)
Proteinase K	AppliChem (Darmstadt, Germany)
Restriction enzymes: (AhdI, BamHI, SmaI, ScaI, HindIII, MluI)	New England Biolabs ,NEB (Frankfurt, Germany)
Reverse transcriptase ProtoscriptII	New England Biolabs ,NEB (Frankfurt, Germany)
Taq DNA Polymerase	GenScript (New York, USA)
Trypsin	ThermoFisher Scientific (Surrey, United Kingdom)

2.5 DNA and protein marker

Precision Plus Protein™ All Blue Standards	BioRad (Hercules, USA)
DNA ladder100 bp DNA ladder (25ng/µl)	New England Biolabs ,NEB (Frankfurt, Germany)

100bp DNA ladder	30 µl
Loading buffer (5x)	120 µl
TAE buffer (1x)	450 µl

1000bp DNA ladder (25ng/µl)	New England Biolabs ,NEB (Frankfurt, Germany)

1000bp DNA ladder	30 µl
Loading buffer (5x)	120 µl
TAE buffer (1x)	450 µl

2.6 Antibodies

Primary antibodies for Western Blot

Anti - CCN1 (ab24448)	Abcam (Cambridge, United Kingdom)
Anti - p53 (ab26; ab28; ab1101)	Abcam (Cambridge, United Kingdom)
Anti - p16 ^{INK4a} (ab54210)	Abcam (Cambridge, United Kingdom)
Anti - p21$^{CIP1/WAF1}$ (ab7960; ab109199)	Abcam (Cambridge, United Kingdom)
Anti - HSP90	Santa Cruz (Heidelberg, Germany)

Secondary antibodies for Western Blot

HRP mouse (#7076)	Cell Signaling Technology (Danvers, USA)
HRP rabbit (#7074)	Cell Signaling Technology (Danvers, USA)

Primary antibodies for immunohistology

Anti - p16 ^{INK4a} (ab54210)	Abcam (Cambridge, United Kingdom)
Anti - p21$^{CIP1/WAF1}$ (ab7960; ab109199)	Abcam (Cambridge, United Kingdom)
Anti - CCN1 (ab24448)	Abcam (Cambridge, United Kingdom)
Anti - vimentin (ab24525)	Abcam (Cambridge, United Kingdom)
Anti - HP1beta (ab10478)	Abcam (Cambridge, United Kingdom)
Anti - PDGFRalpha (AF1062)	R&D Systems (Minneapolis, Canada)
Anti - aplha SMA (A5228)	Sigma Aldrich (Taufkirchen, Germany)
Anti - CD31 (ab28364)	Abcam (Cambridge, United Kingdom)
Anti - CD31 (#550274)	BD Pharmingen (Heidelberg, Germany)
Anti - TroponinT (ab8295)	Abcam (Cambridge, United Kingdom)

Secondary antibodies for immunohistology

All secondary luorophore coupled antibodies were obtained from ThermoFisherScientific (Surrey, United Kingdom).

Anti - rabbit - 488
Anti – rabbit - 594
Anti - mouse - 488
Anti – mouse - 594
Anti – chicken - 488
Anti – goat - 488
Anti – rat - 594

2.7 Cell lines and primary cells

HEK293T Cell line

The human embryonic kidney cell line HEK293T were originally obtained from ATCC and maintained as described (3.3.1).

AMCM

Adult mouse cardiomyocytes were isolated as described elsewhere (3.4.3).

AMCF

Adult mouse cardiofibriblasts were isolated as described elsewhere (3.4.3).

NRCM

Adult mouse cardiofibriblasts were isolated as described elsewhere (3.4.2).

NRCF

Adult mouse cardiofibriblasts were isolated as described elsewhere (3.4.2).

2.7 Bacterial strains

Stable competent E.coli cells were originally obtained from New England Biolabs , NEB (Frankfurt, Germany) and maintained according the instruction.

SURE competent E.coli cells were originally obtained from Biocompare (San Francisco, USA) and maintained according the instruction.

DH10B competent E.coli cells were originally obtained from ThermoFisher Scientific (Surrey, United Kingdom) and maintained according the instruction.

2.8 Viral strains

Adeno-associated virus serotype 9 (AAV9)

AAV9-CCN1, AAV9-DN and AAV9-GFP

Plasmids with the appropriate insert for AAV9 generation were cloned as described elsewhere (3.7.4.1) and used for virus production (3.3).

Adenovirus

pAd-CCN1 and pAd-CCN1-DN

Plasmids with the appropriate insert for Adenovirus generation were cloned as described elsewhere (3.7.4.1) and used for virus production (3.3).

2.10 Plasmids and cloned vectors

Gateaway cloning

Cloning was performed according the Gateway manual ThermoFisher Scientific (Surrey, United Kingdom).

DsAAV-CMV9-CCN1 and DsAAV-CMV9-CCN1-DN

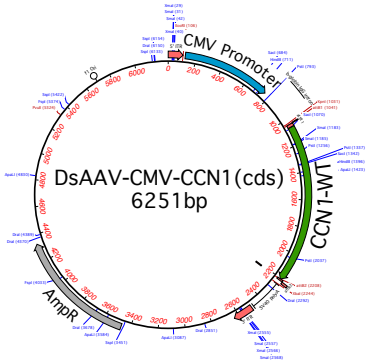

DsAAV-CMV9-CCN1

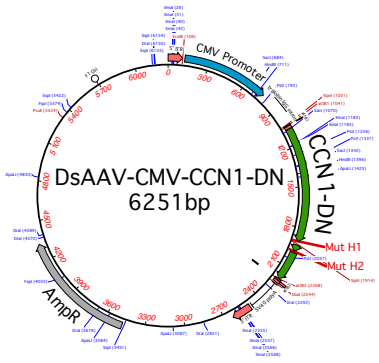

DsAAV-CMV9-CCN1-DN

pAd-CMV-V5- CCN1 and pAd-CMV-V5- CCN1-DN

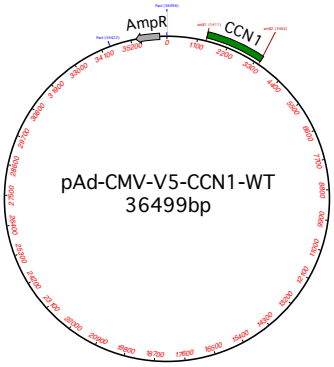

pAd-CMV-V5-CCN1

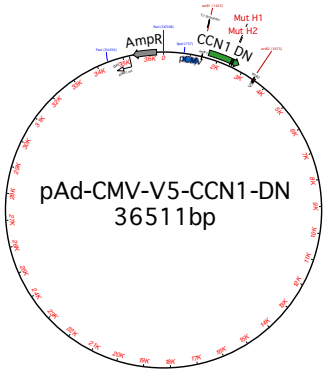

Ad-CMV-V5-CCN1-DN

2.11 Oligonucleotides

Oligonucleotides for DNA amplification via PCR for genotyping: All primers were ordered from Eurofins MWG Operon (Ebersberg, Germany).

Gene	Primer sequence
CDKN2A WT :	5'-GTGATCCCTCTACTTTTTCTTCTGACTT - 3' (forward) 5'- CGGAACGCAAATATCGCAC-3' (reverse)

CDKN2A KO:	5’-GTGATCCCTCTACTTTTTCTTCTGACTT - 3’ (forward) 5'-GAGACTAGTGAGACGTGCTACTTCCA -3' (reverse)
TP53 WT:	5’-ACACACCTGTAGCTCCAGCAC-3’ (forward) 5’-AGCGTCTCACGACCTCCGTC-3’ (reverse)
TP53 KO:	5’-ACACACCTGTAGCTCCAGCAC-3’ (forward) 5’-GTGTTCCGGCTGTCAGCGCA-3’ (reverse)
TG^{Adrb1}:	5’-ACATGGAGTCCTGGTGGGAG-3’ (forward) 5’-TGCGGCCGACGACAGGTTAC-3’ (reverse)
CTSD:	5’-GCAACCCGGAGGAGAACTAA-3’ (forward) 5’-CCACAGGCCCCACCAGAAGA-3’ (reverse)

Oligonucleotides for DNA amplification via PCR for cloning: All primers were ordered from Eurofins MWG Operon (Ebersberg, Germany). CCN1 was cloned from CDKN2A WT genomic DNA and CCN1-DN from the plasmid received from Prof. Lau (Chicago, USA).

Gene	Primer sequence
CCN1 and CCN1-DN	5’-GGGGACAAGTTTGTACAAAAAAGCAGGCTTC ATGAGCTCCAGCACCTTCAGGACG-3’ (Attb1; forward)
	5’-GGGACCACTTTGTACAAGAAAGCTGGGTCTTAGTCCCTGAAC TTGTGGATGTC-3’ (Attb2; reverse)

Oligonucleotides for cDNA amplification via qRT-PCR: All primers were ordered from Eurofins MWG Operon (Ebersberg, Germany)

Gene	Primer sequence
Rpl32	5’-GCCAAGATCGTCAAAAAGA-3’ (forwa 5’-GTCAATGCCTCTGGGTTT-3’ (reverse)
Gapdh	5’-TGGCAAAGTGGAGATTGTTG-3’ (forward) 5’-CATTATCGGCCTTGACTGTG-3’ (reverse)
Col3a1	5’-ACAGCAAATTCACTTACACAGTTC-3’ (forward) 5’-CTCATTGCCTTGCGTGTTT-3’ (reverse)
Nppa	5’-GCTTCCAGGCCATATTGGAG-3’ (forward) 5’-GGGGGCATGACCTCATCTT-3’ (reverse)

Col1a2	5’-AGGTCTTCCTGGAGCTGATG-3’ (forward) 5’-ACCCACAGGGCCTTCTTTAC-3’ (reverse)
Cdkn2a	5’-CGAACTCTTTCGGTCGTACCC-3’ (forward) 5’-CGAATCTGAACCGTAGTTGAGC-3’ (reverse)
Cdkn1a	5’-CAAGCGCCGATTGGTCTT-3’ (forward) 5’-CCTCCCGTGGGCACTTC-3’ (reverse)
Glb1	5’-CCTGTCACTGCTGCAACT-3’ (forward) 5’-AATGGCTGTCCATCCTGTAG-3’ (reverse)
Cyr61	5’-ACCGCTCTGAAAGGGATCTG-3’ (forward) 5’-TGTTTACAGTTGGGCTGGAAG-3’ (reverse)
Cdkn2d	5’-GTTCTTGGTCACTGTGAGGATTCAG-3’ (forward) 5’-CCATCATCATCACCTGGTCCAG-3’ (reverse)
Trp53	5’-GGGACAGCCAAGTCTGTTATGTGC-3’ (forward) 5’-CTGTCTTCCAGATACTCGGGATAC-3’ (reverse)

2.12 Kits

Avidin-Biotin Blocking Kit	Vector Laboratories (Burlingame, USA)
DAB Reagent Set	KPL (Gaithersburg, USA)
Histo Mark Biotin-Streptavidin-HRP System	KPL (Gaithersburg, USA)
ABC Kit	Santa Cruz (Dallas, USA)
Goat anti-rabbit IgG (H+L)	KPL (Gaithersburg, USA)
PureLink® Plasmid Midi/Maxi Kit	Invitrogen (Karlsruhe, Germay)
PureLink® HiPure Plasmid DNA Gigaprep Kit	ThermoScientific (Surrey, England)
ECL Plus detection reagents	GE Healthcare (Munich, Germany)
QIAquick Gel Extraction Kit	Qiagen (Hilden, Germany)
QIAquick PCR Purification Kit	Qiagen (Hilden, Germany)

2.13 Instruments

StepOnePlus Real-Time PCR System	Applied Biosystem (Foster City, USA)
Centrifuge 5417R	Eppendorf (Hamburg, Germany)
Bornstead Nanopure	ThermoScientific (Surrey, England)
Electrophoresis Power Supply –EPS 301	GE Healthcare (Munich, Germany)
Fluorescence microscope Observer.Z1 Axio	Zeiss (Oberkochen, Germany)

Gel documentation instrument UV	
Trans illuminator	Wealtec (Wilhelmsthal, Germany)
Gel electrophoresis chamber	Peqlab (Erlangen, Germany)
Cryostat Leica CM 1900	Leica (Wetzlar, Germany)
Leica SP5 confocal microscope	Leica (Wetzlar, Germany)
Metamorph	Visitron Systems (Puchheim, Germany)
Nanodrop ND-1000	Thermo Scientific (Surrey, England)
Prism 5 for Mac OS X Version 5.Ob, GraphPad	Software (San Diego, California)
Thermo cycler	Biometra (Göttingen, Germany)
Thermomixer comfort	Eppendorf (Hamburg, Germany)
Turrax (tissue homogenizer)	

2.14 Software

Metamorph	Visitron Systems (Puchheim, Germany)
Prism 5 for Mac OS X Version 5.Ob GraphPad	Software (San Diego, USA)
Illustrator	Adobe (Mountain View, USA)
Photoshop	Adobe (Mountain View, USA)
MacVector	MacVctor Inc. (Cambrodge, United Kingdom)

2.15 Others

MicroAmp® Fast Optical 96-Well	Applied Biosystems (Foster City, USA)
Reaction Plate with Barcode, 0.1 ml	Applied Biosystems (Foster City, USA)
MicroAmp® Optical Adhesive Film	Applied Biosystems (Foster City, USA)
Millipore Immobilon PVDF Membran, IPFL00010	Roth (Karlsruhe, Germany)
Pap pen	Vector Laboratories (Peterborough, United Kingdom)
TripleFlask (Nunc)	VWR (Darmstadt, Germany)

2.16 Mouse lines

C57B6/N	Charles River (Freiburg, Germany)
TG ^{Adrb1}/ FvB/N	Institute breeding
CDKN2A KO / B6.129	NCI mouse repository (Frederick, USA)

TSG-p53 (B6.129)	Taconic Biosciences Inc. (Köln, Germany)
CDKN2A/TP53 DKO / B6.129	Institute breeding

2.17 Human tissue samples

Human tissue samples were provided by Prof. R. Hajjar (New York, USA).

3 Methods

3.1 Animal work

3.1.1 Mouse lines

C57BL6/N

The C57BL6/N mouse line was originally obtained from Charles River Laboratories and expanded according to national and institutional guidelines. C57BL6/N is a standardized model system for multiple purposes. Only male mice were used for animal experiments and cardiac disease models.

TG ^{Adrb1}/ FvB/N

The TG^{Adrb1} mouse line was generated by Engelhardt et al. 1999. The ß$_1$-adrenoceptor is specifically overexpressed in cardiac myocytes. This results in remarkable cardiomyocyte hypertrophy and progressive heart failure with increased age. Only male transgenic and wildtype littermates were used for investigation and animal experiments.

CDKN2A KO / B6.129

The CDKN2A KO / B6.129 mouse line was generated in 1996 (M. Serrano et al. 1996) and carries a targeted deletion of exon 2/3 of the INK4A gene locus by a neomycin cassette insertion, thus eliminating the gene products p16 ^{INK4a} and p19 ^{ARF}. The knockout is conditional affecting all organs. Homozygous knockout mice are viable and fertile, but exhibit early tumor development with an average age of 5-6 months. Heterozygous mice show longer tumor latency.

TSG-p53 (B6.129)

The TSG-p53 mouse line was developed in 1992 (Donehower et al. 1992) The p53 gene is interrupted at exon 5 by the integration of a neomycin cassette. The knockout is conditional affecting all organs. Homozygous TSG-p53 mice show complete loss of the p53 protein and are prone to early tumor development. Heterozygous TSG-p53 mice have lower risk of developing spontaneous tumors.

CDKN2A/TRP53 DKO (B6.129)

The CDKN2A/p53 DKO mouse line was generated by cross breeding the CDKN2A KO (see 3.1.1.3) and the TSG-p53 (see 3.1.1.4) mouse lines. Heterozygous parents were bred to produce homozygous CDKN2A/p53 knockout animals and wild type animals within the same

litter. The knockout is conditional. Homozygous CDKN2A/p53 animals develop spontaneous tumors at an average age of 3-4 months.

3.1.2 Genotyping

A biopsy of the tail (around 0.5 mm) was cut and put in an 1.5 ml reaction tube. Afterwards, the tip was stored or used directly for DNA isolation. 500 µl of Phenol/Chloroform buffer and 2.5 µl proteinase K were added to the biopsy and incubated at 56 °C over night while shaking at 950 rpm. Next day, DNA was extracted by adding 500 µl of Phenol/Chloroform and centrifugation at 14000 rpm at room temperature for 10 minutes. The upper DNA containing phase was transferred into a new 1.5 ml reaction tube and 500 µl of isopropanol was added, mixed rigorously and centrifuged at 4 °C, 14000 rpm and for 10 minutes. The supernatant was discarded and the DNA pellet washed twice with 70 % ethanol and centrifuged as described before. The supernatant was discarded and the pellet dried to remove the remaining ethanol. Finally, the DNA was dissolved in 50 µl of water and stored at 4 °C until performing the PCR (see 3.7.1).

3.1.3 Transverse aortic constriction (TAC) disease model

8-9 week old mice were analgized with an opioid analgesic (Temgesic (Buprenorphine)) more than 30 minutes prior anesthetsia with 4 % Isofluorane and 96 % oxygen by inhalation. Then, the mouse was fixed on a 40 °C heating plate and the Isofluran concentration reduced to 1-2 %. The thoracotomy was performed by opening the thorax at the second rib. The aorta was dissected to free it from fat tissue and thymus. Constriction was conducted at the aortic arch between the left common carotid artery and the brachiocephalic artery by putting a 27 gauge cannula at the aorta and constrict it with a 7-0 nylon thread and two knots. The cannula was removed and the aorta diameter decreased by approximately 0.4 mm. The thorax was closed with a nylon thread and the mouse put into a heated cage. The next two to three days, analgesic treatment was performed. The control operation, termed Sham, was performed by doing the thoracotomy without aortic constriction. To determine the success of the disease model, macroscopic and functional cardiac monitoring were performed.

3.1.4 Cardiac monitoring

Functional cardiac monitoring

Functional cardiac monitoring was done before 2 or 6 weeks after surgery with an ultrasound machine Vevo 770 High-Resolution Imaging System (Visual Sonics, Ontario, Canada). The mouse was anesthetized with 4 % isofluorane and 96 % oxygen by inhalation. Then it was fixed on electrodes with electrode gel (Spectra 236 Parker, Medic, Gemany) to the desk of the ultrasound stage. The hair of the abdomen was removed with an electrical shaver and depilatory cream. The isoflurane concentration was reduced to 1-2 % and prewarmed ultrasound gel (Aquasonic 100, Medic, Germany) applied to the abdomen. The scanhead of the ultrasound machine was turned to an angle of 30 ° to the mouse and the desk moved until the long axis of the heart was visible (B-mode measurement). Afterwards, the scan head was turned to 90 ° to the mouse to visualize the short axis of the heart (M-mode measurement). The parameters *fractional shortening (FS)*, *ejection fraction (EF), left ventricular internal diameter (LVID d/s,) right ventricular internal diameter (RVID d/s), intraventricular septum (IVS d/s) and left ventricular posterior wall (d/s)* were calculated with the obtained measurements. To validate the TAC operation, pulse wave Doppler measurement was performed and the blood flow of the left coronary artery and the right coronary artery visualized and calculated.

Macroscopic cardiac monitoring

To determine hypertrophy and heart failure, heart and lung weight were analyzed. Therefore, the mouse was sacrificed 2 or 6 weeks after TAC by Isoflurane treatment and following cervical dislocation. The mouse was weighted, the abdomen cleaned with 80 % EtOH and the chest opened. The heart was removed and washed with PBS and remaining blood was pulled out. After determining the heart weight, atria were removed and the heart was cut into four pieces. Two pieces were put into 1.5 ml reaction tubes and marked with the mouse ID, organ type as well as date and shock frozen in liquid nitrogen. Later on, these pieces were used for RNA and protein isolation (see 3.8.1 and 3.5.1). The third tissue sample was put into 4 % paraformaldehyde at room temperature over night and paraffin preservation was continued next day (see 3.2.1). Another tissue piece was put into 30 % sucrose at 4 °C over night for cryopreservation (see 3.2.2). The lung was removed and washed in PBS and dried rigorously before weighing. It was cut into two pieces, one fore paraffin preservation and one for cryopreservation as described. In addition, other organs, like spleen, liver and kidney were removed, washed in PBS and cut into two parts and proceeded as before. Finally, the

leg was cut off and the bone removed from the surrounding tissue. The remaining bone was stored in 80 % ethanol until transferring it to the digestion solution (see 3.1.2). Next day, the tissue was completely removed and the tibia length was measured and documented.

To determine heart and lung weight, the ratio of heart and lung compared to body weight or tibia length were calculated. A heart weight/tibia length ratio of 5-7 showed healthy heart conditions and a ratio between 8-11 determined heart failure.

Histologic cardiac monitoring

To determine the degree of hypertrophy and fibrosis, senescence or protein expression levels, animals were euthanized 5 days, 2 or 6 weeks after TAC and heart tissue preserved. For this, two preservation methods were employed, cryopreservation (3.2.2) and paraffin-embedding (3.2.1). After cutting the sections, respective slides were used for fibrosis staining (Sirius red/fast green, 3.2.3 and 3.2.4), senescence staining (SA-ß-galactosiadase-assay, 3.2.5) or protein expression analysis by western blot or immunofluorescence.

Molecular cardiac monitoring

To study mRNA and protein expression, heart tissue was frozen at -80 °C and RNA or protein lysates prepared. Further analysis, like qRT-PCR (see 3.8.3) and western blot (see 3.5.2 and 3.5.3), allowed quantification of mRNA and proteins, respectively.

3.1.5 Tail vein injection

To inject AAV9 in adult mice, tail vein injection was performed. 3-4 weeks old Bl6/N mice were anesthetized with isoflurane and fixed in a small box where only the tail was exposed. The tail was put into hot water to visualize the veins. When the color of the veins was blue, a 1 ml syringe needle was inserted into the vein by keeping it parallel to the vein. Injection was carried out with 2x10^12 virus particles or 40 % iodixanol in a total volume of 200-300 µl.

3.2 Histology

3.2.1 Paraffin preservation and paraffin-sectioning

After removal, organs were transferred into 4 % paraformaldehyde and incubated at RT overnight. The next day the PFA was discarded and tissues washed 3 times with PBS. The following embedding step was performed by an automated Spin Tissue Processor (STP 120, Thermo Scientific, Braunschweig, Germany). The tissue was incubated in serial concentrations of ethanol for 2 hours each: 50 %, 60 %, 70 %, 80 %, 90 %, 2 x 100 %. Afterwards, the tissue was treated with Roti-Histol as well as liquid paraffin 2 times for 2 hours. Then, it was embedded manually in a paraffin block by putting the plastic device on ice, inserting the tissue and adding hot, fluid paraffin. The tissue was sectioned at 6 µm and 8 µm slices, transferred on polylysine coated slides (Thermo Scientific, Braunschweig, Germany) and dried at 42 °C. The slides were stored at room temperature.

3.2.2 Cryopreservation and Cryo-sectioning

Organs were removed from the mouse and cut into several pieces. The pieces were washed with PBS and put into 30 % sucrose over night at 4 °C while shaking. Next day, the tissue was dried rigorously with a kimwipe and put into a plastic box. OCT (Thermo Scientific, Braunschweig, Germany) was added and the tissue was frozen at -80 °C.

For sectioning, the frozen OCT block was put from -80 °C in to -20 °C for approximately 30 minutes and fixed within the cryotome machine. The thickness of each slice was adjusted to 5 µm. The tissue was cut and the slice was transferred on the slide by putting it onto the section. Minimum two slices were put on one slide. The slides were stored at -80 °C and used for histological or immunological stainings.

3.2.3 Histochemistry I: Hematoxyline /Eosine (H/E) staining of paraffin and cryopreserved sections

Paraffin sections were deparaffinized and rehydrated by putting the slides successively into 100 % toluol twice for 10 minutes, twice in 100 % ethanol for 5 minutes and afterwards for 5 minutes in 90 %, 70 %, 50 % and 30 % ethanol and finally into water.

Cryo-preserved sections were air dried at room temperature for a minimum of one hour and then incubated for one hour at 58 °C in bouin's solution before washed rigorously 20-25

minutes with running tap water.

The rehydrated paraffin sections and the cryosections were treated equally from now on and incubated for 2 minutes in hematoxyline solution and washed 3 times with tap water. Then the clarifier solution was added for 10 seconds and the slides washed for 1 min with tap water. The sections were transferred into the bluing reagent for 1 minute and washed for 1 minute in tap water. For counterstaining, the sections were put in 0.1 % eosin solution for 1 minute. Finally, the sections were dehydrated by incubating successively in 80 % ethanol for 30 seconds, 100 % ethanol for 1 minute and 100% toluol for 3 minutes. The slides were covered with approximately 50-100 µl DEPEX and a 24x55 mm coverslip.

3.2.4 Histochemistry II: Sirius red/fast green staining of paraffin and cryopreserved sections

The deparaffinization and rehydration of the paraffin sections was done as described in 3.2.3. After this, sections were incubated in Bouin's solution for 1 hour at 58 °C and washed for 20 min with running tap water. The cryopreserved sections were treated in the same way as in 3.2.3. Cryopreserved and deparaffinized sections were incubated in 0,1 % fast green staining for 20-30 minutes at room temperature and afterwards incubated in 1 % acetic acid for 1 minute at room temperature. Then a washing step in tap water for 5 minutes followed prior 0,1 % picrosirius red solution incubation for minimum of 30 minutes. Afterwards, sections were dehydrated as described previously and covered with DEPEX. The quantitative analysis was done with the metamorph software and an analysis journal that quantifies the percentage of fibrotic areas in the left ventricle or in the perivascular regions.

3.2.5 Histochemistry III: Senescence associated (SA)-ß-galactosidase staining

SA-ß-gal staining of cryopreserved heart sections

In principle, cryopreserved sections were fixed with SA-ß-gal fixation solution for 15 minutes at room temperature and washed 2 times with PBS for a total 20 of minutes. Subsequently, the staining solution with 1 mg/ml X-gal and pH 5.5 for mouse and pH 6 for human heart sections was added and incubated overnight at 37 °C in a CO_2 -free incubator. The next day, sections were washed with water and covered with aquatex and a 24x50 mm coverslip. The

slides were air dried for a few hours and then analyzed by bright field microscopy and the metamorph software using a journal measuring the blue intensity and the percentage of the blue area.

SA-ß-gal staining of NRCF

Medium of NRFC was removed and the cells washed twice with PBS prior to putting the fixation solution for 15 min at RT. Afterwards, the fixation solution was removed rigorously by 3 washing steps with PBS. The SA-ß-gal staining solution with 1 mg/ml X-Gal and pH 6 was added (200 µl per well in a 96 well plate). The plate was put into a plastic bag to avoid evaporation of the solution and transferred into a CO_2-free incubator at 37 °C overnight. The next day, the staining solution was discarded and cells washed twice with PBS. To normalize to the cell number during analysis, cells were incubated for 30 min with DAPI 1:100 in PBS and washed again with PBS. For storage, 80 % glycerol was added. The analysis was done by microscopy and a software detecting the blue pixels per area and DAPI positive cells. The area was manually divided by the DAPI number.

3.2.6 Immunohistochemistry

Generally, paraffin embedded sections were deparaffinized and rehydrated as described in 3.2.3. Afterwards, sections were treated to unmask the epitope, which was cross-linked by paraformaldehyde treatment during paraffin-conservation. For this, several protocols were established, including enzyme or heat mediated based methods. Here, only heat induced epitope retrieval (HIER) was used. Sections were incubated for 10 minutes in sodium citrate buffer and cooked for 4 min at 100°C in a microwave. Slides were cooled down and then incubated with 1% triton x in PBS for 30 minutes at room temperature. The blocking step was performed after circling the tissue sections with a pap pen. 10 % goat serum for minimum one hour at room temperature was added. Immunohistochemistry was only performed to detect p16 ^{INK4a}. The primary p16 ^{INK4a} antibody (abcam, ab54210) was diluted 1:3500 in 10 % goat serum and applied over night at 4 °C. The next day, the slides were washed 3 times for a total of 30 minutes in PBST followed by an incubation step in 3 % H_2O_2/PBS in the dark at room temperature for 30 minutes. After this, the biotnylated secondary F(ab)2 - anti - mouse was added for 30 minutes. The incubation with the biotinylated Streptavidin peroxidase (from Santa Cruz Kit) followed after a washing step in PBST for 30 minutes. Detection followed by adding the substrate DAB (from Santa Cruz Kit) for 5-10 minutes. The

slides were put into water and covered with aquatex. Analysis was performed by bright field microscopy and counting the dark brown nuclei.

3.2.7 Immunofluorescence

All fluorescence-based stainings were conducted on cryopreserved sections. For this, the slides were dried at room temperature for 30 min followed by a methanol/acetone fixation step. Sections were incubated for 10 minutes in methanol at -20 °C, washed rigorously in running tap water for approximately 2-3 minutes and then incubated in acetone for 1 minute at -20 °C. The slides were air dried for 30 minutes at room temperature. Prior blocking in 10 % goat serum or horse serum for a minimum of 1 hour, samples were briefly washed in PBS and the sections circled with the pap pen. The primary antibody was added as shown in table 1 overnight at 4 °C. The next day, the sections were washed with PBST for a total of 30 minutes and then the secondary, fluorophore-labelled antibody added. The secondary antibody was diluted 1:400 in PBS and added for 30 minutes at RT. A final washing step followed before the slides were covered with DAPI mounting medium. If a double staining was performed, the second primary antibody was added after the last washing step and incubated over night at 4 °C. The dilutions of the second primary antibodies are listed in table 1. The next day, sections were washed for 30 minutes in PBST and the second secondary antibody was applied as listed below for 30 minutes followed by a 30 minutes washing step in PBST. Finally, the slides were covered with DAPI mounting medium. For double staining, the primary antibodies have to be generated in different species and the fluorophores of the secondary antibodies have to emit light within a different spectrum.

Table 1: Antibody dilutions for single and double staining

Primary antibody	**dilution**	**dilution buffer**
Anti-p21 $^{CIP1/WAF1}$	1: 100	10 % goat serum or 10 % horse serum
Ani-HP1ß	1: 100	10 % goat serum or 10 % horse serum
Anti-CCN1	1: 1000	10 % goat serum
Anti-CD31	1: 200	10 % goat serum
Secondary primary antibody		
Anti-vimentin	1: 50	10 % goat serum
Anti-PDFRα	1: 200	10 % horse serum

Anti- CD31	1: 200	10 % goat serum
Anti-troponinT	1: 500	10 % goat serum
Anti-smooth muscle actin	1: 200	10 % goat serum
Secondary antibody		
Anti-mouse-Alexa 488	1: 400	PBS
Anti-rabbit-Alexa 594	1: 400	PBS
Anti-chicken-Alexa 488	1: 400	PBS
Anti goat-Alexa 488	1: 400	PBS
Anti-rat-Alexa 488	1: 400	PBS

3.3 Virus production

3.3.1 Adeno-associated virus serotype 9 (AAV9)

Within this study, three virus types of adeno-associated viruses have been obtained: AAV9-CCN1 and AAV9-CCN1-DN and AAV9-dsred.

HEK293T/17 cells were cultivated in HEK medium. The amount of 15 cm dishes needed for the triple flask was calculated as follows: The amount of triple flasks wanted by 3 and divided by 2.5 ((x TFs x3)/2.5). Usually, five triple flasks per condition with three conditions were produced, so 18 15 cm dishes were grown up to 90-100% confluency and transferred into 15 triple flasks. For this, the medium was removed, cells washed with PBS and Trypsin added for 5 minutes. Then, the solution was taken up in HEK medium and cells of 6 dishes pooled in 1 DMEM (HEK medium) medium bottle with 500 ml in total. 100 ml of each flask were then put into one 75 cm triple flask and cultured for one day. The next day, the cells were transfected with the virus producing plasmid (AAV9-CCN1 or AAV9-DM backbone vector) as well as one helper plasmid Pdp9. 35 µg of the vector and 120 ug of pdp9 and 310 µl of the transfection reagent PEI were used for transfection of a triple flask. Since one vector or condition was pooled for five triple flasks, the transfection mix was calculated as follows:

Mix 1 and 2 were vortexed and incubated for 15 minutes at room temperature before added to the prewarmed HEK medium. 60 ml of total mix per condition were added to one 500 ml bottle. The medium of the HEK cells was removed by decanting carefully. 100 ml of the new medium together with the transfection mix was added to a triple flask and incubated for 72 hours. Then, the cells were harvested by shaking the triple flasks roughly and putting the

medium with the cells into a 500 ml conical centrifuge bucket. 50 ml of PBS were added to the triple flasks to remove remaining cells by shaking vigorously and adding them to the centrifuge bucket. Five triple flasks of one condition were pooled into two buckets and spinned down at 1000 rpm (220 g) (Beckmann, Germany), 4 °C and 15 minutes before resolving the pellets of one condition in 50 ml of PBS in a 50 ml tube. After a second centrifugation step at 220 g, 4 °C and 15 minutes, the pellet was mixed with 3 ml of AAV9 lysis buffer and stored at -80 °C. To lyse the cells, the lysate was incubated at 37 °C for 15 minutes before freezing in liquid nitrogen for 15 minutes. This cycle was repeated 3 times before storing the lysed cells at -80 °C or continuing with the purification procedure by adding 0.5 µl of benzonase per 1 ml lysate and incubation at 37 °C for 30 minutes. The solution was centrifuged at 3000 g for 15 minutes and 4 °C. The virus containing supernatant was added to the iodixanol gradient in a quick seal tube in following order:

1. AAV9 lysate: around 4 ml
2. 15 % Iodixanol (2 ml)
3. 25 % Iodixanol (2 ml)
4. 40 % Iodixanol (2ml)
5. 60 % Iodixanol (2 ml)

Importantly, the solutions had to be added without any air bubbles in between. Afterwards, the tubes were balanced with a difference smaller than 0.01 g and sealed (Quick seal Cordless Tube Tupper kit 50 HZ, Germany) prior centrifugation with an ultracentrifuge (Beckman, Germany) in a 75Ti Rotor at4°C, at 60000 rpm and 2 hours. Afterwards, the tubes were fixed and two needles inserted, one on the top and one with a syringe in the 40 % iodixanol to suck off the virus containing solution, which was transferred into a sterile cry vial and stored at 4 °C or for long term at -80 °C. To determine the virus titer, a quantitative PCR was performed. Therefore, 10 µl of virus containing solution, 10 µl of TE buffer and 20 µl 2M NaOH were mixed and incubated at 56 °C for 30 minutes while shaking at 1000 rpm. Then, 960 µl of 40 mM HCl were added to the virus lysate and used for a titration PCR as shown in table 2. For determination of the concentration, viral DNA standards were used for each PCR as shown in table 3, to perform a concentration standard curve.

Table 2: qPCR reaction for AAV9 titration

Component	Volume	Final concentration
Virus lysate or plasmid standard	1 µl	x µg/ µl
SV40 primer mix	1 µl	5 pM
SYBR Green Master Mix	12.5 µl	
H_2O bidest	10.5 µl	

Table 3: qPCR program for AAV9 titration

Reaction step	Temperature	Time	
Initial denaturation	95°C	10 min	
Denaturation	95°C	15 sec	**40x**
Elongation	60°C	1 min	

Typical viral concentrations ranged from 5x10^12 to 1x10^13 viral particles per milliliter solution. For adult tail vein injections, 2x10^12 virus particles were used. Before large scale production of AAV9-CCN1 and AAV9-CCN1-DN was performed, pilot studies with protein expression level validation have been validated.

dilution 1/x	Ct	copies/ml
Standard 8		
Standard 9	26.42	1.00E+09
Standard 10	23.40	1.00E+10
Standard 11	20.02	1.00E+11
Standard 12	15.69	1.00E+12
Standard 13	11.60	1.00E+13
dsAAV9-CMV-dsRed DR	12.18	8.51E+12
dsAAV9-CMV-dsRed 1	11.75	1.11E+13
dsAAV9-CMV-dsRed 2	12.86	5.61E+12
dsAAV9-CCN1 1	13.88	2.99E+12
dsAAV9-CCN1 2	14.69	1.82E+12
dsAAV9-CCN1 DM 1	16.09	7.74E+11
dsAAV9-CCN1 DM 2	12.96	5.28E+12
dsAAV9-CCN1 DM 3	13.20	4.54E+12
dsAAV9-CCN1 DM 4	14.0717	2.66E+12

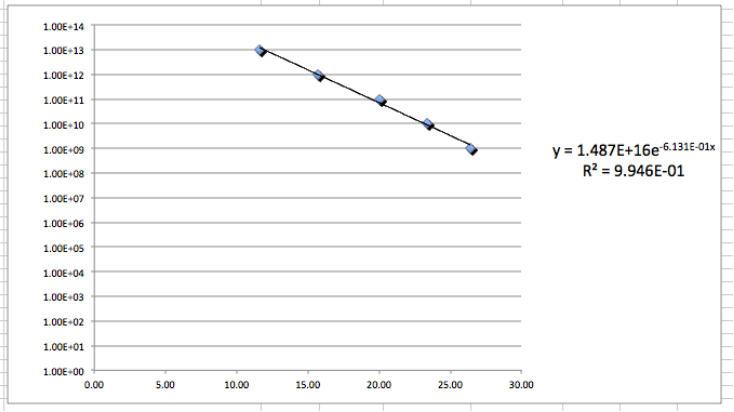

Figure M1: Example of a standard AAV9 titration curve. Evaluation of the AAV9 titer by implementing the formula of the standard curve as shown above.

3.3.2 Adenovirus production

Within this study, two adenoviral vectors were produced: pAd-CCN1 and pAd CCN1-DN with the viral backbone plasmid pAd-CMV-V5-DEST.

First, around 30 µg of the vector DNA for adenovirus production were digested with PacI before precipitating with 0.1 volume of 3 M sodium acetate and 100 % Ethanol at -80 °C for 15 minutes. Then, the DNA was pelleted by spinning at 13000 rpm and 4 °C for 10 minutes. The DNA was washed once with 500 µl 70 % ethanol and centrifugation prior to resolving in 20-30 µl water. The linearized DNA was transfected into the HEK293 cell line. The transfection was conducted with Lipofectamine 2000. For this, a confluent 6 cm dish was transfected with 3-5 µg of DNA using two mixtures as shown below:

Mix 1: X µl DNA + 250 µl Optimem

Mix 2: 10 µl Lipofectamine2000 + 250 µl Optimem

Mix 1 and Mix 2 were put together and incubated for 20 minutes at RT before adding the solution to the cells growing in antibiotic free HEK culture medium. After one day, the medium was exchanged by HEK culture medium. Around 10-13 days post transfection, the cythopathic effect of the evolving adenoviruses was observed. When 80 % of the cells had a roundish shape, the virus was harvested by pipetting the cell suspension up and down and

transferring it into a 15 ml falcon tube. The virus containing cells were centrifuged at 850 g, 4 °C for 10 minutes. The pellet was taken up in 1 ml 10 mM Tris solution, frozen in liquid nitrogen and thawed at 37 °C to lyse the cells and release the virus. This was repeated 3 times before cell debris were removed by centrifugation at 850 g, 4 °C for 10 minutes. The virus containing supernatant was aliquoted and stored at -80 °C. For the second and third amplification step, 500 µl of the virus was used to infect a confluent 10 cm dish with HEK293 cells and after observing 80-90 % cytopathic effect, the virus was harvested as described before. After the third amplification step, the virus was aliquoted and used for experiments after performing the titration step. For titering the adenoviruses, HEK293 cells were seeded in a 12 well plate. The virus was prepared in serial dilutions and 100 µl of the dilution was added to each well and incubated for 48 hours at 37 °C and 5 % CO_2. Then, the medium was removed and 1 ml ice cold 100 % methanol was added gently to the cells and the cells were incubated at -20 °C for 10 minutes. The cells were washed with washing solution and anti-hexon antibody (1:1000) was added for 1 hour at 37 °C. The cells were washed with washing solution for 3 times and the secondary rat-anti-mouse antibody (1:500) was added and incubated for 1 hour at 37 °C. The DAB detecting solution was added for 10 minutes at room temperature before aspirating the solution and adding PBS. The brown cells were counted as positive cells and the infection units per milliliter or ifu calculated as follows:

$$\frac{\text{(infected cells/ field) x (fields/ well)}}{\text{volume virus (ml) x (dilution factor)}}$$

The desired ifu was determined as follows:

$$\frac{\text{Cell number (cells) x ifu wanted}}{\text{Ifu (ifu/ ml)}}$$

3.4 Cell culture

3.4.1 HEK293T cultivation

293 cells were mainly used for AAV9 production. For this, freshly thawed cells were incubated in HEK293 medium in a 15 cm dish (Sarstedt, Nürnbrecht, Germany) and cultivated until the cell layer was confluent. Then, the cells were passaged by removing the culture medium, washing once with PBS and adding 0.05 % 5 ml Trypsin-EDTA (Life Technologies, Darmstadt, Germany) for 3-5 minutes at 37 °C, 5 % CO_2. When the cells were detached from the dish, which was controlled by microscopy, they were taken up with around

5 ml of medium. Then, a centrifugation step at 250 g and 5 minutes at room temperature followed. The supernatant was discarded and the pelleted cells were resuspended in 10 ml medium, and 1 ml was added to maximum 10 new cell culture dishes. The dishes were incubated at 37 °C until the cell layer was confluent and split or transferred into triple flasks for virus production.

3.4.2 NRCM and NRCF isolation and cultivation

The hearts of newborn rats were isolated by cutting off the head, opening the chest and taking out the organ. The hearts were transferred into a 50 ml falcon tube with CBFHH solution on ice. Then, they were put into a 10 cm dish filled with CBFHH and the atria were cut off. After the ventricles were transferred into another 6 cm dish with CBFHH and cleaned from blood, they were cut into small pieces. 10 ml of trypsin solution was added. 5 ml of the solution were put into two bakers and continuously stirred by a magnetic stirrer for 15 minutes at room temperature for 2 times after adding 10 ml trypsin solution and discarding the supernatant in between. Finally, 15 ml were added to the digesting hearts and the solution was stirred for 10 minutes. Next, the solution was mixed by pipetting up and down and the supernatant transferred into 7.5 ml FCS solution. The tube was centrifuged at 800 g for 10 minutes at room temperature, the supernatant discarded and preplating medium was added to the cell pellet. The cell suspension was added onto a 40 µm cell strainer into a 50 ml falcon tube and diluted continuously by adding preplating medium (10 ml medium per 5 hearts). The filtrate was put into 10 cm dishes and incubated for 1 hour at 37 °C and 1 % CO_2. The NRCFs adhered to the cell dish, and the myocytes were still in the suspension, which was transferred into a new falcon and 10 µl, mixed with 10 µl of trypan blue were used to count the cells and validate the cell viability. The remaining suspension was used for cultivation. Depending on the cell number, the desired concentration of 700 000 cells per well was generated with NRCM culture medium and put into a 12 well plate and cultivated at 37 °C and 1 % CO_2. Meanwhile, the dishes with the fibroblasts were washed 3 times with 10 ml PBS and shaking at 37 °C, 100 rounds per minute for 5-10 minutes. Finally, 10 % NRCF medium was put to the cells, which were incubated at 37 °C and 1 % CO_2. NRCFs were grown until the dish was confluent.

Cultivation and medium transfer of NRCM and NRCF for senescence induction in NRCF

To induce senescence in NRCFs, the NRCMs were cultured in a 12 well plate for 1 day. The following day, the medium was discarded and the cells were washed three times with NRCM medium to remove dead cells. Finally, 1 ml Penicillin free 1 % NRCM medium was added and the cells were infected with the adenoviral constructs pAd-CCN1, pAd-CCN-DN with an ifu of 300 (reaching 15-30 fold overexpression of CCN1 and CCN1-DN compared to mock) and mock (PBS only). The cells were incubated for 24 hours over night at 37 °C and 1 % CO_2. The medium was removed and cells washed 3 times with culture medium and finally 500 µl of 1 % NRCM medium was added per well. The cells were incubated for 3 days before the first medium transfer took place. Meanwhile, the NRCFs were passaged one day before medium transfer and seeded in a 96 well plate with 5000 cells per well and triplicates for each condition with 5 % NRCF medium. In addition, 50 000 cells per well in a 6 well plate were seeded with 5 % NRCF medium. The medium transfer was done by removing and pooling the medium of each condition (usually 4 wells of a 12 well plate with 500 µl / well) and adding 500 µl fresh 1 % NRCM medium to the wells. The medium of the NRCF plates was discarded and the conditioned medium of the NRCM was added, and 1 ml was put onto the well of a 6 well plate (one per condition) and 200 µl in a well of a 96 well plate (3 per condition) and cultivation continued. A medium transfer was done after 2 days and 5 days (see timeline at **Fig. M2**) before the 6 well plate was washed with PBS once and then directly frozen at -80 °C for mRNA analysis and the 96 well plate investigated for SA-ß-Gal expression.

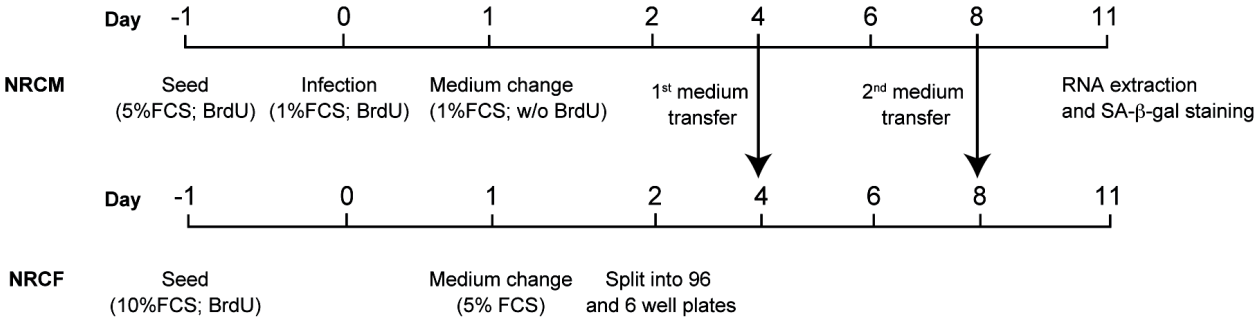

Figure M2: Experimental scheme for senescence induction in CF *in vitro*.

3.4.3 AMCM and ARCF isolation and cultivation

Before starting the procedure, all the buffers were prepared freshly. Afterwards, ketonhydrochloride was thawed and the Langendorf perfusion system prepared. Then, the self made yellow cannula was put on a 1 ml syringe and filled with perfusion buffer (without bubbles) and fixed with the clue in a 6 cm dish underneath the stereo magnifier. Then, the mouse was heparinized intraperitoneally with 0.05 µl heparin and 0.15 ml NaCl for 5 min. Around 800 µl ketonhydrochloride was intraperitoneally applied. When the mouse was narcotised completely (which was controlled by pinching heavily the toes), the chest was cleaned with 70 % ethanol, opened and the heart cut out and transferred into a 6 cm dish filled with perfusion buffer. Then, the blood was removed by slightly pressing the heart for several times. Afterwards, the aorta was attached to the cannula and fixed with a thread. Then, the perfusion buffer in the syringe was pulled through the heart to clean it from the remaining blood. The cannula with the heart was attached to the perfusion system, which was turned on for 2 minutes with a flow rate of 4x10. Then, the digestion system was turned on with a flow rate of 4x10 for 6-10 minutes, depending on the digestion condition of the heart. When the heart became fluffy and loose, it was transferred into a 6 cm dish with perfusion buffer and released from the atria and fat. The ventricles were put into approximately 2.5 ml digestion buffer in a beaker and cut into small pieces. To singularize the cells, the solution was pulled up and down with a 1 ml syringe for approximately 40 times. Then, 2.5 ml of P1 buffer were added and the solution was pulled up and down for around 20 times prior adding the solution to a 100 µm cell strainer and filtering it in a 50 ml falcon. Finally, the cells were transferred into a 15 ml falcon and incubated for 10 minutes at 37 °C, after validating the quality of the preparation by putting 100-200 µl onto a glass slide under a bright field microscope. After sedimentation of the cardiomyocytes, the supernatant was spinned down at 55 g for 5 min and the supernatant transferred into a new 15 ml falcon for cardiac fibroblast isolation. For this, the supernatant was spinned down at 220 g for 5 minutes and the pellet mixed with 10 ml of 10 % NRCF medium, put onto a 10 cm dish and incubated for two hours at 37 °C and 5 % CO_2. The sediment and pellet was pooled in 10 ml P2 and transferred into a 25 ml canonical flask for calcium reconstitution. Subsequently, calcium chloride with rising concentrations was added to the myocytes in following order: 50 µl of 10 mM $CaCl_2$ for 4 minutes, 50 µl of 10 mM $CaCl_2$ for 4 minutes, 100 µl of 10 mM $CaCl_2$ for 4 minutes, 30 µl of 100 mM $CaCl_2$ for 4 min and finally 50 µl of 100 mM $CaCl_2$. The solution was put into a 15 ml falcon and incubated for 10 minutes at 37 °C for sedimentation before spinning at 55 g for 5 minutes. The sediment and pellet was pooled in 10 ml of AMCM plating medium and put onto a 10 cm dish at 37 °C and 5 % CO_2 for two hours. After two

hours, the cardiomyocytes and cardiofibroblasts were washed twice with PBS and frozen at -80 °C. RNA or protein isolation followed.

3.5 Protein methods

3.5.1 Protein isolation from tissue and cells

To isolate proteins from tissues and cells, the cell signaling cell lysis buffer has been used and protease and phosphatase inhibitors were added freshly by putting a tablet or soluble inhibitors as shown below.

Table 4: Protease and phosphatase inhibitor concentrations

Reagent	Stock concentration	Final concentration
DTT	100 mM	1 mM
NaF	500 mM	12.5 mM
Na_3VO_4	100 mM	1 mM
PAO	40 mM	400 µM
PMSF	0.5 M	1 mM
Leupeptin	25 mg/ml	10 µg/ml
Antipain	25 mg/ml	10 µg/ml

One tablet was added to 10 ml of lysis buffer solution.

The complete lysis buffer was added to the tissue (500-800 µl) or to the cell dish (100-500 µl). The tissue was homogenized using the turrax machine and the cells were scraped from the dish using an appropriate cell scraper and pipetting up and down and finally putting the lysate into an 1.5 ml reaction tube. The solution was incubated on ice for 10-20 min and vortexed in between to lyse the cells. After this, the lysate was incubated in an ice-cooled ultrasound bath for 10-15 min. The final centrifugation step at 14000 rpm, 4 °C and 10 min isolated the proteins in the upper phase from the cell compartments left in the pellet. The protein containing supernatant was put into a new tube and protein concentration was determined.

Protein concentration measurement with the Bradford assay

In general, 2 µl of the protein sample was transferred into 1 ml of 1x Bradford solution. Then, 200 µl were put into 3 wells of a 96 well plate and absorbance was measured at 595 nm. The mean of the values was transferred into an excel sheet with a protein standard curve generated before (with protein solutions of known concentration) thus calculating the concentration of the sample.

3.5.2 SDS Polyacrylamide gel electrophoresis (SDS-PAGE)

Preparation of an SDS gel

An SDS gel matrix consists of linearized polymerized acrylamide cross-linked by N,N'-Methyl-Bisacrylamide. The polymerization is induced by ammoniumpersulfate and catalyzed by N,N,N',N'-tetramethylethylendiamine (TEMED). The matrix pore size and thereby the separation properties depend on the concentration of the acrylamide and bisacrylamide. For this work, only discontinuous gel systems were used, thus containing 2 different gel matrixes, the upper and lower gel with discontinuous pH values of the gel buffers and the running buffer. Depending on the size of the analyzed protein, an appropriate gel matrix concentration was used (see table 5).

8 %, 10 %, 12 % and 14 % SDS gel matrices were used. Thus, the upper and the lower gel buffers were made in 50 ml and 15 ml falcon tubes as shown below:

Table 5: Separation range of proteins

Gel percentage	Optimal separation range of proteins [kDa]
8	50- 500
10	20- 300
12	10- 200
14	5- 100

After this, APS and TEMED were given to the lower buffer and the solution was transferred between two fixed glass plates with 1 mm distance in between (Mini PROTEAN® System, BIO-RAD, München, Germany). Water served as a cover until the gel polymerized after about 20 min. Then, APS and TEMED were added to the upper buffer and the solution put

above the lower gel. A chamber comb (BIO-RAD, München, Germany) was put into the solution, which then polymerized within about 15 min. The gel was ready to use for electrophoresis or could be stored for several days at 4 °C.

Protein sample preparation

The Bradford assay was performed to load always 40 ug protein of each sample. The samples were mixed with 1-2 µl 4x LAEMMLI buffer and then boiled for 10 min at 99 °C. After a short centrifugation step, the samples were cooled down and ready to use.

Gel electrophoresis

The gel was put into the gel chambers with running buffer. The protein marker and protein samples were carefully transferred into the pockets of the upper gel. The electrical field was applied having a current of 25 mA while the samples ran through the upper gel, and 35 mA for the lower gel. The run was stopped when the blue protein running front reached the end of the separating gel.

3.5.3 Western Blot (Immunoblot)

Ponceau S staining

The protein transfer to the PVDF membrane was verified by Ponceau S staining.
The membrane was incubated with Ponceau S solution on a shaker for 10 min at room temperature. Red staining was reversed by washing with water for 5 min and then continued with the Immunoblot.

Immunological detection of the proteins

Before putting the specific antibody onto the membrane, unspecific binding sites were masked with blocking buffer, either BSA or non-fat dry milk powder. Blocking was carried out on a shaker at room temperature for 3- 5 hours. After that, the membrane was incubated with the specific antibody over night at 4 °C. The antibody was diluted in 5 % BSA and 0.02 % sodiumacide. For primary antibodies the following dilutions were used:

Table 6: Antibody dilution

Primary antibody	dilution
Anti-HSP90	1: 5000
Anti-CCN1	1: 1000
Anti-p53	1: 1000
Anti-p16 ^{INK4a}	1: 1000
Secondary antibody	
Anti-mouse	1: 10000
Anti-rabbit	1: 10000

Afterwards, the membrane was washed with PBST several times for approximately 1 hour. Then, the secondary antibody was added in PBST in a dilution of 1:10 000 for 1 hour at room temperature. The blot was washed several times for about 1 hour. The secondary antibody, obtained from mouse or rabbit, is coupled to a horseradish peroxidase. This enzyme catalyzes the oxidation of chromogenic substrates which are then spectrophotometrically detectable. The membrane was incubated with ECL Plus (Life Technologies, Darmstadt, Germany), which was then detected with a photometer equipped with an integrated camera (LAS 4000 Mini, Fujifilm, Düsseldorf, Germany). The intensity of the protein bands is directly proportional to the protein amount, which was measured and analyzed with a special software (Multi Gauge Software; Fujifilm, Düsseldorf, Germany).

3.6 Bacteria work

3.6.1 DNA transformation in bacteria

50 µl of the electrocompetent DH10B, SURE or Stabl2 bacteria were thawed on ice. 2 µl of the ligation or 100 ng of plasmid DNA were added and transferred into the pre-chilled cuvette (Gene Pulser®, BIO-RAD, München, Germany) and stimulated with a short 1.8 kV pulse with a gene pulser (Micro-Pulser®, BIO-RAD, München, Germany). Afterwards, 500 µl LB medium were added and the bacteria cultured at 37 °C for 45 min until 1 hour in a thermo shaker. The suspension was then transferred onto agar plates with an appropriate selection antibiotic (ampicillin: 100 µg/ ml; kanamycin: 33 µg/ml) and incubated overnight at 37 °C. The grown colonies were used for further DNA amplification in small or large scale production. For a small scale production, only one clone was put into 4 ml of LB medium (minipreparation) with selection antibiotics and cultured over night. After isolating the pure plasmid and sequencing

the DNA, a part of the solution was taken for large scale production in 100 ml (midipreparation), 500 ml (Maxipreparation) LB medium or 2000 ml (giga preparation) TB medium with antibiotics and grown over night.

3.6.2 Plasmid purification

After amplifying the plasmid DNA in bacteria, it had to be purified from genomic DNA, proteins, ribosomes and other bacterial components. For this purpose Life technology kits were used (PureLink® Quick Plasmid Miniprep Kit; Darmstadt, Germany; Life Technologies PureLink^{tm} HiPure Plasmid Midi- / Maxi prep Kit, Life Technologies, Darmstadt, Germany; PureLink HiPure Plasmid DNA Gigaprep Kits, Life Technologies, Darmstadt, Germany). In general, the bacteria were pelleted by centrifugation at 4000 g for 15 min and 4 °C to remove the LB or TB medium. Then, the bacteria were resuspended in the resuspension buffer (with RNase) and the cells lysed with an instructed lysis buffer. Meanwhile, the DNA capturing columns were equilibrated by putting the equilibration buffer on the filtration cartridge. Afterwards, the lysed bacterial suspension was mixed with precipitation buffer to bind and modify the plasmid DNA. The solution was added to the column and spinned down. The lysate passed through the pre-packed anion exchange column where the negatively charged phosphates of the DNA backbone interacted with the positive charges on the surface of the resin. Afterwards, 2 washing steps removed RNA, proteins, carbohydrates and other impurities. The plasmid DNA was eluted by putting the high salt elution buffer to the column and spinned down. The DNA precipitation was performed by incubation with isopropanol and followed centrifugation at 12000 g, for 30 min at 4 °C. The DNA pellet was washed twice with 75 % EtOH and then resuspended in 300-500 µl water. The concentration was measured with a Nanodrop spektrophotometer ND 1000 (Peqlab, Erlangen, Germany).

3.7 DNA methods

3.7.1 Polymerase chain reaction (PCR)

PCR was used to genotype mouse lines and for cloning purposes. For genotyping, a specific part of the genomic DNA (gDNA) was amplified after isolation from the mouse tail tip (see 3.1.2). For cloning, the complementary DNA (cDNA), obtained by an RT reaction or a plasmid was amplified. A PCR reaction was carried out as shown in table 7 and table 9 with the reaction times and temperatures taking place in a thermo cycler (Master cycler,

Eppendorf, Hamburg, Germany or Biometra, Göttingen; Germany) as shown in table 8 and table 10.

Table 7: PCR reaction for cloning purpose:

Component	Volume	Final concentration
10xreaction buffer (including dNTPs)	5 µl	1x
5'-Primer forward	1 µl	0.5 pmol/ µl
3'-Primer reverse	1 µl	0.5 pmol/ µl
Template cDNA	1- 5 µl	20 ng/ µl
DNA Polymerase (Accu Prime Pfx)	1.2 µl	0. 12 U/ µl
H_2O bidest	ad 50 µl	

Table 8: Typical PCR program for cloning purpose

Reaction step	Temperature	Time	
Denaturation	95 °C	12 min	
Denaturation	95 °C	15 sec	**35-40x**
Annealing	62 °C	30 sec	
Extension	68 °C	2 min	
Denaturation	95 °C	2 min	
Extension	68 °C	1 min 30 sec	

Table 9: PCR reaction for genotyping purpose:

Component	Volume	Final concentration
10x reaction buffer	2 µl	1x
dNTPs (10mM)	0.4 µl	0.2 mmol/l each
($MgCl_2$ 50mM)	0.6 µl	1.5 mmol/l
5'-Primer forward	1 µl	0.5 pmol/ µl
3'-Primer reverse	1 µl	0.5 pmol/ µl
Template gDNA	1- 5 µl	2 ng/ µl
DNA Polymerase (Taq)	0.08	0.02 U/ µl
H_2O bidest	ad 20 µl	

Table 10: Typical PCR program for genotyping purpose

Reaction step	Temperature	Time	
Denaturation	94 °C	2 min	
Denaturation	94 °C	1 min	**30-40x**
Annealing	depending on primer	0,5 -1 min	
Extension	72 °C	1 min	
Last Extension	72 °C	3 min	

3.7.2 Agarose gel electrophoresis

Preparation of an agarose gel

Depending on the desired gel density (1-2 % w/v), 1-2 grams of agarose were put into 100 ml 1x TAE buffer, mixed and boiled until the powder was dissolved completely. After cooling down the solution, ethidiumbromide was added. The solution was filled into a gel carrier equipped with a gel comb and cooled down for polymerizing. The gel carrier was put into an electrophoresis chamber connected to a gel power supply.

Table 11: Separation of DNA fragments according to their size

Agarose concentration [% w/v]	Optimal separation range of linear, double stranded DNA fragments [kbp]
0.3	5- 60
0.6	1- 20
0.7	0.8- 10
0.9	0.5- 7
1.2	0.4- 6
1.5	0.2- 3
2.0	0.1- 2

Electrophoresis

The DNA samples were mixed with DNA loading buffer to increase the mass density of the sample. At the same time, DNA marker was put into the pocket to identify DNA molecules by their size. An electrical field was employed with 120-130 Volts and 400 mA for 30-45 minutes. The DNA visualization was carried out with a gel documentation system (UV-light at λ= 254-366 nm,) and light was emitted at the orange-red range (590 nm). For analysis, the detection was carried out at energetic short wave UV (λ = 254 nm), for cloning purposes, the visualization was carried out at low energetic long wave (λ= 366 nm) detection. In the latter case, the DNA was extracted out of the gel.

DNA gel extraction

After electrophoresis and visualization, the DNA was isolated with the *QiaQuick Gel Extraction Kit* (Qiagen, Venlo, NL) prior using it for further experiments. The DNA fragment of the desired size was cut out of the gel with a scalpel and transferred into a 1.5 ml reaction tube. The gel piece was weighted and 300 µl of buffer QG was added to 100 mg gel. The tube was vortexed and incubated at 50 °C for around 10 minutes until the gel was dissolved. One gel volume isopropanol was added to the solution and mixed. A QIAquick spin column was placed into a 2 ml tube, the gel solution transferred onto the column and spinned down at 18000 g for one minute. The flow-through was discarded, 500 µl buffer QG was added and spinned again. 750 µl buffer PE was applied to the column, spinned down and the flow through discarded. A final centrifugation step followed to remove the remaining solution. For

DNA elution, the column was placed into a new 1.5 ml centrifuge tube, 30 µl buffer EB added, incubated for two to three minutes and spinned down. The concentration of the isolated DNA was measured.

3.7.3 DNA restriction

A restriction reaction is shown in table 12 and performed at 37 °C for 3 hours. The result was analyzed with gel electrophoresis.

Table 12: Standard restriction reaction

Component	Volume	Final concentration
Restriction enzyme 1	1- 2 µl	1-2 U/ µl
(Restriction enzyme 2)	1- 2 µl	1-2 U/ µl
2x Restriction buffer	2 µl	1x
DNA	0.5- 5 µl	0,025- 0,1µg/µl
H_2O bidest	ad 20 µl	

3.7.4 DNA ligation

DNA ligation was exclusively performed with the Gateway cloning system to produce the destination vectors for AAV9 and adenoviruses

Gateway cloning

Mouse CCN1 cDNA (PubMed #NM_010516.2) has been amplified with attB containing primer from cDNA after an RT reaction (generated according to the manual) of RNA isolated from p16 ^{INK4a} and p53 wild type mice. The CCN1-DN cDNA was amplified with attB containing primer (generated according to the manual) from a plasmid including the desired mutation, obtained from Prof. Lau (University of Illinois, Chicago, USA). After amplification, the cDNA was mixed with DNA loading dye and loaded on a gel. A 1200 bp band was extracted and purified. 100 femtomoles of the cDNA was used for the following BP reaction to introduce CCN1 or CCN1-DN cDNA into the gateway entry vector pDONR. The BP reaction was carried out as shown in table 13 and the PCR product was the coding sequence

of CCN1 or the mutated CCN1, CCN1-DN.

Table 13: BP reaction

Component	amount
pDONR™221	150 ng
BP Clonase®	2 µl
PCR product PCR product	50 fmols
TE buffer	ad 10 µl

Afterwards, the ligation mix was transformed into bacteria and transferred on a kanamycin containing agar plate. On the next day, positive colonies were selected and grown in 4 ml of LB medium overnight. The plasmid was purified and DNA sent for sequencing. After verification of the sequence, the plasmid was used for producing the destination plasmid by an LR reaction. For this, the AAV9 destination plasmid and an adenoviral destination plasmid were used for insertion of the CCN1 or CCN1-DN cDNA out of the pDONR plasmid (pDONR-PCR product). The LR reaction was performed as shown in table 14.

Table 14: LR reaction

Component	amount
pAd/CMV/V5-DEST™ or pAAV/CMV DEST	150 ng
LR Clonase®	2 µl
pDONR-PCRproduct	50 fmols
TE buffer	ad 10 µl

After this, the reaction was transformed into the bacteria strain Sure2 and put on an ampicillin containing agar plate. The next day, positive colonies were selected and grown in a mini culture setting over night. The following day, the DNA was isolated and sent for sequencing. After verification of the sequence, the plasmid was amplified by taking 1 ml of the mini culture and transferring it into 400 ml of LB medium followed by incubation over night. The following day, the plasmid was isolated and used for adenovirus production (3.3.2) or AAV9 production (see 3.3.1).

3.7.5 DNA concentration measurement

For measuring the DNA concentration, 1.5 µl of the solvent (usually EB buffer or water) were transferred onto the Nanodrop measurement device, the absorbance measured and the solution removed with a kimwipe. 1.5 µl of the sample was transferred onto the device and measured. The 260 nm absorbance, 280 nm absorbance, 230 nm absorbance, the ratio and the concentration were noted on the screen.

3.7.6 DNA sequencing

Sequencing was performed by Eurofins Genomics (Ebersberg, Germany). 2 µg of DNA were diluted in 20 µl of water, labeled and sent to the company. The primers for sequencing were ordered and stored at Eurofins and chosen for each sequencing procedure. The obtained data by Eurofins were analyzed with the program MacVector (MacVector, Cary NC, US).

3.8 RNA methods

3.8.1 RNA isolation of tissue and cells

RNA was isolated from cells or tissue using the RNAPure^{TM} reagent (Peqlab, Erlangen, Germany). For tissues, 1 ml of the reagent was added and then the tissue was homogenized by the turrax machine. For cells, 1 ml was put to the cell dish and the cells scraped from the surface with a cell scraper. The solution was transferred into a 1.5 ml reaction tube and incubated at room temperature for 5-10 min. 200 µl chloroform was added and the mixture vortexed for minimum 50 seconds until the solution turned white. After this, a 10 minute incubation step followed, where the phases started to separate and finally the tube was centrifuged at 12000 g for 10 min and 4 °C. The upper RNA containing phase was carefully transferred into a new 1.5 ml reaction tube and isopropanol was added. The precipitation of RNA was performed at 4 °C and a minimum of 10 minutes incubation time. The solution was spinned down and the Isopropanol removed from the pellet, which was washed 2 times with 75 % ethanol. The RNA pellet was dried and then resuspended in 10-100 µl RNAse free water. For concentration and quality control, the RNA was measured with a Nanodrop spektrophotometer ND 1000 (Peqlab, Erlangen, Germany).

3.8.2 RNA concentration measurement

The RNA was measured to adopt the amount of RNA for quantitative analysis, like RT-qPCR. An optical density based spectrophotometry using a Nano Drop™ spectrophotometer was used. For measuring the RNA concentration, 1.5 µl of the solvent (usually water) was transferred onto the Nanodrop measurement device, the absorbance measured and the solution removed with a kimwipe. 1.5 µl of the sample was transferred to the device and measured. The 260 nm absorbance, 280 nm absorbance and 230 nm absorbance were determined and the ratio and the concentration were ncalculated.

3.8.3 qRT- PCR

The reverse transcription- PCR is a variation of the polymerase chain reaction (see 3.7.1) to study gene expression qualitatively and quantitatively by converting the messenger RNA (mRNA) to its complementary DNA (cDNA) and quantitatively amplifying it. It can be done by a one-step or a two- step procedure.

Within this study, RT was exclusively combined with quantitative Real Time PCR (qRT-PCR) in a 2- step protocol, thus reverse transcription and qPCR were performed in two different steps. Reverse transcription is an enzymatic reaction performed by a viral reverse transcriptase. Oligo dT primers are used to bind the poly A tail of all mRNAs, which serves as the binding site for the reverse transcriptase. This enzyme produces cDNA. A typical RT reaction was conducted as shown below.

Table 15: First step (RT)

Component	**amount**	**final concentration**
RNA	x µl (100-1000 ng)	
Oligo(dT)-Primer (10 mM)	1 µl	0.83 mM
dNTPs (10 mM)	1 µl	0.83 mM
RNAse free water	ad 12 µl	
1) incubation for 5 minutes at 65 °C; 2) incubation for 2 minutes at 4 °C		
Protoscript II reaction buffer (5x)	4 µl	1x
DTT (0,1 M)	2 µl	0.0 1M
Murine RNAse Inhibitor	1 µl	2000 U/ml

ProtoScript® II Reverse Transcriptase	1 µl	10000U/ml
3) incubation for 60 minutes at 42 °C; 4) incubation for 5 minutes at 80 °C		

After the RT reaction, quantitative detectable amplification of the cDNA was performed. The principle is the same as that of a standard PCR procedure with an additional fluorophore, SYBR Green, binding the double stranded DNA. The fluorescence intensity was detected by a Real Time PCR instrument (StepOne Plus, Applied Biosystems, New Jersey, USA). The Ct value is defined as the number of cycles required for the fluorescent signal to exceed the threshold of the background fluorescence dye ROX. The calculation of the change of a target cDNA (A) compared to a reference cDNA (B) was done with the 2^-(ΔΔCt) method: ΔCt =Ct (A)-Ct (B). The Ct values are logarithmically plotted and inverse proportional to the amount of cDNA, so that Ct (A)-Ct (B) = - log N (A)- (- log N (B), which is the same as + logN (B)-log N (A) or log N (B)/N (A)). So the fold change is $2^{-(\Delta Ct(\text{mean target (A)})-\Delta Ct(\text{mean reference (B)}))}$. A typical qPCR reactions was performed as followed:

Table 16: Second step (q- PCR) reaction

Component	amount	final concentration
cDNA	2- 4 µl	8- 80 ng/ µl
Primer (20 pM)	0.25 µl	5 pM
SYBR Green Master Mix	3.75 µl- 1.75 µl	
RNAse free water	ad 12.5 µl	

Table 17: Second step (q- PCR) program

Reaction step	Temperature	Time	
Initial denaturation	95 °C	10 min	
Denaturation	95 °C	15 sec	40x
Hybridization	60 °C	1 min	
Elongation	65 °C	1 min 30 sec	
Melting curve			
	95 °C	15 sec	
	60 °C	1 min	
	95 °C	15 sec	

After PCR, a post amplification analysis was carried out to validate the reaction for specificity. For this, a melting curve was conducted after each reaction. When high temperature was applied after PCR, the double stranded, SYBR Green bound DNA products dissociate into single stranded DNA and the fluorescence change with the time is plotted against the time. Every DNA molecule has characteristic melting properties. Ideally, only one peak was observed per product.

4 Results

4.1 Accumulation of senescent cells in fibrotic heart tissue

4.1.1 Validation of the transverse aortic constriction model for heart failure and fibrosis

The transverse aortic constriction (TAC) is an extensively used small animal model system to study heart failure (Rockman et al. 1991). After an initial compensatory phase with transiently increased heart function, TAC induces chronic hemodynamic pressure overload, causing maladaptive hypertrophy and fibrosis. To figure out if cardiac fibrosis is associated with premature senescence, cardiac monitoring was performed. To evaluate cardiac disease, first hypertrophy was assessed by determining the heart weight/ tibia length ratio. After 2 and 6 weeks TAC, the heart weight/ tibia length ratio increased significantly 1.5 - 1.6 fold, due to the increase in heart weight (n = 6-16, $P < 0.001$) (**Fig. 1A**), indicating a hypertrophic response after insult. To analyze heart failure, lung weight/ tibia length ratio was measured. It increased by trend 1.2 - fold 2 weeks and 6 weeks after TAC. However, this was not significant (**Fig. 1A**). Left ventricular mass and left ventricular posterior wall (LVPV) were assessed by echocardiography and increased significantly ~ 1.5 - fold 2 and 6 weeks after TAC when compared to sham controls after surgery or to TAC animals before surgery (n = 6-9, $P < 0.001$) (**Fig. 1A)**, underlying the macroscopic observation of hypertrophy. Left ventricular internal diameter (LVID) changed significantly only 6 weeks after TAC 1.12 - fold when compared to sham animals and TAC animals before surgery (n = 6-9, $P < 0.05$, $P < 0.01$). 2 weeks after TAC no changes were observed between sham and TAC before and after surgery (sham vs. TAC after surgery: 1.0 - fold change). To measure heart function, fractional shortening was investigated for the respective groups. Fractional shortening decreased 6 weeks after TAC by 50 % (27.63 % ± 1.9 7 % for sham animals vs. 15.82 % ± 3 % for TAC animals, n = 6-9, p < 0.01). After 2 weeks of intervention, there was a significant decrease between sham and TAC animals of 25 % (33.32 % ± 3.2 % vs. 25.3 % ± 2.2 %; n = 6-9, $P < 0.05$). However, there was no reduction for TAC when compared to the groups before surgery (26.1 % ± 1.7 % and 26.3 % ± 1.1 %). To investigate fibrosis, quantitative PCR of collagen1a2 (*Col1a2*) and collagen3a1 (*Col3a1*), which are produced and secreted by fibroblasts during fibrogenesis, were analyzed. *Col1a2* is significantly higher expressed with a 1.6 - and 3.7 - fold increase in cardiac fibroblasts 2 and 6 weeks after TAC, respectively (n = 4-5, p < 0.05). Additionally, there is a significant increase of *Col1a2* expression 2 and 6 weeks after TAC in the CF fraction when compared to cardiomyocytes,

which is also already abundant in sham conditions (TAC: 12 - 15 fold increase, n = 4-5, P < 0.01, *P* < 0.001). The ratio between cardiac fibroblasts and myocytes did not change after TAC due to an increase in collagen production of the myocyte fraction. *Col3a1* is 60- fold higher expressed in fibroblasts 6 weeks after TAC when compared to cardiac myocytes after TAC (n = 4-5, *P* < 0.05) and 3 - fold when compared to cardiac fibroblasts of sham animals. (**Fig. 1B**).

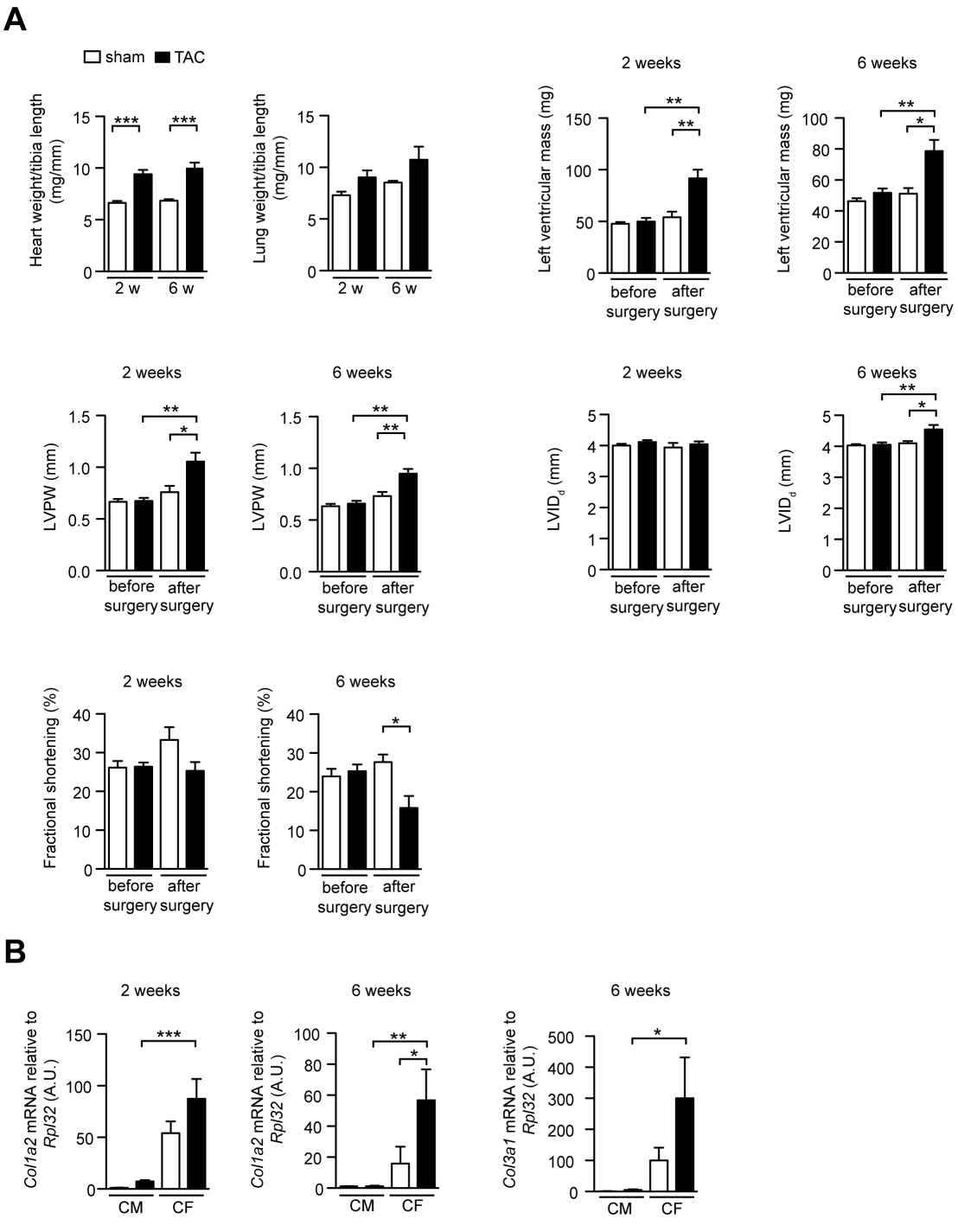

Fig. 1: Assessment of parameters for cardiac morphology, function and gene expression after TAC and sham surgery. 8-week-old male C57BL/6N mice were subjected to transverse aortic constriction (TAC; causing chronic pressure overload and fibrosis). Cardiac dimensions and function were analyzed by pulse-wave doppler echocardiography before TAC/sham surgery and before the animals were euthanized 2 and 6 weeks after surgery, respectively. (**A**) Assessment of parameters for cardiac morphology and function. Left ventricular internal diameter (LVID d/s) and left ventricular posterior wall (LVPW d/s). n = 6-9; * $P < 0.05$, ** $P < 0.01$, *** $P < 0.001$ (t-test). (**B)** Quantitative PCR analysis for collagen gene expression in freshly isolated primary CM and CF 2 or 6 weeks after TAC or sham surgery. n = 4-5; * $P < 0.05$, ** $P < 0.01$, *** $P < 0.001$ (ANOVA).

4.1.2 Senescent cells accumulate in perivascular fibrotic tissue after TAC

In TAC, fibrosis typically originates from areas surrounding the coronary arteries (perivascular regions, reactive fibrosis) and spreads throughout the myocardium. Therefore, perivascular areas were primarily investigated. Perivascular fibrosis, visualized by sirius red/fast green staining, was increased in TAC hearts when compared to sham controls 2 and 6 weeks after surgery (~ 1.7 - and ~ 1.3 - fold, respectively) (**Fig. 2A).** To detect senescent cells, heart sections were stained for a panel of senescence markers that included senescence-associated ß-galactosidase (SA-ß-gal), p16 ^{INK4a} and p21 $^{CIP1/WAF1}$. SA-ß-gal is the most established assay for senescence detection *in vitro* and *in vivo* (Collado & Serrano 2006a; Dimri et al. 1995) and based on the increased lysosomal content of senescent cells (Kurz et al. 2000). In addition, p16 ^{INK4A} and p21 $^{CIP1/WAF1}$ expression is a hallmark of senescent cells (Ohtani et al. 2004), which prevent cell cycle progression by inhibiting cyclin-dependent kinases (Sherr & Roberts 1999). TAC animals exhibited a constant increase in the expression of the senescence marker p21 $^{CIP1/WAF1}$, SA-ß-gal and p16 ^{INK4a} (2-, 8- and 20 - fold, respectively), when compared to sham controls 6 weeks after TAC (n = 5-7; $P < 0.01$) (**Fig. 2 B-D**).

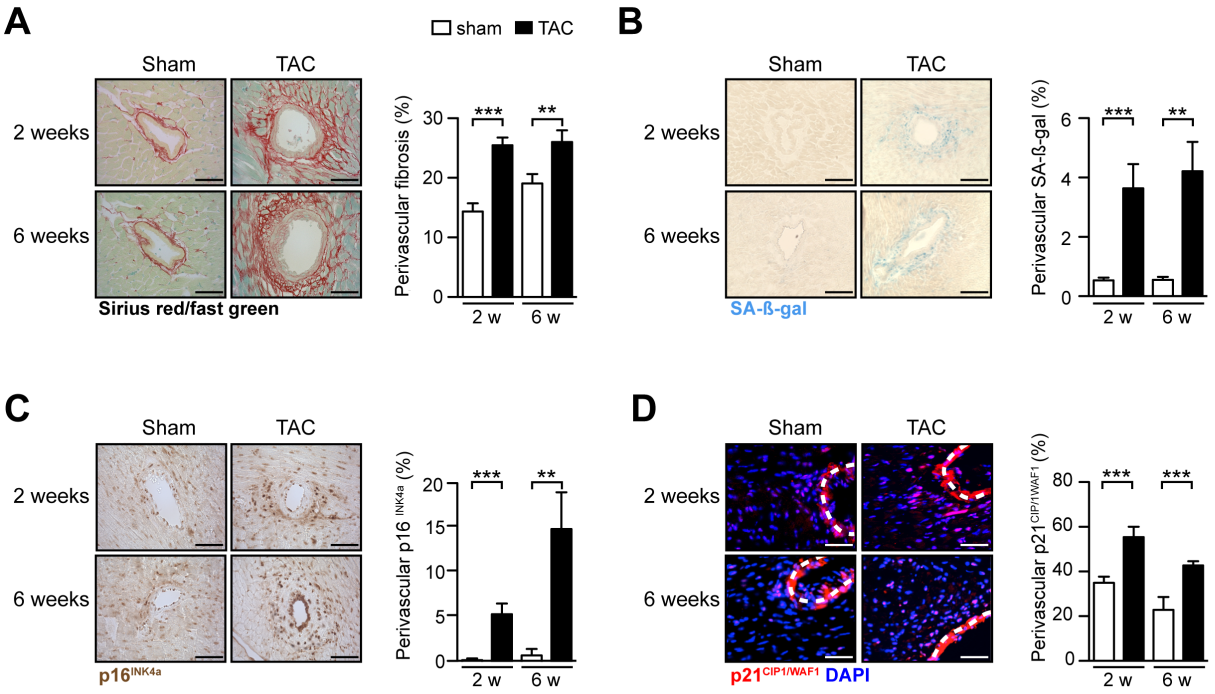

Fig. 2: Perivascular fibrosis is associated with premature senescence. Transverse aortic constriction (TAC; causing chronic pressure overload and fibrosis) or sham surgery was performed in 8-week-old male C57BL/6N mice and the degree of perivascular fibrosis and senescence examined 2 and 6 weeks after intervention. (A) Sirius red/fast green fibrosis staining and quantification. n = 12-15. * $P < 0.05$, *** $P < 0.001$ (t-test). (B) Histochemistry for Senescence-associated beta-galactosidase (SA-ß-gal). (C) Immunhistology for p16 ^{INK4a}, (D) Immunofluorescence for p21 $^{CIP1/WAF1}$ (red) and DAPI (blue). n = 5-7. * $P < 0.05$, ** $P < 0.01$, *** $P < 0.001$ (t-test). Cells were analyzed in an automated manner by pixel counting on digitized images. Scale bar = 150 µm.

To determine perivascular proliferation, KI-67 was analyzed. The percentage of perivascular KI-67-positive cells was increased 5 days after TAC when compared to sham (6.4 ± 1.1 % vs. 1.5 ± 0.4 %, n = 4-10. *** $P < 0.001$), and declined thereafter (**Fig. 3A**). To investigate which cells are proliferating, KI-67 was co-stained with the fibroblast marker vimentin and over 95 % of the KI-67 positive cells were also positive for vimentin (**Fig. 3B**). This indicates a proliferative impulse immediately after TAC-induced pressure overload (n = 3-6 , $P < 0.001$).

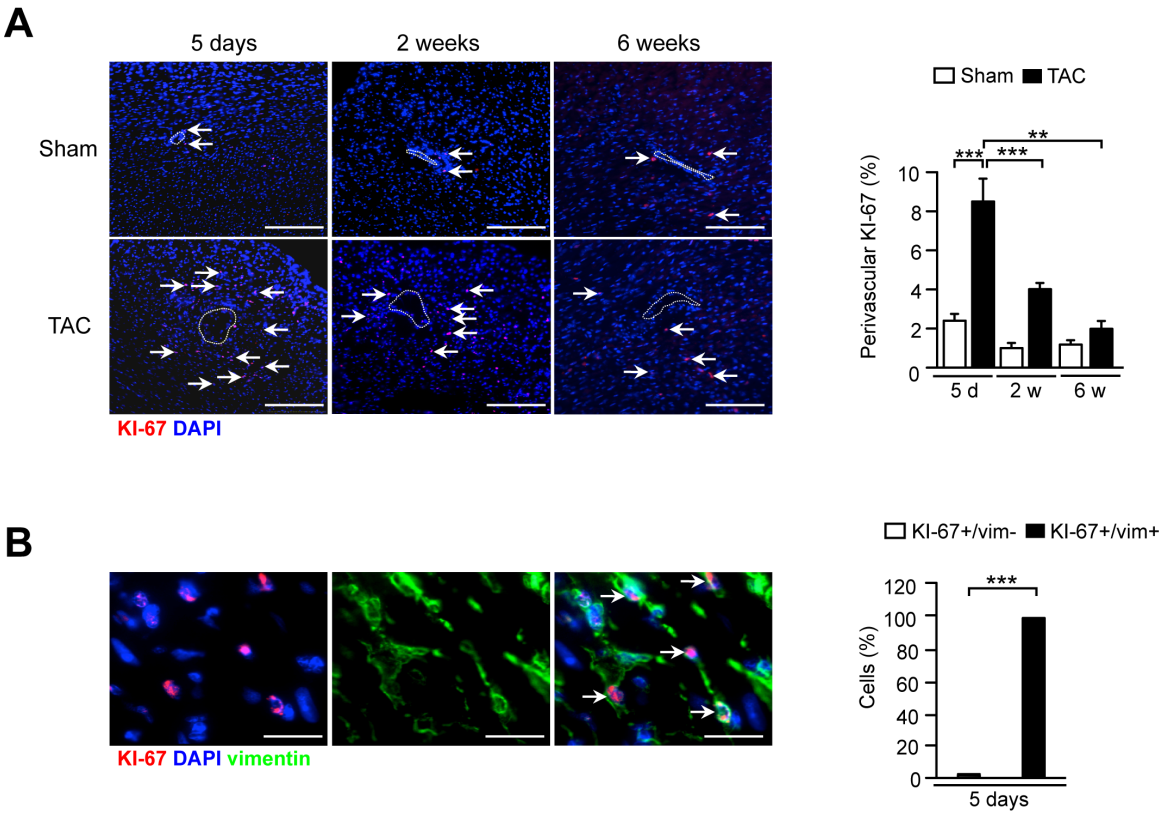

Fig. 3: Analysis of the proliferation marker KI-67 after TAC or sham surgery. 8-week-old male C57BL/6N mice were subjected to TAC or sham surgery, euthanized at week 10 and left ventricular heart sections analyzed. (**A**) Left, representative immunofluorescence image of KI-67 (red) and DAPI (blue) of heart sections at 5 days, 2 and 6 weeks after surgery. Scale bar = 200 µm. Right, quantification of perivascular KI-67 positive cells; n = 4-10. *** $P < 0.001$ (2-way ANOVA). (**B**) Left, representative immunofluorescence image of KI-67, DAPI and fibroblast marker vimentin 5 days after surgery. Scale bar = 200 µm. Right, quantification of KI-67 and vimentin positive cells. n = 3-6 *** $P < 0.001$ (t-test).

4.1.3 Validation of the ß$_1$-adrenoceptor transgenic mice for heart failure and fibrosis

The ß$_1$-adrenoceptor transgenic mice mimic the chronic overstimulation of the ß$_1$-adrenoeceptor of cardiomyocytes during heart failure leading to progressive cardiomyocyte hypertrophy, apoptosis and thereby to interstitial fibrosis (Engelhardt et al. 1999). Heart failure and fibrosis progress over time and with the age. To verify the ß$_1$-adrenoceptor transgenic mouse model (referred to as “TG”, and the wild type littermates are referred to as “WT”) as a valid disease model for studying senescence, macroscopic cardiac monitoring and fibrosis analysis were performed at the age of 2.5, 5 and 10 months. The heart weight/ tibia length ratio was not different in transgenic animals, although heart failure progressed extensively. 10 months old transgenic animals did not show an increase in heart weight/ tibia length ratio when compared to 5 months or 2.5 months old transgenic mice (5 months vs. 2.5 months: 0.9 - fold; 10 months vs. 5 months: 1.06 - fold; 10 months vs. 2.5 months: 0.87 - fold;

n = 4-9, *P* < 0.01) (**Fig 4**). Hypertrophy also did not differ at any time point between wild type and transgenic animals (2.5 months, WT vs. TG: 0.96 - fold; 5 months WT vs. TG: 1.06 - fold; 10 months WT vs. TG: 0.87 – fold, 4-9). A significant physiological hypertrophy was observed between 10 months old and 2.5 months old wild type mice, and also between 5 months compared to 10 months old wild type animals (5 months vs. 2.5 months: 1.18 - fold, n = 4-9, *P* < 0.05; 10 months vs. 5 months: 1.1 - fold; 10 months vs. 2.5 months: 1.3 - fold, n = 4-9, *P* < 0-01). Concerning the significant physiological hypertrophy in WT animals and the fact that chronic stimulation of the adrenergic system in the heart leads to cardiomyocyte apoptosis (Engelhardt et al., 1999), no differences in heart weight/ tibia length ratios between transgenic mice and age matched wild type littermates were observed at any time point or in between the transgenic group at 10 months of age compared to 5 or 2.5 months of age. The lung weight/ tibia length ratios increased by trend between transgenic mice and wild type littermates at an age of 2.5 months, but were the same for older transgenic mice and their wild type littermates (2.5 months, WT vs. TG: 1.16 - fold; 5 months WT vs. TG: 1.06 - fold; 10 months WT vs. TG: 1.04 - fold) (**Fig 4)**. To address fibrosis, a quantitative PCR analysis of the *Col1a2* gene in isolated cardiac myocytes and fibroblasts of 5 and 10 months old mice was performed, resulting in a 2.2 - fold change in the collagen expression in cardiac fibroblasts, showing an advanced remodeling state of the transgenic mice compared to wild type littermate controls (n = 2-6, *P* < 0.001). There was also an increase of *Col1a2* expression in the cardiomyocyte fraction in 10 months old transgenic mice (17.5 - fold, n = 2-6; *P* < 0.01). This shows severe heart failure and remodeling at an advanced age leading to collagen production by cardiomyocytes. Moreover, severe interstitial fibrosis increased progressively over time with age (**Fig. 5A**), qualifying the ß$_1$-adrenoceptor transgenic mice for a fibrosis-senescence association study.

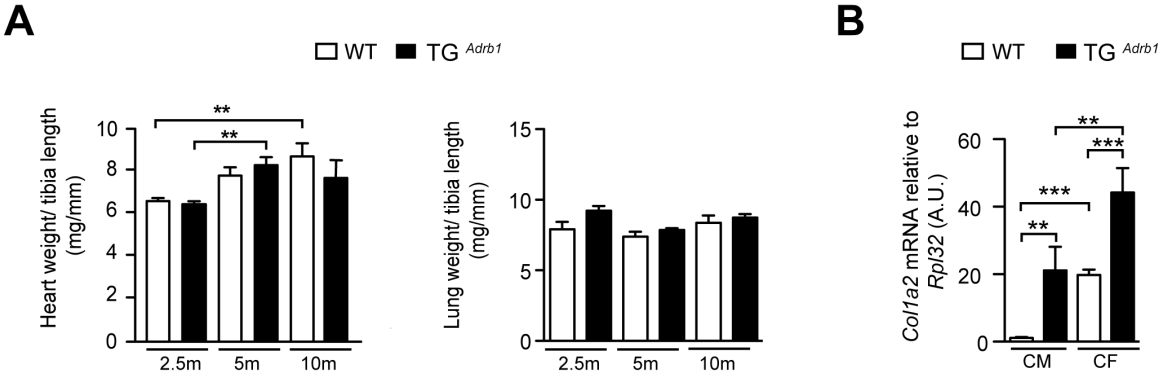

Fig. 4: Assessment of parameter for cardiac morphology in the ß$_1$-adrenoceptor transgenic (TG ^{Adrb1}) mice. (A) TG ^{Adrb1} and wild type littermate controls (WT) were analyzed at 2.5, 5 and 10 months of age for hypertrophy and heart failure by assessment of heart weight/ tibia length and lung weight/ tibia length ratio. n = 3-

9. ** $P < 0.01$ *** $P < 0.001$ (2-way ANOVA). **(B)** Real-time qPCR analysis for *Col1a2* gene expression in isolated CM and CF of 5-month-old TG ^{Adrb1} mice and WT controls. n = 3-9. ** $P < 0.01$ *** $P < 0.001$ (2-way ANOVA).

4.1.4 Senescent cells accumulate in interstitial fibrotic tissue of ß$_1$-adrenoceptor transgenic mice

In the ß$_1$- adrenoceptor transgenic disease model, fibrosis typically originates from interstitial areas as compensatory or replacement fibrosis to replace apoptotic cardiomyocytes. Fibrosis infiltrates the left ventricle. Therefore, interstitial areas of the left ventricular myocardium were primarily investigated. As shown in **Fig. 5A**, TG ^{Adrb1} mice displayed marked fibrosis at 5 and 10 months of age (~ 2.0 - and ~ 4.1 - fold, respectively; n = 3-9, $P < 0.05$ and $P < 0.001$) when compared to WT controls as quantified by Sirius red/fast green staining. Between transgenic animals, fibrosis increased progressively with a significant increase in 10 months old compared to 5 months old animals. Consistent with the TAC model, a significant accumulation of the senescence marker SA-ß-gal, p16 ^{INK4a} and p21 $^{CIP1/WAF1}$ were observed in TG ^{Adrb1} mice in the course of fibrogenesis when compared to WT controls and in between the transgenic group starting from 5 months of age (**Fig. 5B-D)**.

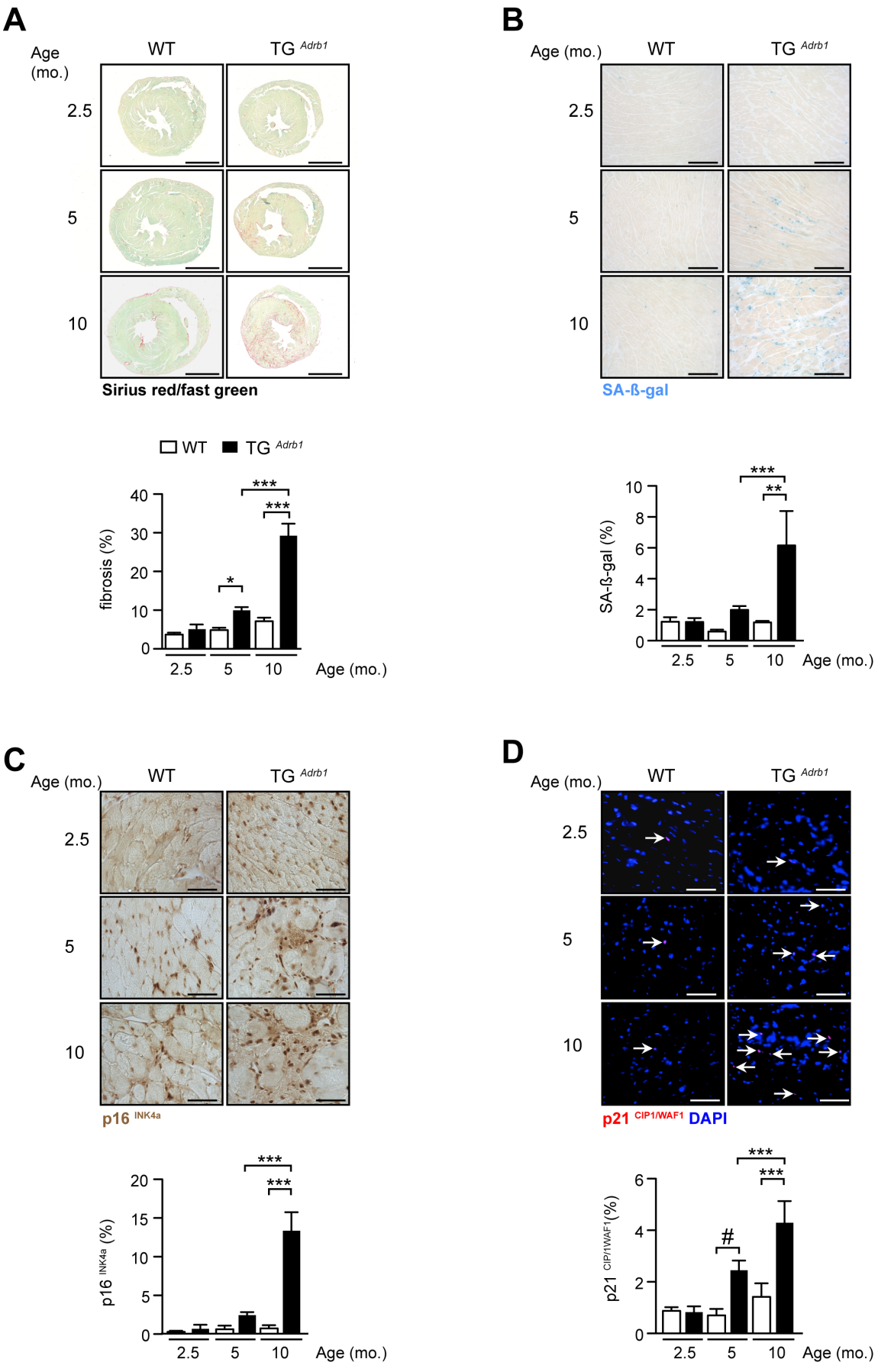
A
Age (mo.)
WT
TG Adrb1
2.5
5
10
Sirius red/fast green
WT
TG Adrb1
fibrosis (%)
40
30
20
10
0
*
***
***
2.5
5
10
Age (mo.)
B
Age (mo.)
WT
TG Adrb1
2.5
5
10
SA-ß-gal
SA-ß-gal (%)
10
8
6
4
2
0
***
**
2.5
5
10
Age (mo.)
C
Age (mo.)
WT
TG Adrb1
2.5
5
10
p16 INK4a
p16 INK4a (%)
20
15
10
5
0
***
***
2.5
5
10
Age (mo.)
D
Age (mo.)
WT
TG Adrb1
2.5
5
10
p21 CIP1/WAF1 DAPI
p21 CIP1/WAF1 (%)
6
4
2
0
***
***
#
2.5
5
10
Age (mo.)

Fig. 5: Interstitial fibrosis in myocardial tissue of ß$_1$-adrenoceptor transgenic mice is associated with premature senescence. TG ^{Adrb1} mice or WT littermates were analyzed for interstitial fibrosis and senescence markers SA-ß-gal, p16 ^{INK4a} and p21 $^{CIP1/WAF1}$ at 2.5, 5 and 10 months of age. Representative images and quantifications of cryo- or paraffin-embedded sections of left ventricular myocardium (**A**) fibrosis (red; Sirius red/fast green). n = 12-15. * $P < 0.05$, *** $P < 0.001$. (**B**) SA-ß-gal (blue). (**C**) p16 ^{INK4a} (brown). (**D**) p21 $^{CIP1/WAF1}$(red) and DAPI (blue). n = 3-7. * $P < 0.05$, ** $P < 0.01$ *** $P < 0.001$ (2-way ANOVA). Individual cells were analyzed in an automated manner by pixel counting on digitized images. Scale bar = 200 µm.

KI-67-positive cells were constantly increased ~ 1,7 - fold in TG ^{Adrb1} mice when compared to WT from 2.5 to 10 month of age (n = 3-9) (**Fig. 6**), consistent with a continuous tissue remodeling process due to cardiomyocyte degeneration and replacement fibrosis. Finally, and in line with the observations of the TAC study senescent cells accumulate in the hearts of TG ^{Adrb1} animals within interstitial fibrotic areas along with the severity of fibrosis.

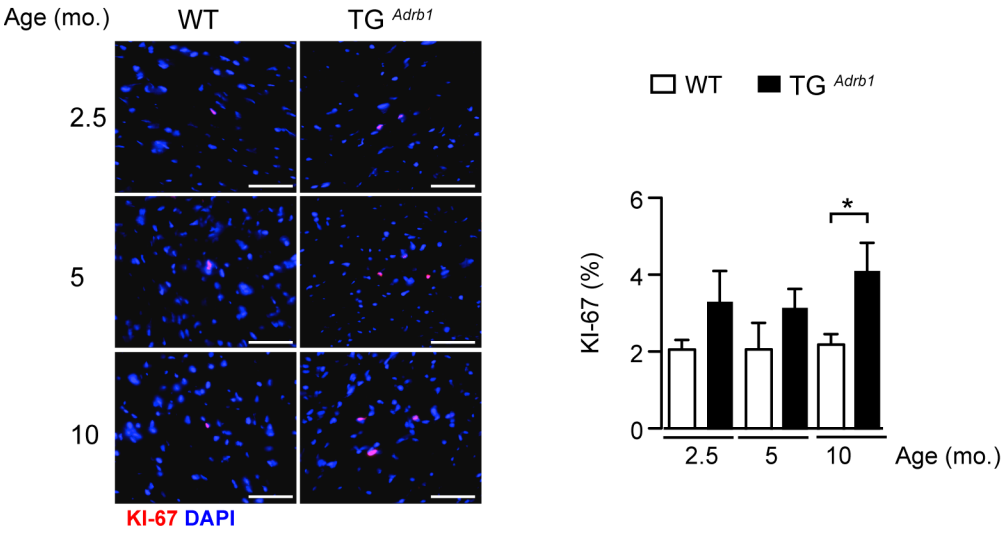

Fig. 6: Analysis of proliferation marker KI-67 in ß$_1$-adrenoceptor transgenic mice. Paraffin-embedded left ventricular myocardium of TG ^{Adrb1} mice or WT littermates were analyzed for proliferation marker KI-67 (red) at 2.5, 5 and 10 months of age. Co-staining with DAPI (blue). **Left**, representative images. **Right**, quantification of KI-67 positive cells; n = 3-9. * $P < 0.05$ (2-way ANOVA). Individual cells were analyzed in an automated manner by pixel counting on digitized images. Scale bar = 200 µm.

4.1.5 Senescent cells accumulate in perivascular and interstitial fibrotic tissue in human heart biopsies of idiopathic cardiomyopathy

To asses the biological relevance for cellular senescence within human cardiac pathologies, heart samples of patients with different heart diseases were analyzed for senescence markers and fibrosis. There was a trend towards an increase in the SA-ß-gal area of mixed pathologic left ventricular samples when compared to control tissue (**Fig. 7A**). However, this did not reach significance due to an unknown kinetic of senescence as well as the variable mixture of tissues concerning age, medical treatment, and systemic condition of the patients (n = 5-15). Nevertheless, in line with the data obtained from the animal disease models, expression of senescence markers SA-ß-gal (R^2 = 0.70; *P* < 0.001; n = 25) and p16 ^{INK4a} (R^2 = 0.62; *P* < 0.0001; n = 22) correlated positively with fibrosis in heart biopsies of patients suffering idiopathic cardiomyopathy (**Fig. 7B-C**).

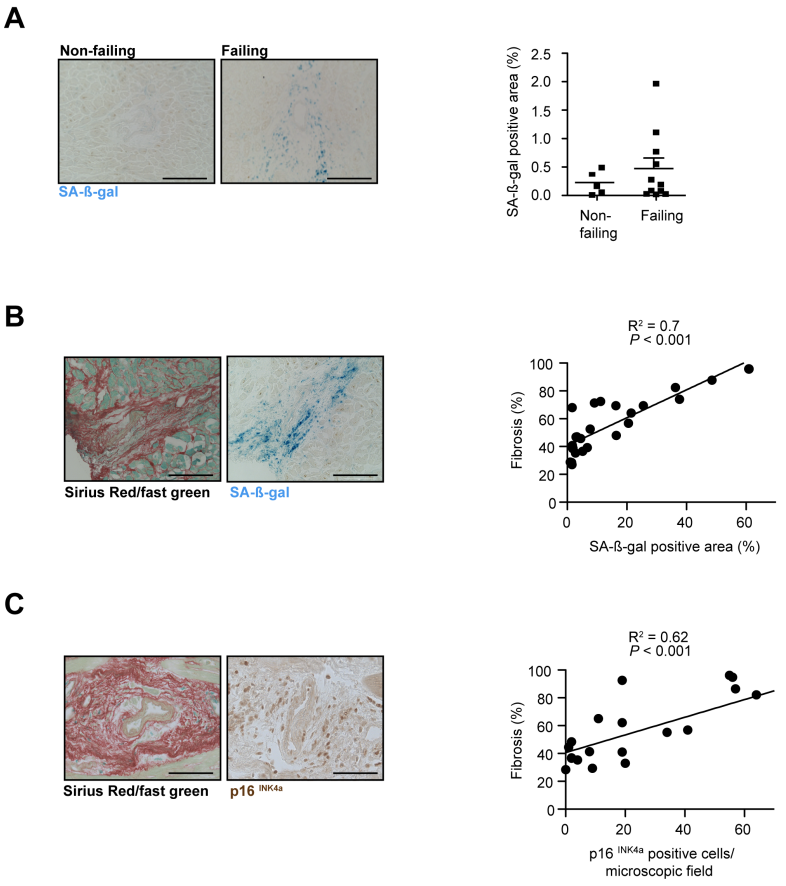

Fig. 7: Analysis of fibrosis and senescence markers in human heart tissue. Human heart biopsies from patients suffering from different etiologies of cardiac disease (failing) or non-failing control hearts were used to analyze the expression of the senescence marker SA-ß-galactosidase (SA-ß-gal) and $p16^{INK4a}$. Representative images and quantifications of cryo-embedded heart biopsies. n = 5-15. **(A) Left,** representative image of SA-ß-gal staining of failing and non-failing human heart biopsies. **Right**, quantitative assessment of SA-ß-gal positive area. (**B**) Human heart biopsies from patients suffering from idiopathic cardiomyopathy were used to analyze the expression of senescence markers in diseased human myocardium. Representative images and quantifications of cryo-embedded heart biopsies. **Left**, representative image of fibrotic lesions (Sirius red/fast green) and co-staining for senescence markers SA-ß-gal. **Right**, regression analysis of Sirius red/fast green and SA-ß-gal staining intensities. $R^2 = 0.70$; $P < 0.001$; n = 25. (**C**) **Left**, representative image of fibrotic lesions (Sirius red/fast green), and staining for senescence markers $p16^{INK4a}$. **Right**, regression analysis of Sirius red/fast green and $p16^{INK4a}$ staining intensities. $R^2 = 0.62$; $P < 0.0001$; n = 22.

Taken together, the data obtained from the animal disease models of cardiac fibrosis and the human heart biopsies demonstrate that senescent cells accumulate in the fibrotic myocardium.

4.2 Cardiac (myo)fibroblasts are the main cell population undergoing cellular senescence

Fibroblasts are the principal effector cells of cardiac fibrosis and play a critical role for ECM turnover and pathological remodeling of scar tissue (Leask 2015). The observation that senescent cells accumulate within fibrotic areas **(Fig. 2, 5, 8, 9)** suggested that CF may constitute the main cell population undergoing senescence upon fibrosis induction. Indeed, the majority of cells expressing the senescence marker $p21^{CIP1/WAF1}$ were positive for the mesenchymal cell marker vimentin (92 ± 0.9%; **Fig. 8**) and the fibroblast marker platelet-derived growth factor receptor α (92 ± 0.9 %; **Fig. 9A**). Additionally, 65.7 ± 10,47 % of $p21^{CIP1/WAF1}$ positive cells expressed α-smooth muscle actin (α-SMA) (**Fig. 9A**), indicating that the majority of CF undergoing senescence are myofibroblasts. Moreover, only 10.25 ± 1.9 % of $p21^{CIP1/WAF1}$ - positive cells were positive for the endothelial cell marker CD31, indicating that only a small population of the endothelial cells were senescent within fibrotic areas (n = 3). 5.88 ± 2.28 % of senescent cells were positive for the cardiomyocyte cell marker troponin T demonstrating that cardiomyocytes are not affected by senescence during fibrogenesis. In alignment with these data, more than 95 % ± 0.17 % of the cells expressing the senescence marker HP1ß also expressed PDGFRα. 63.19 % ± 3.84 % of them were activated synthetic myofibroblasts and therefore positive for α-SMA (n = 3-9) (**Fig. 9B**). A small cell population expressing HP1ß was positive for the endothelial cell marker CD31 and cardiomyocyte cell marker Troponin T (7.14 % ± 3.55 and 2.39 % ± 0.89, respectively). To further corroborate these findings, the SA-ß-gal (*Glb1)* transcript level was measured by quantitative Real- time

PCR in CM and CF isolated from TAC- or sham- treated mice or TG ^{Adrb1} mice and their WT littermates (**Fig. 9C, D**). Basal *Glb1* gene expression was 4.4 - fold higher in CF when compared to CM in sham-treated hearts. In addition, *Glb1* expression significantly increased in CF (+ 125 %, n = 4, $P < 0.05$), but not in CM, after TAC (**Fig. 9C**). Accordingly, the *Glb1* gene expression was 1.67 - fold higher in CF of WT mice when compared to CF in TG ^{Adrb1} animals. (**Fig. 9D**). These results indicate that SA-ß-gal is mainly expressed in CF and significantly increases in fibrogenic conditions.

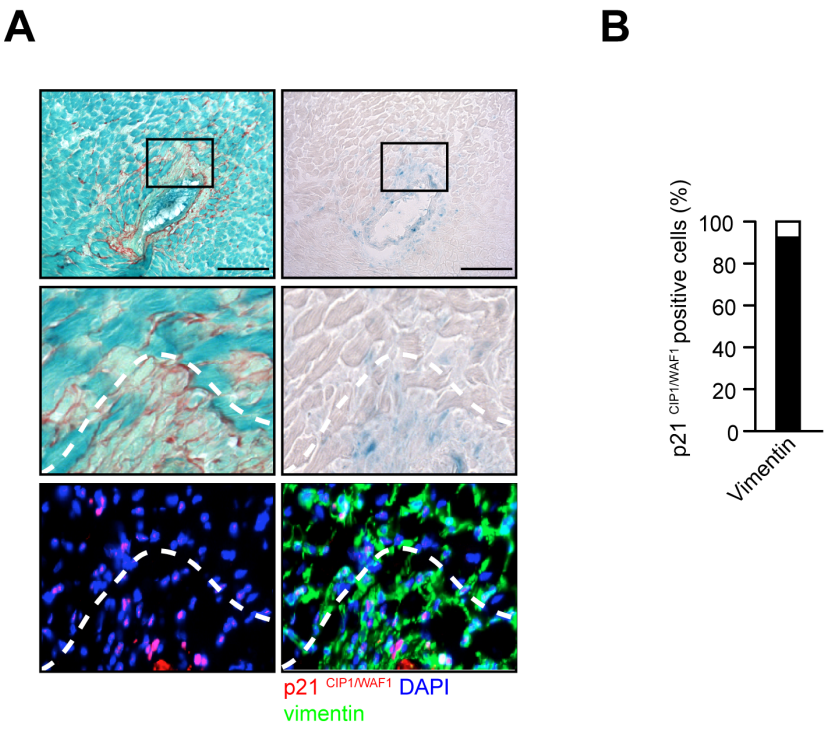

Fig. 8: Cardiac mesenchymal cells are predominantly undergoing premature senescence in the heart after TAC. (**A**) Representative image of perivascular areas stained for fibrosis (red; Sirius red/fast green; left upper and left middle image), senescence marker SA-ß-gal (blue; right upper and right middle image) and p21 $^{CIP1/WAF1}$ (red; left lower image) and fibroblast marker vimentin (green; right lower image); overlay of p21 $^{CIP1/WAF1}$, vimentin and DAPI (right lower image); (**B**) Quantification of p21 $^{CIP1/WAF1}$ positive cells in perivascular fibrotic areas that express the fibroblast marker vimentin. Individual cells were analyzed in an automated manner by pixel counting on digitized images. Scale bar = 100 µm. n = 3.

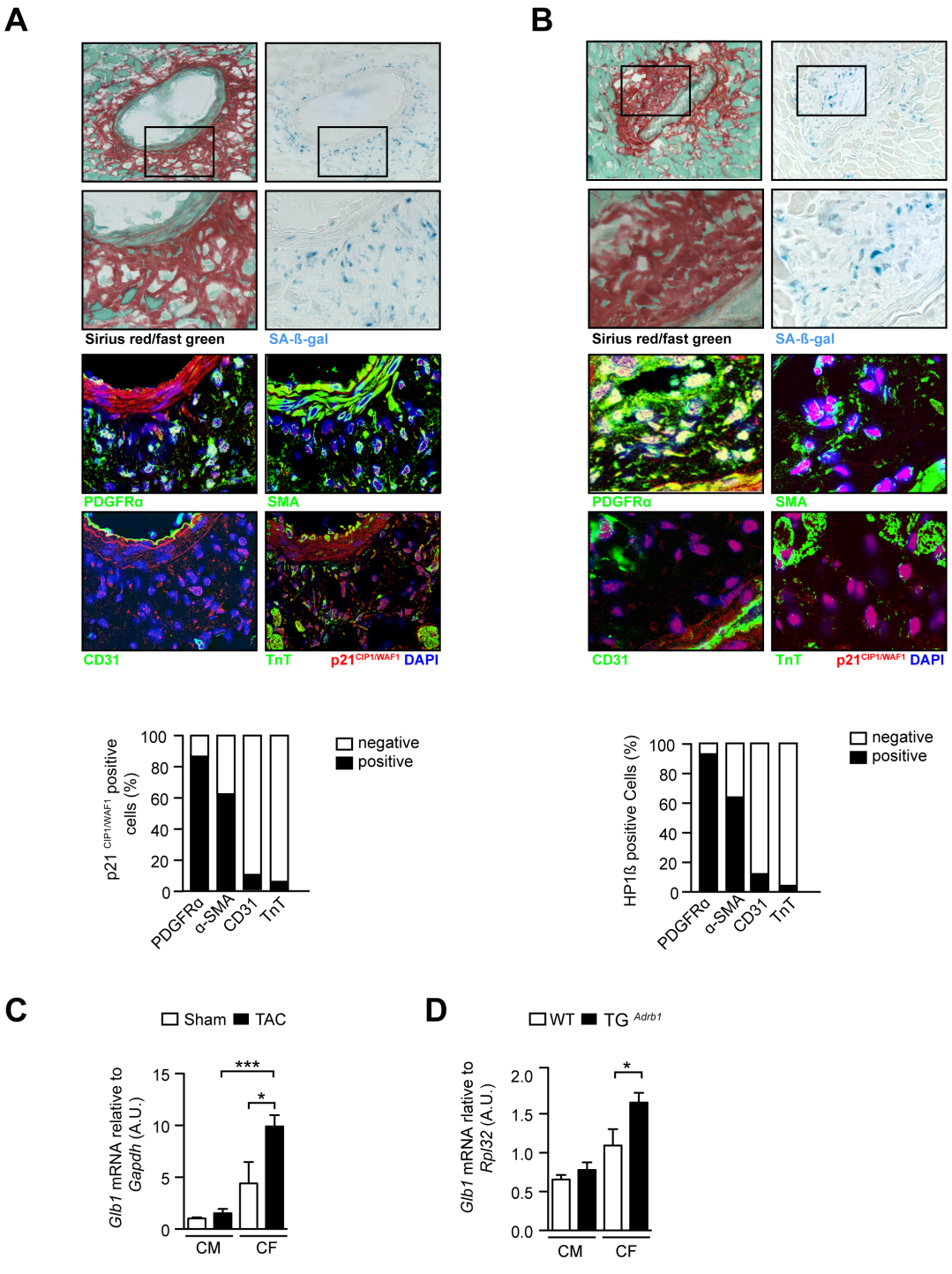

Fig. 9: Cardiac myofibroblasts are the predominant cell population undergoing premature senescence in the heart. Staining of perivascular areas for fibrosis (Sirius red/fast green), (**A**) and **(B) left upper two images.** Staining for senescence marker SA-ß-gal, (**A**) and **(B) right upper two images**. **(A)** p21 $^{CIP1/WAF1}$ /DAPI overlay or **(B)** HP1ß/ DAPI overlay with fibroblast marker PDGFRα (**third panel, left**), myofibroblast marker α-smooth muscle actin (α -SMA) (**third panel, right**), the endothelial cell marker CD31 (**fourth panel, left image**) and the cardiac myocyte marker troponin T (TnT) (**fourth panel, right**). Quantification of p21 $^{CIP1/WAF1}$- or HP1ß-positive cells in perivascular fibrotic areas that express the fibroblast marker PDGFRα, myofibroblast marker α-SMA, the endothelial cell marker CD31 and the cardiac myocyte marker troponin T (TnT). n = 3-9. Individual cells were analyzed in an automated manner by pixel counting on digitized images Scale bar = 100 µm. (**C**) and (**D**) Real-

time qPCR analysis of *Glb1* gene expression (SA-ß-gal) of freshly isolated murine cardiac myocytes (CM) and CF 3 weeks after TAC or at 5 months of age in TG ^{Adrb1} mice. n= 4, * $P < 0.05$, *** $P < 0.001$ (2-way ANOVA).

4.3 Fibrosis progression is enhanced by a dysfunctional senescence machinery

To evaluate the biological relevance of premature senescence in cardiac fibrogenesis, the cardiac phenotype of global *Trp53* $^{-/-}$ (referred to as p53-KO) and *Cdkn2a* $^{-/-}$ (also referred to as p16 ^{INK4a}-KO) mice were studied. In many cell types, p53 and p16 ^{INK4a} pathways contribute to cellular senescence to a varying degree (Collado et al. 2007). *Trp53* $^{-/-}$ mice hearts did not show detectable *Trp53* mRNA expression, validating the gene deletion (n = 3-5) (**Fig. 10A**). In sham treated animals, no SA-ß-gal expression was observed, neither in the wild type, nor in the p53 knockout condition (0.71 % ± 0.28% and 1.25 % ± 0.37 % respectively). However, there was no decrease in the SA-ß-gal expression 2 or 6 weeks after TAC when compared to the wild type littermate controls (2 weeks after TAC, WT vs. p53-KO: 3.24 % ± 0.69 % vs. 5.871 % ±1.38 %; 6 weeks after TAC WT vs. p53-KO: 2.37 % ±0.64 % vs. 4.16 % ± 3.32 %, n = 3-12) (**Fig. 10B**), indicating that senescence was functional independently of Trp53 repression under pathologic conditions. Although a high variability of the SA-ß-gal activity was observed in insulted hearts of p53 knockout animals, the expression of Sa-ß-gal was even higher by trend in the p53 depleted hearts (**Fig. 10B**). Nonetheless, there was no significant difference in the senescence staining between p53 knockout and p53 wild type animals after TAC. Likewise, no differences could be observed in perivascular fibrosis 2 or 6 weeks after TAC (Sirius red/ fast green staining, 2 weeks after TAC, WT vs. p53-KO: 65.95 % ± 3.12 % vs. 72.18 % ± 2.97 %, 6 weeks after TAC, WT vs. p53-KO: 69.82 % ± 3.08 % vs. 53.54 % ± 6.05 % n = 3-12) **(Fig. 10C)**. In alignment with these data, no differences were observed in heart function, determined by fractional shortening (FS), of knockout animals when compared to their p53 wild type littermates adter TAC (FS: WT sham vs. WT and p53-KO after TAC: 26.65 % ± 2.92 % vs. 15.34 % ± 2.64 % and 15.36 % ± 1.51 %) (**Fig 10D**).

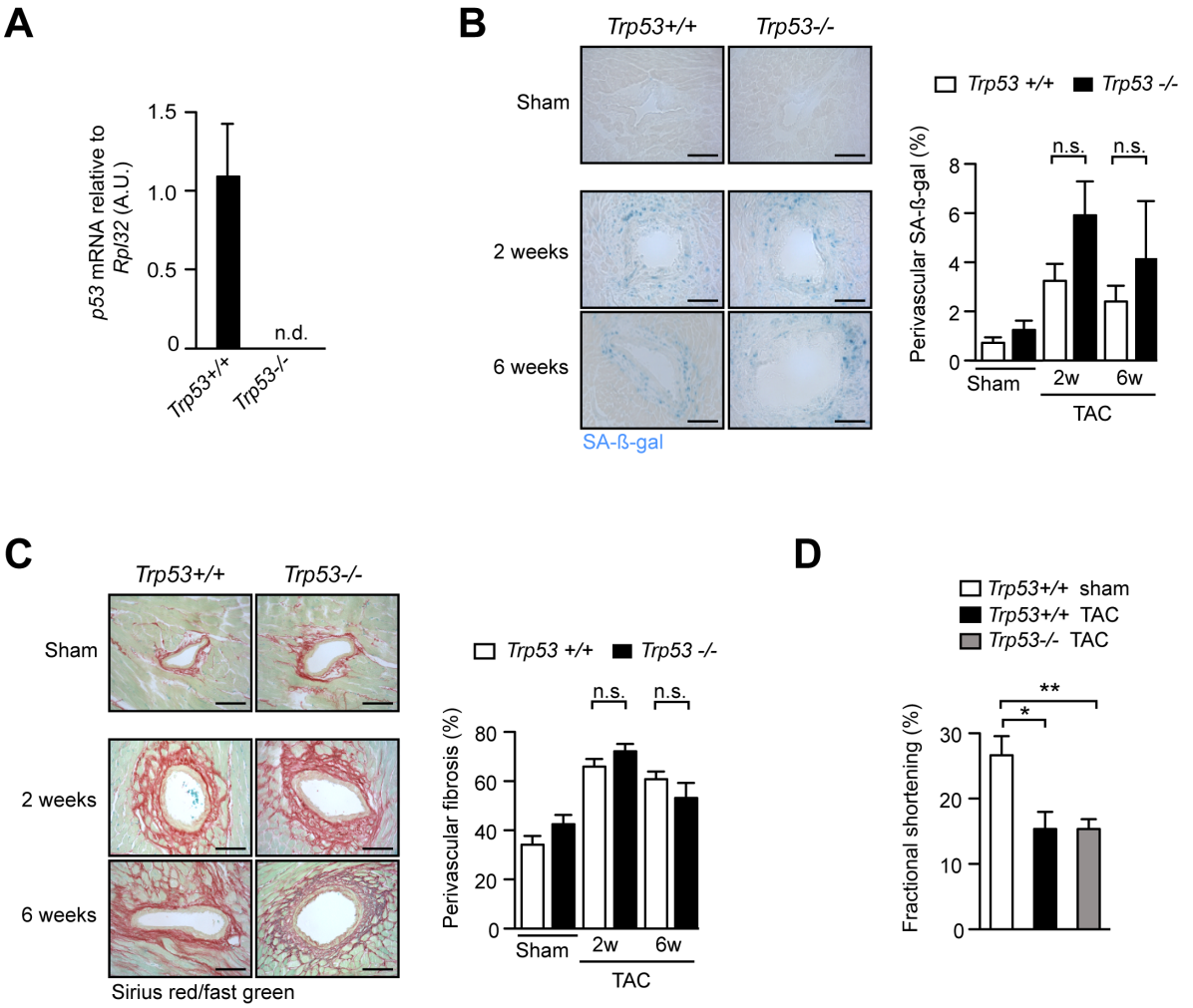

Fig. 10: Genetic ablation of *Trp53* does not affect the extent of premature senescence or perivascular fibrosis in the heart after TAC. Transverse aortic constriction (TAC) or sham surgery was performed in 8-week-old male *Trp53* $^{-/-}$ or *Trp53* $^{+/+}$ mice and the degree of perivascular fibrosis and senescence examined 2 and 6 weeks after intervention. Images were analyzed in an automated manner by pixel counting. Scale bar = 100 µm. (**A**) Real-time qPCR analysis of *Trp53* gene expression of whole heart lysates 2 weeks after TAC. n=3-4. N.d. = not determined. (**B**) SA-ß-gal histochemistry and quantification. n = 3-12. n.s. not significant. (**C**) Sirius red/fast green fibrosis staining and quantification. n = 3-12. n.s. not significant. (**D**) Assessment of cardiac function by echocardiography. Fractional shortening (FS). n = 4-6, * $P < 0.05$, ** $P < 0.01$ (1-way ANOVA).

Similar results were obtained for the *Cdkn2a* $^{-/-}$ mice. After knockout validation by qPCR (**Fig 11A**), where no detectable mRNA expression was observed for p16 ^{INK4a} and p19 ^{ARF} (alternative reading frame of the *Cdkn2a* gene, n = 3-4), senescence functionality was assessed. In sham treated animals, no SA-ß-gal expression was observed in the wild type and in the *Cdkn2a* depleted mice 2 and 6 weeks after TAC (0.84 % ± 0.21 % and 0.75 % ± 0.13 % respectively, n = 4-13) (**Fig. 11B**, first two bars). As shown in **Fig.11B**, 4 last bars, senescence activity was equal in p16 ^{INK4a}- knockout and wild type animals 2 and 6 weeks after TAC, indicating no differences in the senescence functionality (2 weeks after TAC, WT vs. p16 ^{INK4a} -KO: 6.34 % ± 1.47 % vs. 5.94 % ±1.29 %; 6 weeks after TAC WT vs. p16^{INK4a} -

KO: 3.84 % ±0.63 % vs. 3.52 % ±0.52 %, n = 4-13). Additionally, there was no difference in perivascular fibrosis between wild type and Knock out animals, as determined by Sirius red/ fast green staining (2 weeks after TAC, WT vs. p16 ^{INK4a} -KO: 62.16 % ± 5.68 % vs. 58.02 % ± 4.08 %; 6 weeks after TAC WT vs. p16 ^{INK4a} -KO: 64.14 % ± 4.16 % vs. 69.09 % ± 2.50 %, n = 4-13) (**Fig. 11 C**). According to these data, heart function was the same between wild type and p16 ^{INK4a} -KO animals after TAC (FS: WT sham vs. WT and p16 ^{INK4a} -KO after TAC: 24.76 % ± 1.15 % vs. 12.45 % ± 0.84 % and 15.11 % ± 2.38 %, n = 3-5) (**Fig. 11D**).

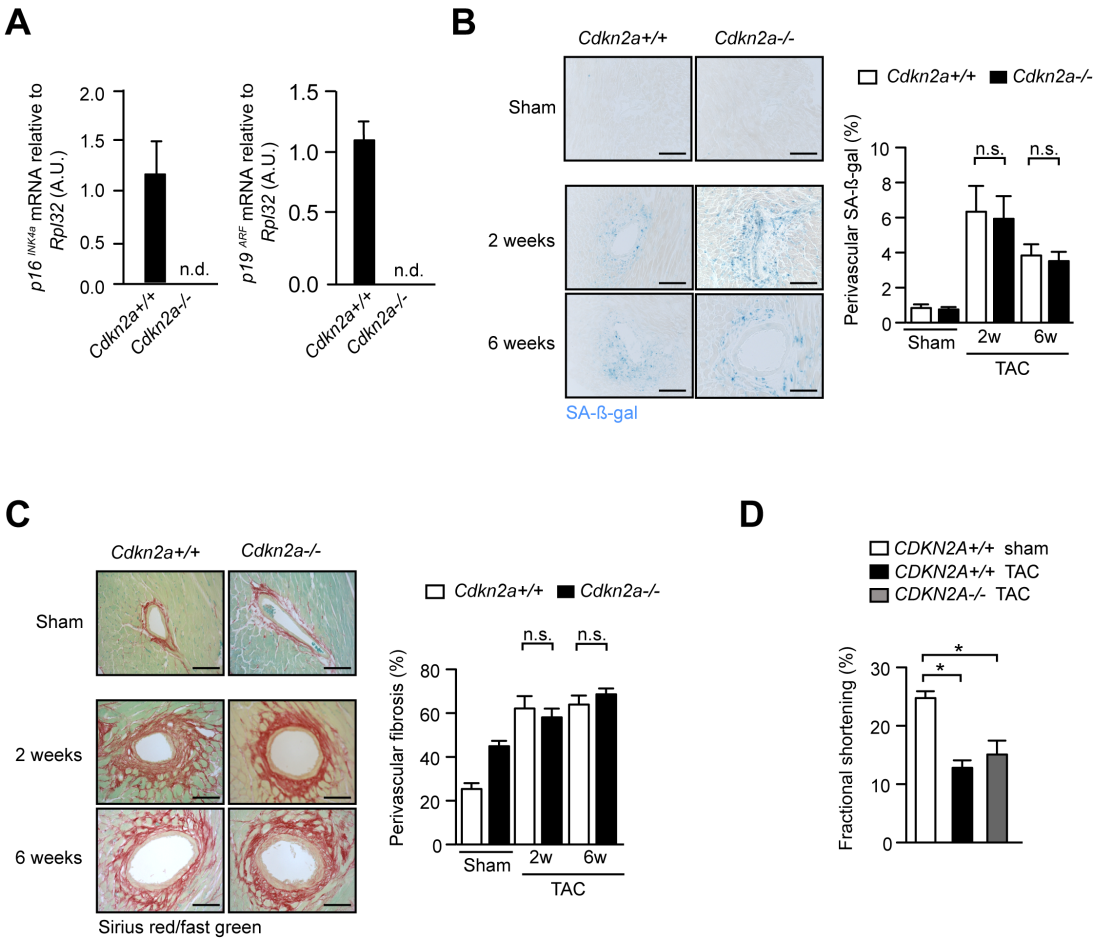

Fig. 11: Genetic ablation of *Cdkn2a* does not effect the extent of premature senescence or perivascular fibrosis in the heart after TAC. Transverse aortic constriction (TAC) or sham surgery was performed in 8-week-old male *Cdkn2a* $^{-/-}$ or *Cdkn2a* $^{+/+}$ mice and the degree of perivascular fibrosis and senescence examined 2 and 6 weeks after intervention. Images were analyzed in an automated manner by pixel counting. Scale bar = 100 µm. (**A**) Quantitative qPCR analysis of *Cdkn2a* gene locus and quantitative examination of the *p16* ^{INK4a} and the *p19* ^{ARF} gene expression of whole heart lysates 2 weeks after TAC. n = 3-4. N.d. = not determined. (**B**) SA-ß-gal histochemistry and quantification. n = 4-13. n.s. not significant. (**C**) Sirius red/fast green fibrosis staining and quantification. n = 4-13. n.s. not significant. (**D**) Assessment for cardiac function by echocardiography. Fractional shortening (FS). n = 4-6, * $P < 0.05$ (1-way ANOVA).

To determine the impact of disrupting both gene loci on the development of premature senescence and fibrosis in the heart, I generated *Trp53* $^{-/-}$ *Cdkn2a* $^{-/-}$ compound mutant mice and subjected them to TAC (**Fig. 12 A)**. The double knockout (also referred to as DKO) was verified by mRNA and protein expression, as determined by qPCR and western blot analysis, respectively. No detectable mRNA and only faint signals in the protein level (coming from unspecific antibody reactions) of Trp53 and p16^{INK4a} in the hearts of double knockout animals could be found, Thus validating the gene depletion (n = 3-4) (**Fig. 12 B, C)**. Consistent with a critical role of p53 and p16 ^{INK4a} for cellular senescence, heart sections of *Trp53* $^{-/-}$ *Cdkn2a* $^{-/-}$ mice contained a markedly reduced number of SA-ß-gal positive CF after TAC when compared to WT littermates (WT sham. 0.17 % ± 0.06 %, WT TAC: 1.52 % ± 0.23 %, DKO TAC: 0.47 % ± 0.08 %) (**Fig. 12 D**). Remarkably, *Trp53* $^{-/-}$ *Cdkn2a* $^{-/-}$ mice developed a more severe perivascular fibrotic phenotype after TAC when compared to *Trp53* $^{+/+}$ *Cdkn2a* $^{+/+}$ mice (49 ± 4.9 % vs. 33 ± 2.7 %, n = 4-8, $P < 0.01$) (**Fig. 12 D)** that was associated with impaired cardiac function as judged by ejection fraction (WT sham: 51.55 % ± 1.47 %, WT TAC: 38.44 %± 3.08 %, DKO TAC: 25.89 % ± 2.4 %, n = 3-8, $P < 0.01$), fractional shortening (WT sham: 26.06 ±0.94 %, WT TAC: 18.56 % ± 1.65 %, DKO TAC: 11.98 % ± 1.2 %, n = 3-8, $P < 0.01$)**,** left ventricular end-systolic (WT sham: 75.2% ± 5.04%, WT TAC: 84.27 % ± 2.38 % , DKO TAC: 96.23 % ± 1.49 %, n = 3-8, $P < 0.01$) and end-diastolic volume (WT sham: 79.29 µl ± 2.75 µl, WT TAC: 82.63 µ ± 2.34 µl , DKO TAC: 97.23 µl ± 3.25 µl, n = 3-8, $P < 0.01$), as well as left ventricular internal diameter (WT sham: 3.98 mm ± 0.1 mm WT TAC: 4.36 mm ± 0.05 mm , DKO TAC: 4.57 mm ± 0.03 mm, n = 3-8, $P < 0.01$) (**Fig. 13C**).

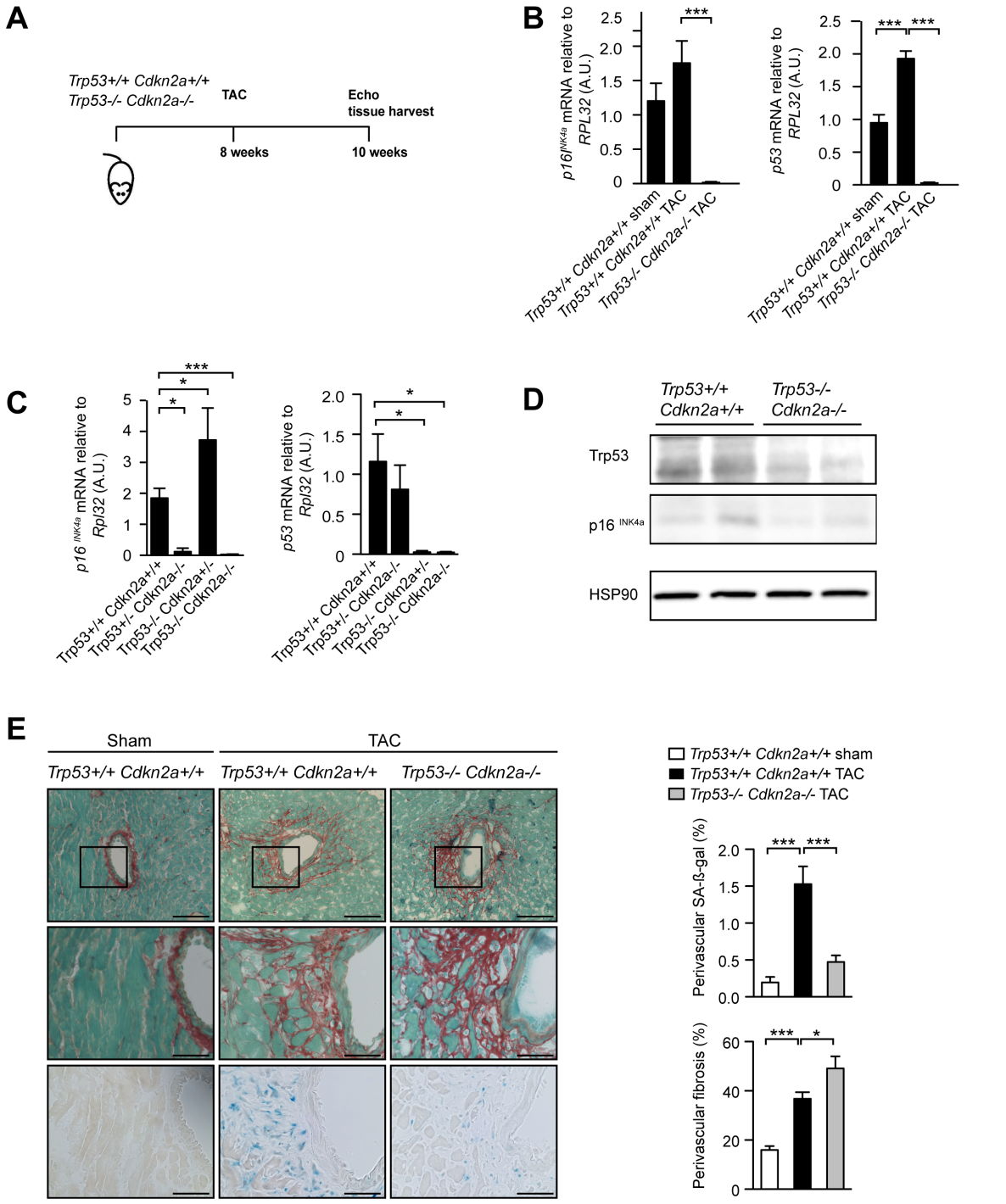

Fig. 12: Genetic ablation of *Trp53* and *Cdkn2a* results in diminished senescence and increased perivascular fibrosis. 8-week-old *Trp53* $^{+/+}$ *Cdkn2a* $^{+/+}$ or *Trp53* $^{-/-}$ *Cdkn2a* $^{-/-}$ mice were subjected to TAC or control (sham) surgery. At week 10, animals were euthanized for further analysis. (**A**) Experimental strategy and timeline. (**B**) Quantitative PCR analysis of the *Trp53* and the *p16* ^{INK4a} gene for validation of the double knockout (DKO). **(C)** Quantitative PCR analysis of *Trp53* and the *p16* ^{INK4a} gene in wild type, heterozygous and homozygous animals after TAC. (**D**) Western blot for Trp53 and the p16 ^{INK4a} proteins in wild type and homozygous DKO animals. (**E**) Representative images of fibrosis (Sirius red/fast green) and premature senescence (SA-ß-gal). Individual cells were analyzed in an automated manner by pixel counting on digitized images. Scale bar = 100 µm. Quantification of panel (E). n = 4-8. ** $P < 0.01$ *** $P < 0.001$ (t-test).

Interstitial fibrosis also increased by trend in *Trp53* $^{-/-}$ *Cdkn2a* $^{-/-}$ mice when compared to wild type mice. However, this was not significant (WT sham: 2.72 % ± 0.07 % vs. WT TAC: 6.82 % ± 0.82 % vs. KO TAC: 11.43 %± 2.41 % n = 4-8) **(Fig. 13A)** probably due to global effects of the *Trp53* and *Cdkn2a* depletion, i.e. on cardiac myocytes and endothelial cells. *Trp53* depletion was shown to induce angiogenesis after TAC (Sano et al., 2007). In order to determine the impact of the *Trp53* /*Cdkn2a* knockout on angiogenesis, mRNA levels were determined and heart sections of *Trp53* $^{-/-}$ *Cdkn2a* $^{-/-}$ and *Trp53* $^{+/+}$ *Cdkn2a* $^{+/+}$ CD31 were stained and quantified for the endothelial cell marker CD31 (**Fig.13B**). In alignment with published data, CD31 positive cells increase significantly 2 weeks after TAC when compared to sham control hearts (WT sham: 41.65 % ± 0.99 %, WT TAC: 54.81 % ± 2.93 %, n = 3-8, $p < 0.05$) (**Fig. 13 B**). Angiogenesis was significantly increased in p53-KO mice when compared to wildtype hearts 2 weeks after TAC (WT TAC vs. p53-KO TAC: 54.81 % ± 2.93 % vs. 65.97 % ±2,18 %, n = 3-8, $p < 0.01$) (**Fig. 13 B**). Similar results were observed in *Cdkn2a* knock out animals, but without statistical significance (WT TAC vs. $p16^{INK4a}$-KO TAC: 54.81 % ±2.93 % vs. 62.86 % ± 2,99 %) (**Fig. 13 B**). However, there was no increase of angiogenesis anymore in the *Trp53* $^{-/-}$ *Cdkn2a* $^{-/-}$ mice (53.02 % ± 3.31 %) 2 weeks after TAC (**Fig. 13 B**), indicating that angiogenesis does not impact the phenotype concerning fibrosis within this time period.

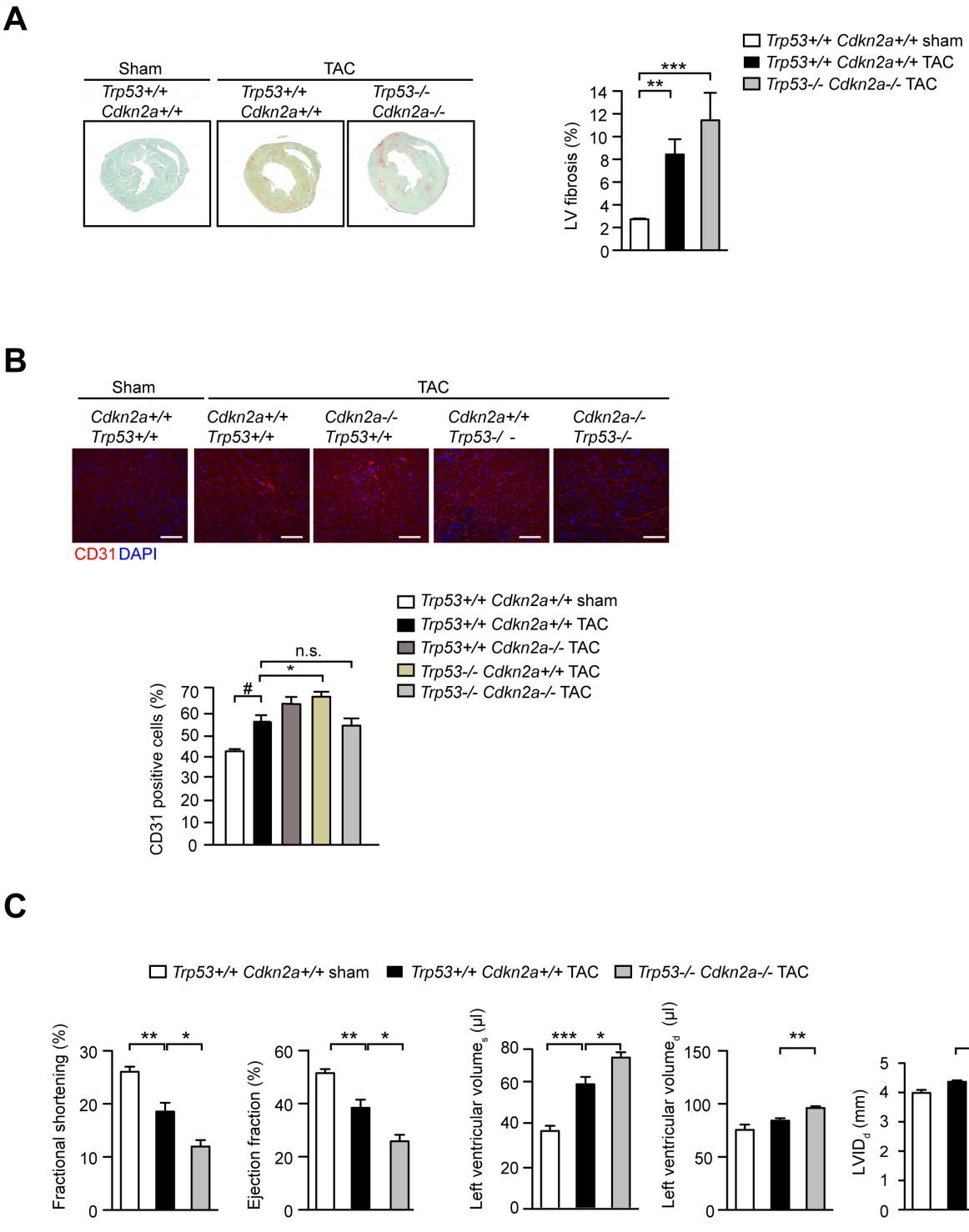

Fig 13: Genetic ablation of *Trp53* and *Cdkn2a* results in increased left ventricular fibrosis, unchanged angiogenesis and reduced cardiac function. *Trp53* $^{+/+}$ *Cdkn2a* $^{+/+}$ or *Trp53* $^{-/-}$ *Cdkn2a* $^{-/-}$ mice were treated as described and euthanized for further analysis. Representative images and quantifications of cryo- or paraffin-embedded sections of left ventricular myocardium. (**A**) **Left**, *Trp53* $^{+/+}$ *Cdkn2a* $^{+/+}$ or *Trp53* $^{-/-}$ *Cdkn2a* $^{-/-}$ mice were analyzed for left ventricular interstitial fibrosis, representative images (Sirius red/fast green). **Right**, quantification of left ventricular interstitial fibrosis. n = 4-8. $P < 0.01$ *** $P < 0.001$ (ANOVA). (**B**) Representative images and quantification for immunofluorescence analysis of CD31 (red) and DAPI (blue). n = 4-8. * $P < 0.05$ (ANOVA). Individual cells were analyzed in an automated manner by pixel counting on digitized images. Scale bar = 200 µm. (**C**) Assessment of parameter for cardiac morphology and function. Left ventricular internal diameter (LVID d/s). n = 4-8. ** $P < 0.01$ *** $P < 0.001$ (t-test).

In summary, these data demonstrate that CF lacking both the *Trp53* and *Cdkn2a* genes (and thus having dysfunctional ARF/p53 and p16 ^{INK4a}/Rb pathways) fail to senesce, which results in exacerbated fibrosis and impaired cardiac function.

4.4 Induction of cellular senescence restricts cardiac fibrosis and improves heart function

The observations above suggest that induction of the senescence program in CF may limit fibrosis progression, thus implicating premature senescence as a regulatory mechanism to restrain excess ECM production and tissue remodeling in the heart.

CCN1 (also known as CYR61) is a secretory protein that is expressed at sites of wound healing to induce fibroblast senescence through binding to integrin $\alpha_6\beta_1$ and cell surface heparin sulfate proteoglycans (HSPGs) and activation of p53 and p16 ^{INK4a} pathways (C.-C. Chen & Lau 2009; J.-I. Jun & Lau 2010).

To find out if CCN1 also impacts on senescence during cardiac fibrogenesis, first CCN1 abundance after TAC was investigated. As shown in **Fig. 14A**, perivascular CCN1 protein significantly increased 2 and 6 weeks after TAC, as assessed by immunofluorescence staining (2 weeks, sham vs. TAC: 82.15 % ± 3.97 % vs. 122.6 % ±10.94 %, n= 3-4, $p < 0.001$, 6 weeks, sham vs. TAC: 63.48 % ± 3.38 % vs. 97.77% ± 4.69%, n= 3-4, $p < 0.01$). Moreover CCN1 co-localized with senescent cells, thus positively correlating with the senescence marker SA-ß-galactosidase within diseased heart tissue ($R^2 = 0.55$, n = 8, $p < 0.05$) (**Fig. 14B**). To determine the CCN1 expressing cell type, quantitative PCR analysis of freshly isolated CM and CF was performed. Surprisingly, no increase in CCN1 mRNA was observed 2 and 6 weeks after TAC in each of the cell types, whereas CF constantly show 2 - fold increase in Ccn1 mRNA expression at any time point during sham or TAC conditions when compared to CM sham (**Fig. 14C**). However, there was a significant 3 - fold increase of Ccn1 mRNA expression in CM at 2 and 5 days after TAC (**Fig. 14C**), confirming existing *in vitro* and *in vivo* data showing an immediate increase in CCN1 expression after cardiac insult declining to normal expression levels at later stages. These findings indicate that CCN1 is an early-induced gene upon cardiac injury.

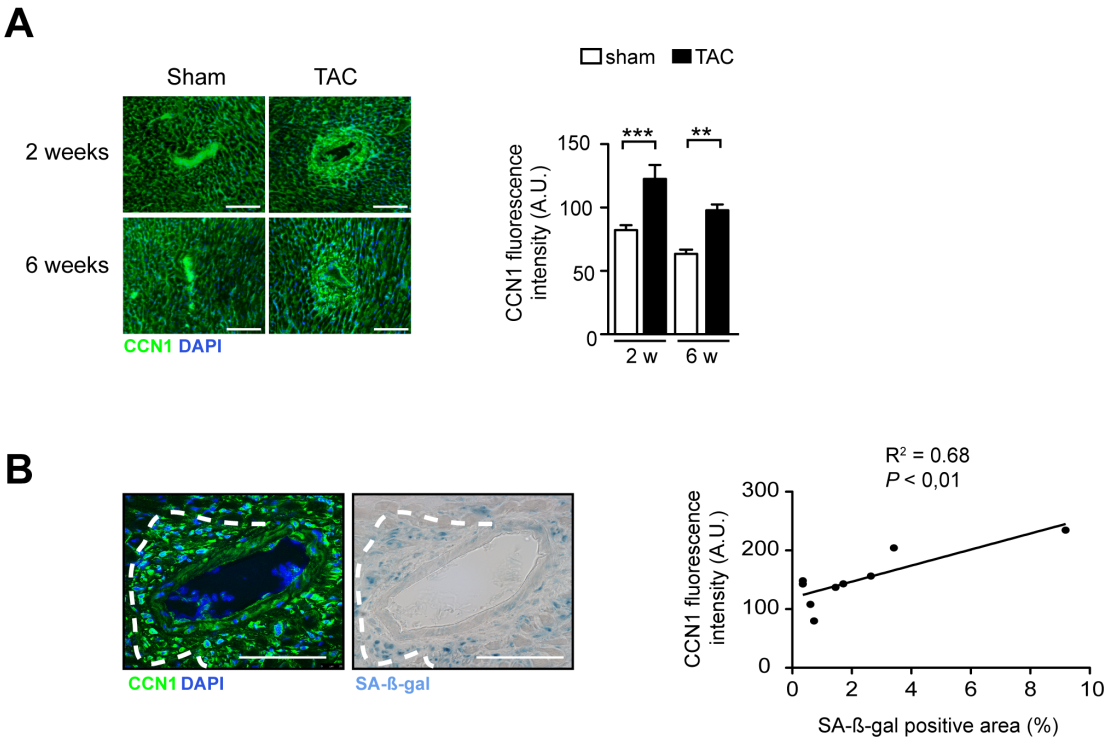

Fig 14.: The senescence inducing secreted matricellular protein CCN1 is increased within fibrotic areas in wildtype animals after TAC. 8-week-old male C57BL/6N mice were subjected to sham or TAC and analyzed for CCN1 expression 5 days, 2 weeks and 6 weeks after intervention. (**A**) **Left**, representative images. **Right,** quantification of immunofluorescence for CCN1 (green) and DAPI (blue) 2 and 6 weeks after TAC. Cells were analyzed in an automated manner by pixel counting on digitized images. Scale bar = 150 µm. n = 3-6. ** $P < 0.01$ *** $P < 0.001$ (t-test). (**B**) **Left,** immunofluorescence for CCN1 (green), DAPI (blue) and SA-ß-gal staining (blue). **Right**, correlation analysis of perivascular CCN1 and SA-ß-gal expression; R = 0,68; * $P < 0.05$. (**C**) Quantitative PCR analysis of *Ccn1* gene expression of freshly isolated murine cardiac myocytes (CM) and cardiac fibroblasts (CF) 2 days, 5 days, 2 weeks and 6 weeks after TAC. n= 4. P = * $P < 0.05$ *** $P < 0.001$ (ANOVA).

To establish the ability of CCN1 triggering senescence in cardiac fibroblasts, first the effect of wild type CCN1 (CCN1-WT) and a dominant-negative CCN1 mutant (CCN1-DN) devoid of integrin $\alpha_6\beta_1$ and HSPGs binding sites critical for senescence induction (J.-I. Jun & Lau 2010) on CF was evaluated *in vitro* **(Fig. 15A)**. Incubation of neonatal rat cardiofibroblasts (NRCF) with conditioned medium of neonatal rat cardiomyocytes (NRCM) infected with adenoviruses expressing CCN1 resulted in a robust induction of cellular senescence as evidenced by SA-

ß-gal staining (+ 83 %, n = 3, $P < 0.01$) and *Cdkn1a* (*p21* $^{CIP1/WAF1}$) gene expression (+ 175 % n = 3, $P < 0.05$). In contrast, no effect was observed with CCN1-DN containing medium (**Fig. 15C-D**), although the protein was abundant in the conditioned medium at equal levels for CCN1-WT and CCN1-DN (**Fig. 15B**).

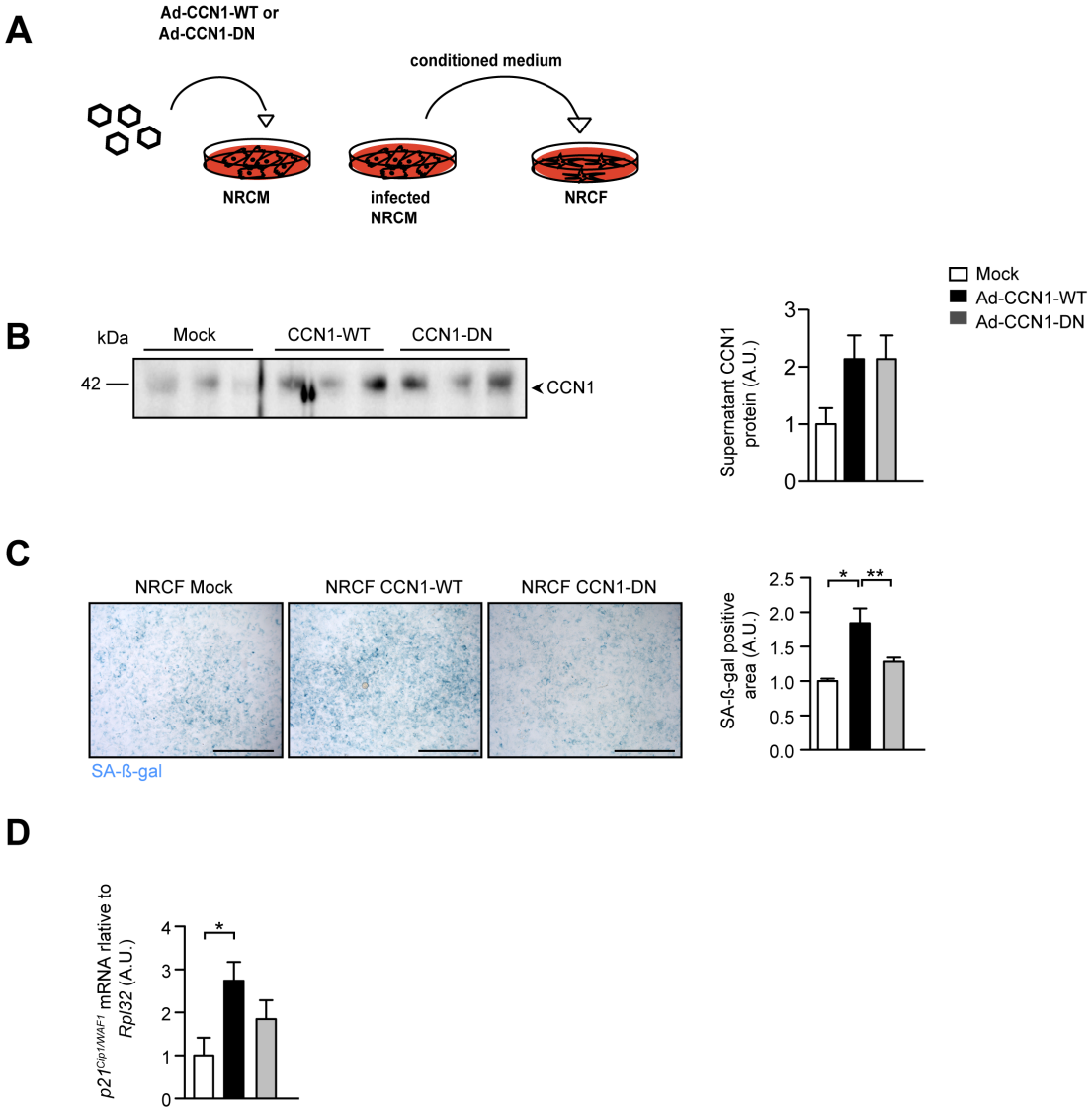

Fig. 15: CCN1 triggers premature senescence of cardiac fibroblasts *in vitro*. (**A**) Experimental strategy. CCN1 was expressed in neonatal rat cardiomyocytes (NRCM) using adenovirus (Ad) vector that encodes wildtype CCN1 (CCN1-WT) or a dominant negative CCN1 mutant (CCN1-DN). After infection, cell culture medium was collected for 72 hrs and transferred to NRCFs. After a 6-day incubation period, NRCFs were analyzed for senescence markers. (**B**) **Left**, CCN1 protein concentrations in cell culture medium of NRCM 4 days after infection with Ad-mock-, Ad-CCN1-WT- and Ad-CCN1-DN. **Right**, quantification. n = 3, * $P < 0.05$, *** $P < 0.001$ (ANOVA). (**C**) **Left**, representative images of SA-ß-gal histochemistry performed with NRCF after incubation with mock-, CCN1-WT- and CCN1-DN-conditioned medium. **Right**, quantification. n = 3, * $P < 0.05$ (ANOVA). (**D**) Quantitative PCR analysis of *Cdkn1a* (p21 $^{CIP1/WAF1}$) gene expression (SA-ß-gal) of NRCF after incubation with mock-, CCN1-WT- and CCN1-DM- conditioned medium. n = 3-5, * $P < 0.05$ (1-way ANOVA).

Next, I assessed whether heart-specific overexpression of CCN1 can induce CF senescence *in vivo* using adeno- associated virus serotype 9 (AAV9)- gene transfer. AAV9 was chosen for its strong heart tropism (Suckau et al. 2009; Hulot et al. 2011). Three-week old mice were injected with AAV9-CCN1, AAV9-CCN1-DN or mock treated, and five weeks later subjected to TAC or sham surgery. After two more weeks, echocardiography was performed and tissue samples collected for further analysis (**Fig. 16A**). Immunoblotting of heart lysates showed a ~1.5 - fold increase of CCN1 and CCN1-DN, respectively, when compared to endogenous CCN1 of uninfected control hearts and an equal distribution of the AAV9 infection pattern throughout the whole heart (n = 3-6). (**Fig. 16B, C**).

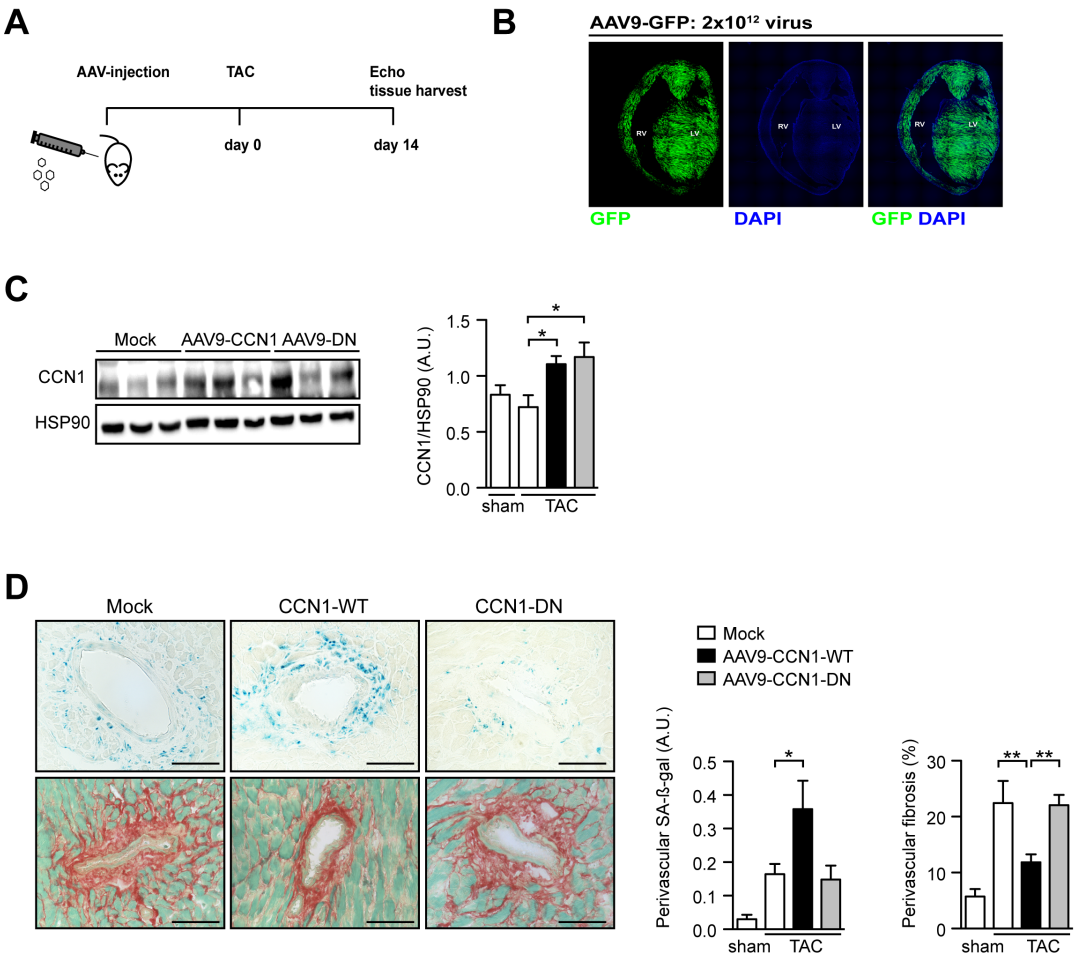

Fig. 16: CCN1 induces senescence and prevents perivascular fibrosis *in vivo*. (**A**) Experimental strategy and timeline for exogenous cardiotropic expression of CCN1 using adeno-associated virus subtype 9 (AAV9) in mice. The 3-week-old mice were infected with an AAV9 vector that encodes wild type CCN1 (CCN1-WT), a dominant- negative mutant (CCN1-DN) or mock (solvent only). At week 8 mice were subjected to TAC or control

(sham) surgery. At week 10 echocardiographic measurements were taken and animals euthanized for further analysis. (**B**) Assessment of AAV9- distribution by visualizing GFP after AAV9-GFP injection (performed as described) with fluorescence microscopy. GFP (green), DAPI (blue). (**C**) Immunoblot analysis and quantification of CCN1 (WT or DN) protein concentrations in heart lysates. (**D**) Representative heart sections (left) stained for senescence (SA-ß-gal) and fibrosis (Sirius red/ fast green) of AAV9-mock-, AAV9-CCN1-WT- and AAV9-CCN1-DN-infected mice after sham or TAC treatment. **Right**, Quantification of perivascular senescence and fibrosis determined from heart sections. Individual cells were analyzed in an automated manner by pixel counting on digitized images. n = 3-6. * $P < 0.05$ (1-way ANOVA), n.s. not significant.

In confirmation with the *in vitro* experiments with NRCF, premature senescence was increased (as evidenced by SA-ß-gal staining normalized to the fibrotic area) in CCN1-infected animals (+ 225 %, $P < 0.05$; and + 240 %, n = 3-6, $P < 0.05$) when compared to mock-treated or CCN1-DN infected controls after TAC, respectively (**Fig. 16D**). Importantly, mice with CCN1-triggered senescence displayed markedly reduced perivascular fibrosis when compared to mock or CCN1-DN infected controls (11.9 ± 1.4 % vs. 22.4 ± 4.0 % and 22.1 ± 1.8 %, respectively; n= 3-6 and both $P < 0.01$) (**Fig. 16D**). In line with these data, also interstitial cardiac fibrosis decreased remarkably in the CCN1-WT infected animals after TAC when compared to mock-or CCN1-DN infected mice (WT sham vs. WT TAC and CCN1- and CCN1-DN TAC: 1.30 % ± 0.14 % vs. 7.07 % ± 1.15 % and 2.18 % ± 0.33 % and 3.31 % ± 0.38 %, n = 4-8. $P < 0.01$) (**Fig. 17A**). To investigate if angiogenesis is altered in the AAV9-treated animals, CD31 was stained and quantified. In Mock infected mice, there was an increase of CD31 positive cells per total area after TAC (**Fig. 17B**). However, no difference between Mock, CCN1-WT or DN infected animals after TAC was observed (WT sham 14.91 ± 1.1, WT TAC: 18.31 ± 1.91, CCN1-WT TAC: 16.96 ± 1.36; CCN1-DN TAC: 18.84 ± 1.84, n = 4), **Fig. 17B**), suggesting, that the mutation of the $\alpha_6\beta_1$ and HSPGs binding sites are not altering angiogenesis. This is in line with findings, showing that $\alpha_5\beta_3$ sites are mainly responsible for endothelial cell proliferation (Chen et al., 2004). Consistently, no changes in the CD31 mRNA expression could be found between Mock, CCN1-WT and CCN1-DN after TAC (WT sham: 1.05 fold ± 0,07, WT TAC: 1.26 fold ± 0.15, CCN1-WT TAC: 1.32 fold ± 0.17, CCN1-DN TAC: 1.34 fold ± 0.12, n = 4), yet there was a clear trend between sham and TAC (1.2 fold increase after TAC) (**Fig. 17C)**. Additionally, the attenuated fibrotic remodeling after TAC in the gain-of-function senescence animal model was accompanied by improved cardiac function as judged by echocardiographic data on ejection fraction (WT sham: 54.10 % ± 2.09, WT TAC: 23.17 % ± 2.49, CCN1-WT TAC: 35.14 % ± 3.26 %, CCN1-DN TAC: 29.18 % ± 2.79 %, n = 3-6, $P < 0.05$), fractional shortening (WT sham: 27.06 % ± 1.33 %, WT TAC: 11.15 % ± 1.02 %, CCN1-WT TAC: 16.26 % ± 1.63 %, CCN1-DN TAC: 13. 47% ± 1.30%, n = 3-6, $P < 0.05$) and end-systolic volume (WT sham: 36.61 µl ± 3.21µl, WT TAC: 75.76 µl ± 6.12 µl, CCN1-WT TAC: 57.33 µl ± 5.05 µl, CCN1-DN TAC: 69.78 µl ± 9.09 µl, n = 3-6, $P < 0.05$) and end-diastolic volume (WT sham: 77.35 µl ± 4.15 µl, WT TAC: 102.8

µl ± 4.71 µl, CCN1-WT TAC: 89.36 µl ± 3.51 µl, CCN1-DN TAC: 96.81 µl ± 8.81 µl, n = 3-6, *P* < 0.05), as well as left ventricular internal diameter (WT sham: 4.10 mm ± 0.08 mm, WT TAC: 4.57 mm ± 0.12mm, CCN1-WT TAC: 4.40 mm ± 0.08, CCN1-DN TAC: 4.61 mm ± 0.11 mm) (**Fig. 17D**).

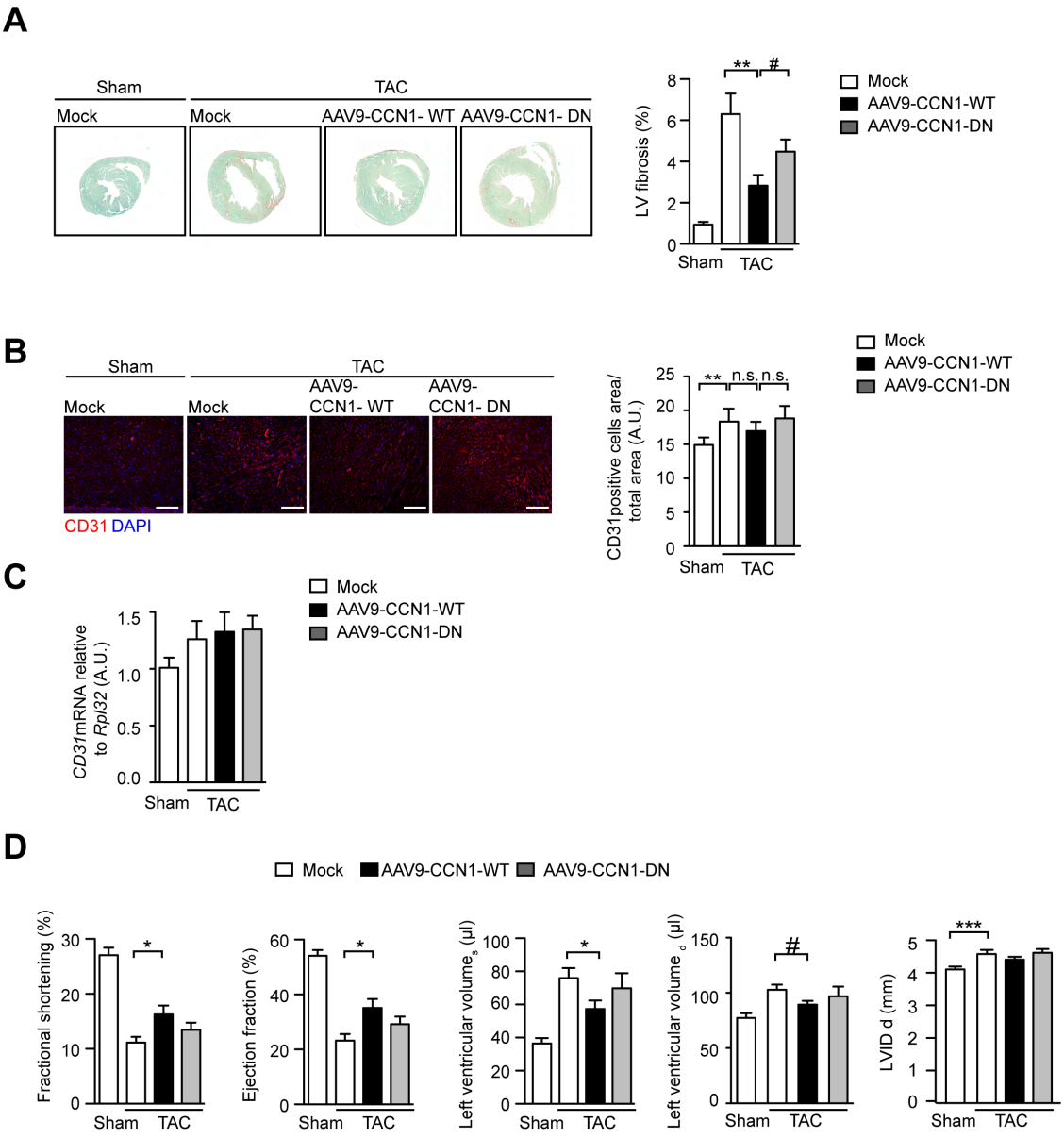

Fig. 17.: CCN1-induced senescence results in decreased left ventricular fibrosis, no changes in angiogenesis and improved heart function. AAV9-CCN1 or AAV9 CCN1-DN or Mock injected mice were treated as described and euthanized for further analysis. Representative images and quantifications of cryo- or paraffin- embedded sections of left ventricular myocardium. (**A**) **Left**, AAV9-CCN1 or AAV9-CCN1-DN or mock injected mice were analyzed for left ventricular interstitial fibrosis, representative images (Sirius red/fast green). **Right**, quantification of left ventricular interstitial fibrosis. n = 4-8. *P* < 0.01 *** *P* < 0.001 (ANOVA). (**B**) Representative images and quantification for immunofluorescence analysis of CD31 (red) and DAPI (blue). n = 4-8. ** *P* < 0.01 (ANOVA), n.s. not significant. Individual cells were analyzed in an automated manner by pixel counting on digitized images. Scale bar = 200 µm. (**C**) Quantitative PCR analysis of the *CD31* gene. n = 4-8. (**D**)

Assessment of parameter for cardiac morphology and function. Left ventricular internal diameter (LVID). n = 4-8. ** $P < 0.05$ *** $P < 0.001$ (t-test). n = 3-6. * $P < 0.05$ (ANOVA), n.s. not significant.

Together, these findings demonstrate that induction of the cellular senescence program in CF restrains perivascular and interstitial fibrosis and improves cardiac function after TAC.

5 Discussion

5.1 Cellular senescence appears within tissue damage and fibrogenesis in the heart

It is demonstrated that senescent cells accumulate within fibrotic tissue after pathologic cardiac challenging, independent of the initial stress stimulus. In TAC, a cardiac pressure overload model with early perivascular reactive fibrosis and interstitial reactive fibrosis, as well as in the ß$_1$-adrenoceptor transgenic mice with compensatory replacement fibrosis due to progressive cardiomyocyte loss, senescent cells accumulate within the scar. This is consistent with studies investigating senescence within fibrogenesis in other organs like liver and skin (Krizhanovsky et al., 2008, J. Il Jun & Lau 2010a, Jun & Lau 2010b, 2010, Kim et al. 2013, Lujambio et al. 2013, Demaria et al. 2014). In the liver, after hepatotoxic CCl_4 treatment, hepatocytes become apoptotic and as a compensatory reaction within the wound healing process, activated stellate cells become synthetic myofibroblasts in order to close the wound by ECM production and finally also become senescent (Krizhanovsky et al., 2008, J. Il Jun & Lau 2010a, Kim et al. 2013, Lujambio et al. 2013). In the skin, after inducing a wound by punching, senescent cells accumulate in the scar after wound closure and fibrogenesis (J. Il Jun & Lau 2010a, Jun & Lau 2010b, Demaria et al. 2014, Baker et al. 2016). Moreover, in human pathologic cardiac samples there is an increase in senescent cells, which are localized at sites of tissue fibrosis. Altogether, this establishes cellular senescence as a basic mechanism during the process of fibrogenesis within wound healing, independent of the organ or the insulting stimulus, and thus independent of the fibrosis type (reactive versus replacement fibrosis). Moreover, senescence accumulates in human fibrotic heart tissue, suggesting senescence as a general phenomenon that also impacts human cardiac pathologies.

5.2 Cardiac (myo)fibroblasts are the senescent cell population within cardiac fibrosis

In alignment with other studies recording that fibroblasts become senescent after insult (Krizhanovsky et al., 2008, J. Il Jun & Lau 2010a, Kim et al. 2013, Lujambio et al. 2013, Demaria et al. 2014, Baker et al. 2016), also (myo)fibroblasts predominantly undergo senescence upon fibrosis induction in the heart. A key event of fibrogenesis in all organs is

the transdifferentiation of fibroblasts into myofibroblasts (Porter & Turner 2009b, Davis & Molkentin 2014). Fibroblasts conduct dynamic ECM homeostasis (Davis & Molkentin 2014). The origins of cardiac fibroblasts are manifold, reaching from proliferation of resident fibroblasts over differentiation from monocytes, fibrocytes, perivascular cells, bone marrow progenitors to endothelial and epithelial cells by EndoMT or EMT. However, the final phenotype of fibroblasts after pathologic cardiac challenging is always a myofibroblast. During a stress situation, fibroblasts become activated and convert into an intermediate state, called proto-myofibroblast. Proto-myofibroblasts are proliferative and produce contractile stress fibers, fibronectin and collagens in order to promote wound healing (van den Borne et al. 2010). Finally, due to tension and other signals, proto-myofibroblastas convert into mature, non-proliferating, mature synthetic myofibroblasts, which express and incorporate α-SMA into complex contractile stress fibers (Davis & Molkentin 2014). Here, evidence for a further differentiation state of a myofibroblast into a senescent myofibroblast is provided. The cardiac senescent myofibroblast is characterized by p21 $^{CIP1/WAF1}$ and p16 ^{INK4a} upregulation and subsequent proliferation arrest. Moreover, SA-ß-galactosidase, as a prominent senescence marker, is upregulated. Several studies have demonstrated that senescent cells (independent of the senescence type) change their gene expression profile towards an ECM degrading shape. Collagens and fibronectins are downregulated, whereas matrix degrading enzymes like and MMP3 and -9 are upregulated (Krizhanovsky et al., 2008). Although it is very likely, that senescent cardiac myofibroblasts exhibit a similar expression profile in the heart, gene expression analysis has to be performed for final proof.

Interestingly, 90 % of p21 $^{CIP1/WAF1}$- or HP1ß- positive cells were positive for the mesenchymal cell marker vimentin or the fibroblast marker PDGFRα, and 60 % were positive for the activated myofibroblast marker α-SMA. Additionally, SA-ß-galactosidase appears already very early at 5 days after TAC (data not shown). This shows, that also fibroblasts or proto-myofibroblasts are senescent, although they do not display the full senescent, anti-proliferative and probably ECM degrading expression profile. However, a recent study demonstrated that SA-ß-gal-positive macrophages are accumulating at sites of senescent cells *in vivo*, which could also account for the SA-ß-gal-positive staining shortly after TAC. The early appearance of senescence in the context of wound healing is consistent with other investigations (J. Il Jun & Lau 2010a, Jun & Lau 2010b, Demaria et al. 2014).

5.3 Triggers of (myo)fibroblast senescence during cardiac fibrosis

According to the different types of cellular senescence, there are several triggers (Muñoz-Espín & Serrano 2014). These are the only criteria discriminating senescence types, since the phenotype is essentially the same in all kinds of senescence.

5.3.1 Telomere-associated senescence

Initially, senescence was described in the context of replicative exhaustion due to telomere attrition (Hayflick & Moorhead 1961). This first *in vitro* phenomenon has been exploited to many *in vivo* findings and is now believed to be the basis of ageing of replication capable tissues and organs. However, it is very unlikely that telomere attrition and telomere-erosion stimuli play a role in inducing senescence after TAC in this study. Although there is an initial hyperproliferation of fibroblasts, which could theoretically lead to telomere shortening, mice in general have very long telomeres (Kipling & Cooke 1990), which do not reach a critical length within this short time period of investigation. Moreover, even telomerase deficient mice have to be bred several generations to sufficiently shorten telomeres to a critical extent (Blasco et al. 1998). Other age-associated stimuli of non-replication capable, post-mitotic tissues (like most adult mammalian organs, also the heart) are also unlikely to be involved in senescence induction after TAC, since the mice operated were not older than 8-9 weeks and have not been investigated for longer than 6 weeks. In summary, age-associated senescence induction does not play a role within this study.

5.3.2 Stress-induced premature senescence

Telomere- and ageing independent senescence is generally termed premature or stress-induced senescence (SIS) and occurs completely independently of the physiological age of organisms, organs or cells (Kuilman et al. 2010, Muñoz-Espín & Serrano 2014). There is now substantial evidence that stressors, e.g. oncogenic signaling, DNA damage or nutrition deprivation can elicit premature types of senescence (Serrano et al. 1997, Campisi & d'Adda di Fagagna 2007). Within the context of cardiac fibrosis it is very likely that the underlying pathology (i.e. hypertrophy or chronic $ß_1$-adrenergic signaling) is the senescence inducing stressor.

CCN1 mediated CM-CF directed senescence induction. It was demonstrated that stress mediated upregulation or ectopic expression of matricellular protein CCN1 elicits senescence of CF *in vitro* and *in vivo*. Mechanistically, CCN1 binds to integrin $\alpha_6\beta_1$ and cell surface heparin sulfate proteoglycans (HSPGs), thereby activating RAC-1-dependent NADPH oxidase1 to trigger a robust and sustained accumulation of reactive oxygen species (ROS). Consequently, CCN1 induces DNA damage response and p53 activation, and triggers the ROS- dependent activation of p38 MAPK and ERK, which in turn activate the $p16^{INK4a}$ / pRb pathways to induce senescence (J.-I. Jun & Lau 2010a). It was observed that endogenous CCN1 is strongly expressed in fibrotic areas after TAC, co-incident with high percentage of senescent cells. This is in accordance with reports of high CCN1 expression levels at sites of tissue repair in liver and skin (C.-C. Chen & Lau 2009). In the heart, ischemia/reperfusion and ischemia alone have been shown to induce a robust CCN1 expression that was associated with cardioprotection (Yoshida et al. 2007, Rother et al. 2010, Zhao et al. 2014, Hinkel et al. 2014).

Whether CCN1-mediated cellular senescence contributes to the beneficial effects observed by Zhao et al. and Hinkel et al. remains to be investigated. It also has to be studied, if CCN1 is one of the key players for senescence induction or if it has only contributing character. Interestingly, CCN1 was shown to be expressed by CM immediately after insult like TAC or myocardial infarction (Hilfiker-Kleiner et al. 2004, Perbal 2013, Zhao et al. 2014, Bonda et al. 2015). In line with these observations, we observed an early CCN1 mRNA increase after TAC only in the CM fraction, although CF display relative high levels of CCN1 mRNA at any time point and without aortic ligation. However, a 3 - fold increase was never observed in CF, whereupon it has been demonstrated in CM 2 and 5 days after TAC, which declines thereafter. In addition, the AAV9-mediated CCN1 overexpression was CM-specific. Due to its secretory nature, the effect on CF and the fact that the protein is detectable 2 and 6 weeks after TAC in scar areas, it is feasible that CCN1 is produced early by stressed CM after TAC (endogenously and exogenously), gets secreted and then associates to the ECM. Likewise, we show that CCN1 is localized at perivascular fibrotic areas. This indicates a CM-CF directed crosstalk after TAC in order to adapt adequately to cardiac insult. In accordance with these data, adenoviral overexpression of CCN1 in neonatal cardiomyocytes and conditioned medium transfer induced senescence in neonatal cardiac fibroblasts *in vitro*. This mimics the in *vivo* situation after increased CCN1 expression and secretion and shows that CM are able to communicate to CF within the heart.

CM-CF directed senescence induction via secreted factors. In addition to CCN1, other factors expressed by CM in the microenvironment of heart injury may promote senescence in fibroblasts and thereby provide evidence for a senescence associated CM-CF crosstalk.

TGF-ß, a key player in cardiac fibrogenesis is upregulated in stretched cardiomyocytes *in vitro* and after pressure overload in CM *in vivo* and finally released into the interstitium. Additionally, TGF-ß is known to induce senescence in many cell types (and is simultaneously able to induce CCN1 mRNA expression) (Leask 2010, Zerlanko et al. 2012, Acosta et al. 2013, Thompson et al. 2014). Moreover, it has been described that TGF-ß induces mRNA expression of the senescence markers $p21^{CIP1/WAF1}$, $p15^{INK4b}$ and $p27^{KIP}$ in fibroblasts and non-fibroblasts (Mulder & Morris 1992, Muñoz-Espín et al. 2013, Morikawa et al. 2016). If TGF-ß is acting upstream of CCN1 and DNA damage or other mediators in this context is not yet known. In developmentally programed senescence TGF-ß signaling plays a crucial role in senescence induction, since DNA microarray analysis and qRT-PCR showed a significant increase in TGF-ß signaling components in senescent versus non-senescent embryonic structures. Moreover, TGF-ß receptor inhibition resulted in remarkable decrease of senescence (Muñoz-Espín et al. 2013). In summary, it is very likely that TGF-ß signaling might play a pivotal role in senescence induction of cardiac fibroblasts. Another factor, which is secreted by cardiac myocytes and released in order to affect non- myocytes is TNF-α (Aoyagi & Matsui 2012). TNF-α is produced by cardiomyocytes after hemodynamic stress and was also found to induce senescence in several cell types (Acosta et al. 2013, Beyne-Rauzy et al. 2004). Thus, a TNF-α dependent senescence induction might play additional roles within the myocardium.

In summary, CCN1, TGF-ß and TNF-α are only some examples, which clearly support a CM-CF directed crosstalk during fibrosis for senescence induction upon cardiac stress.

Non myocyte-CF directed senescence induction. Other factors, released by non-myocytes, underscoring a crosstalk between non-myocyte cell populations, may also contribute to senescence induction after cardiac insult. Endothelial cells, smooth-muscle cells, immune cells or fibroblasts themselves may induce senescence. Myofibroblasts secrete many inflammatory molecules, like Il-1α, IL-1β and IL-6 or ROS, which were shown to induce or reinforce senescence in several cell types (Acosta et al. 2013). As shown in lymphoma studies, attracted immune cells, especially macrophages, contribute to senescence induction by secretion of e.g. TGF-ß (Reimann et al. 2010). Since macrophages accumulate at sites of fibrosis after TAC, this could be another inducing stimulus for fibroblast senescence (Xia et al. 2009, Girgis et al. 2014). Moreover, immune cells are well known to induce inflammation associated reactive oxygen species (ROS), which are known to damage DNA leading to

senescence (Sperka et al. 2012, Muñoz-Espín & Serrano 2014). In summary, compound secretion of inflammatory mediators such as interleukins and ROS as well as fibrosis associated cytokines like TGF-ß or TNF-α and CCN1 can induce fibroblast senescence. Since the expression and release of these senescence triggers is not restricted to one cell type, but rather can be produced by myocytes as well as non-myocytes to a similar extent, senescence might be induced by the coordinated secretion of a cocktail of mediators by many cardiac cells during remodeling.

Senescence induction upon oxygen deregulation. Senescent cells have also been reported to accumulate in the context of hypoxia (Zhu et al. 2013). In alignment with this, CD31 positive cells have been found to be absent in the fibrotic areas after TAC. If hypoxia is contributing to senescence induction within this context has to be figured out. In contrast, there are many findings supporting the fact that hypoxia suppresses senescence (Welford & Giaccia 2011,Lee et al. 2013, Kilic Eren & Tabor 2014).

5.3.3 Maintaining senescence by secondary auto- and paracrine mediators

Once the senescence machinery has been activated, it is known that these cells induce and reinforce senescence in senescence capable neighbor cells in an auto- and paracrine fashion (Kuilman & Peeper 2009, Nelson et al. 2012, Acosta et al. 2013, Hoare & Narita 2013). This happens through direct cell- cell contact or secretory molecules. Direct cell-cell contact enables senescent cells to develop cellular F-actin bridges, transferring proteins to neighboring cells (Biran et al. 2014). The consequences depend strongly on the recipient cell type and it has to be clarified, if senescence can be induced through intercellular protein transfer. In contrast, it has been well described, that senescent cells reinforce senescence by secreted molecules. Especially TNF-α, IL-1α, TGF-ß and IL-6 were prominent candidates in several studies (Kuilman et al. 2008, Acosta et al. 2013). It was shown that IL-6 alone can induce and reinforce senescence in some cell types (Freund et al. 2010), pointing out a key role of the senescence secretome not only in inducing but also in maintaining senescence. Which molecules are secreted by senescent cardiac fibroblasts and their relevance during fibrosis has to be investigated.

5.4 Biological relevance of stress-induced cellular senescence in the heart

5.4.1 A diminished senescence machinery leads to increased fibrosis

Biological relevance of (myo)fibroblast senescence. To determine the biological relevance of senescence, first Trp53 (*Trp53* $^{-/-}$) and p16 ^{INK4a} (*Cdkn2a* $^{-/-}$) single knock out mice have been extensively studied. In contrast to the findings of Zhu et al., but in line with those of Muñoz-Espín et al. (Muñoz-Espín et al. 2013) and Demaria et al. (Demaria et al. 2014), I found that a global genetic ablation of p53 was not sufficient to reduce the number of perivascular SA-ß-gal positive CF. In addition, TAC-induced perivascular and interstitial fibrosis developed to a similar extent in the hearts of *Trp53* $^{+/+}$ and *Trp53* $^{-/-}$ mice 2 and 6 weeks after TAC. In line with these data, no changes in cardiac function were observed. Similar results were obtained with a *Cdkn2a* knockout animal model. These mice display a global deletion of the *Cdkn2a* locus, subsequently eliminating p16 ^{INK4a} and p19 ^{ARF} expression. A decrease in SA-ß-gal positive cells 2 or 6 weeks after TAC could not be observed. Likewise, no effect on fibrosis was found. Similar like the p53 knockout mice, there were no changes in cardiac performance after TAC when compared to wildtype TAC.

Interestingly, heart lysates of *Trp53* $^{-/-}$ *Cdkn2a* $^{+/-}$ mice display a 3.5 - fold compensatory upregulation of p16 ^{INK4a} level when compared to *Trp53* $^{+/+}$ *Cdkn2a* $^{+/+}$ controls. These results underscore that in CF the p53/p21 $^{CIP1/WAF1}$ and p16 ^{INK4a}/Rb pathways act in parallel to execute the cellular senescence program, and that a high degree of functional redundancy exists to perform partially redundant roles. Such a mechanism could provide an extra layer of protection against the bypass of senescence and might be responsible for an undetectable phenotype during pressure overload in the single KO animals. In WT control mice, an upregulation of p16 ^{INK4a} mRNA after TAC was determined, supporting the immunohistochemical data, where an accumulation of p16 ^{INK4a}- positive cells was observed after cardiac insult. Equally, p53 mRNA significantly increases after TAC in WT animals, supporting the finding that the downstream target p21 $^{CIP1/WAF1}$ is increasingly found after cardiac challenging when detected by immunofluorescence staining.

Intriguingly, it was observed that genetic disruption of both *Trp53* and *Cdkn2a* gene loci (DKO) is required to sufficiently reduce CF senescence. As SA-ß-gal was not completely diminished in the DKO, it is likely that other mechanisms than the p53/p21 $^{CIP1/WAF1}$ and p16 ^{INK4a}/Rb pathways can induce senescence, although less efficiently. In the context of

embryonic development, p21 $^{CIP1/WAF1}$ is acting independently of p53 through activation of the TGF-ß pathway (Muñoz-Espín et al. 2013). TGF-ß is highly expressed during cardiac fibrogenesis and it is feasible that a p53 independent p21 $^{CIP1/WAF1}$ activation contributes at least partially to senescence induction. However, in accordance with a significant reduction in senescent cells, there was a significant decrease in perivascular fibrosis 2 weeks after TAC when compared to WT controls or to heterozygous (*Trp53* $^{+/-}$ *Cdkn2a* $^{+/-}$ TAC) littermates. Additionally, interstitial fibrosis increased by trend. However, this was not significant maybe due to the global gene depletion and its consequences on other cell types. In accordance to these observations, a decreased cardiac performance rate of DKO mice was determined after TAC.

Biological relevance of non-fibroblast senescence. Although it was shown that cardiomyocytes and endothelial cells are not becoming senescent after TAC, it does not exclude that senescent fibroblasts influence these cell types in a direct or secretory manner without driving them into senescence. It has been shown that senescent cancer cells influence healthy neighbor cells due to their secretome and immune cell attraction, which can have beneficial or detrimental effects depending on the context (Campisi 2011, Rodier & Campisi 2011). It is likely that senescent fibroblasts in the heart attract immune cells, which in turn act on present cells surrounding the senescent cell population. If and how senescent fibroblasts are communicating towards non-senescence capable neighbor cells in the heart, and which consequences this might have, awaits further investigation.

Roles for Trp53 and Cdkn2a in the cardiovascular system. Since it is a global deletion of *Cdkn2a* and *Trp53*, effects on other cell types may contribute to the detected harmful phenotype during pressure overload. Apart from CF, also CM, endothelial calls, smooth muscle cells and immune cells are of functional relevance in the heart. Considering the fact, that more than 90 % of the senescent cells were fibroblasts, a senescence-associated phenotype of other cell populations may not be of main importance. However, Trp53 and p16 ^{INK4a} may have senescence independent functions in other cardiac cell types that could contribute to the functional outcome observed in the study.

Trp53 function in cardiomyocytes**.** In general it was assumed that p53 expression in CM is proapoptotic and therefore toxic, thus implicating that p53 depletion in CM might be protective during cardiac injury. It was described that p53 expression and subsequently proapoptotic molecules like Bax and PUMA increase after doxorubicin (chemotherapeutic) treatment or hypoxia (Shizukuda et al. 2005; Zhu et al, 2009, Zhu et al. 2014). Nonetheless, a CM specific p53-KO was not sufficient to decrease ROS generation or apoptosis after doxorubicin application. In addition, interstitial as well as perivascular fibrosis was increased.

However, another study showed that antagonizing p53 and Cullin7 (CML7) activity in CM is leading to a cell cycle re-entry of cardiomyocyte after myocardial infarction (Nakajima et al. 2004). In fact, the relevance of p53 in postmitotic cardiomyocyte is not fully understood. Yet, it is unlikely that the described protective p53 depletion in CM is contributing to the rather detrimental phenotype after TAC in the DKO mice.

Trp53 function in endothelial cells. For endothelial cells, p53 depletion is considered to be protective during pressure overload (Sano et al. 2007, Gogiraju et al. 2015). It was found that global and especially endothelial specific p53 depletion de-represses the transcription of hypoxia-inducible factor 1 α f (Hif1α), thus inducing angiogenesis. To test if angiogenesis interferes with this study, CD31 staining was performed and reproduced an increased angiogenesis in both p53 and p16 ^{INK4a} single KO mice when compared to WT during pressure overload. However, this did not lead to changes in cardiac performance or fibrosis development after TAC. Surprisingly, CD31 increase declines in the DKO mice and angiogenesis is similar to WT control animals. For which reasons there is no additive angiogenic effect of p53 and p16 ^{INK4a} depletion in DKO mice, and if angiogenesis is rather a consequence than a modulator within the development of fibrosis after TAC, has to be further investigated.

Trp53 function in immune cells and smooth muscle cells. An effect of p53 depletion on smooth muscle cells and immune cells in the heart has not been investigated yet and was not determined within this study.

Cdkn2a protein functions in the heart. Only little is known about the contribution of p16 ^{INK4a} and p19 ^{ARF} on cardiac remodeling. There are hints that p16 ^{INK4a} is detectable in the heart during norm-oxic conditions and declines after hypoxia, whereas after pressure overload CDKs and cyclins are upregulated (maybe due to a decline in p16I ^{NK4a} levels). In line with these observations, p16 ^{INK4a} overexpression prevents hypertrophy *in vitro* after endothelin 1 (ET-1) stimulation and *in vivo* after pressure overload (Nozato et al. 2001). In accordance CDK4 (target for p16 ^{INK4a} inhibition) overexpression leads to cardiomyocyte hypertrophy in *vitro* (Tamamori-Adachi et al. 2002). Overall, a protective role of p16 ^{INK4a} in the heart is assumed although an accumulation of p16 ^{INK4a} positive cells with age seems to be destructive. In conclusion, the role of p16 ^{INK4a} and p19 ^{ARF} during heart failure and cardiac remodeling has not been fully understood.

In summary, the observed data of the DKO animals clearly demonstrate that deficiency of the senescence machinery (due to Trp53 and p16 ^{INK4a}/p19 ^{ARF} depletion) during pressure

overload is detrimental, which establishes senescence as a protective mechanism within cardiac fibrosis.

5.4.2 An increased senescence machinery leads to extenuated fibrosis

Roles for CCN1 mediated senescence during pressure overload. In order to confirm the hypothesis that senescence is a fibrosis restraining mechanism, cardiac over-activation of senescence was performed. CCN1 is a well established senescence trigger in the liver and in the skin (J. Il Jun & Lau 2010, J.-I. Jun & Lau 2010b, Kim et al. 2013, Borkham-Kamphorst et al. 2014). In line with these observations, it was shown that CCN1-WT can induce senescence *in vitro* and *in vivo* due to its specific integrin $\alpha_6\beta_1$ and heparin sulfate proteoglycan (HSPGs) binding. The double mutant of CCN1 (DN), which is deficient for integrin $\alpha_6\beta_1$ deficient binding was not triggering senescence to the same extent. Therefore, cardiac-specific AAV9-mediated CCN1-WT and CCN1-DN overexpression was performed. As shown, ectopic CCN1-WT and CCN1-DN expression was significantly increased in infected mice on mRNA level as well as on protein level when compared to mock infected mice. In addition, the infection rate (as quantitatively determined by virus particles via qPCR per nucleic acid sample) was directly proportional to the overexpression of the construct (data not shown). Moreover, it was validated that the AAV9 distribution is equal throughout the whole heart and restricted to cardiomyocytes. AAV9 is well known for its strong cardiac, and within the heart, cardiomyocyte specific tropism (Zincarelli et al., 2010). Along with a CCN1 upregulation, there was a significant increase of SA-ß-galactosidase positive cells when normalized to the fibrotic area. However, an overall decrease (%) of perivascular SA-ß-galactosidase accumulation in a non-normalized fashion (which was conducted in the senescence-loss-of-function model) could not be observed (data not shown). A reason for this is the unknown kinetics and fate of senescent cells, so that only the current situation according to fibrosis could be analyzed. In line with that, the SA-ß-galactosidase positive area within a specific fibrotic area was determined. With an increase in senescent cells, a remarkable decrease in fibrosis was observed. Since this effect was not as pronounced in the CCN1-DN injected mice as in the CCN1-WT mice, it is feasible that the fibrosis restriction is mediated through the senescence inducing integrin $\alpha_6\beta_1$ and heparin sulfate proteoglycans (HSPGs) binding to fibroblasts. Although the ectopic expression was CM-specific, the senescence inducing effect was observed in fibroblasts, supporting the notion that CCN1 is secreted and associates to the ECM. In line with these data, CM restricted CCN1

overexpression is able to induce CF senescence *in vitro*. A similar action of CCN1 was observed in the liver, when hepatocyte specific overexpression of CCN1-WT or CCN1-DN mediates stellate cell senescence induction or depletion, respectively (Kim et al., 2013). These observations, together with our findings, clearly demonstrate the secretory nature of CCN1 and thereby establish CCN1 as an intercellular cross-talk mediating molecule during fibrogenesis. Together with the perivascular observations, a prominent overall interstitial fibrosis reduction has been observed, which was significant for CCN1-WT infected mice when compared to mock or CCN1-DN infected animals. Interestingly, also CCN1-DN injected mice show a protection from interstitial fibrosis, indicating that CCN1, despite its integrin $\alpha_6\beta_1$ and heparin sulfate proteoglycan (HSPGs) binding, has protective potential during pressure overload. However, the beneficial outcome is improved, if the senescence inducing domains are functional. As CCN1 is ectopically expressed in CM and is then secreted into the interstitium, an additional CCN1 mediated effect on cell types other than CF may contribute to the protective phenotype. In theory, CCN1 can have an endocrine or autocrine effect on CM itself, as well as consequences on endothelial cells, smooth muscle cells and immune cells. It is shown that CCN1 overexpression can promote cardiomyocyte survival the via $ß_1$-integrin-AKT pathway during oxidative stress (Yoshida et al. 2007). However, it is unlikely that anti-apoptotic effects are playing pivotal roles after TAC, since pressure overload is barely associated with cardiomyocyte death in general and especially after 2 weeks of intervention. In contrast, other investigations claim a toxic effect of CCN1 on cardiomyocytes and show CCN1 mediated CM apoptosis (Hsu et al. 2013). Yet, it is implausible that proapoptotic effects are contributing to the decreased fibrosis and better cardiac performance after TAC.

Further on, a protective role for CCN1 during cardiac challenging has been ruled out and was contributed to its angiogenic ability in previous studies (Grote et al. 2007, Lau 2011b, Hinkel et al. 2014). Although $\alpha_5\beta_3$ integrin binding is mainly responsible for angiogenesis induction (Shimo et al. 1999, Lin et al. 2003, Chen et al. 2004), there is some evidence that also $\alpha_6\beta_1$ binding site (mutated in CCN1-DN) contributes to endothelial tubule formation (Leu et al. 2002). Additionally, one of the $\alpha_5\beta_3$ site is in close proximity to the mutated $\alpha_6\beta_1$ site, which might have some structural and thus functional relevance (C.-C. Chen et al. 2007, Kim et al. 2013). Therefore, endothelial cell proliferation was tested. To test angiogenesis, I performed qRT-PCR analysis and immunofluorescence staining for the endothelial cell marker CD31. As shown, no differences in angiogenesis were observed between the mock or the CCN1-WT and CCN1-DN infected animals after TAC. There was a trend towards increased angiogenesis in the CCN1-DN mice. This slight increase could be the consequence of a

better accessibility of the CCN1 molecule to endothelial cell receptors due to a changed protein folding and thus triggering endothelial cell proliferation. Yet, this effect was not significant.

There are fewer investigations on CCN1 signaling in cardiac immune cells or smooth muscle cells. In the lung, CCN1 suppresses smooth muscle cell contraction resulting in a protective outcome in an animal model of pulmonary hypertension (Lee et al. 2015).

In accordance to the reduced perivascular and interstitial fibrosis after CCN1 overexpression and senescence induction, a better cardiac performance after pressure overload was determined. This is in line with studies investigating CCN1 mediated senescence induction within fibrogenesis in other organs (J. Il Jun & Lau 2010, J.-I. Jun & Lau 2010b, Kim et al. 2013, Borkham-Kamphorst et al. 2014). This is in accordance with previous studies, showing that CCN1 overexpression is protective after cardiac insult, as ischemia/reperfusion, ischemia and myocardial infarction (Hilfiker-Kleiner et al. 2004, Yoshida et al. 2007, Hinkel et al. 2014, Zhao et al. 2014), although the contribution of cellular senescence has not been investigated yet.

In summary, CCN1 mediated CF senescence induction restricts cardiac fibrosis and improves heart function after TAC.

5.5 Chronic senescence and ageing

Some studies have reported an organ destructive outcome for age-associated senescence (Baker et al. 2011, Campisi et al. 2011, Campisi 2013, van Deursen 2014, Baker et al. 2016).

It is known, that the accumulation of senescent cells in many organs (of cardiovascular and non-cardiovascular origin) has detrimental effects, e.g. due to chronic inflammation and regeneration deficiency (Campisi 2013, van Deursen 2014). For the heart, Baker et al. showed that senescent cells accumulate in cardiac tissue with age and that this is negatively associated to cardiac phenotype and function (Baker et al. 2016). This recent study pointed out that depletion of p16 ^{INK4a}- positive cells during ageing reduces age-associated cardiac hypertrophy and improves cardiac function after sub-lethal injection of isoproterenol, indicating that age-associated senescence contributes to tissue ageing and the decline of cardiac function (Baker et al. 2016). However, long-term consequences of CCN1 modulated cardiac senescence induction has not been addressed in this study. Although senescence is by nature initially protective, these cells can turn and become harmful due to an accumulation over time, i.e. during ageing or cancer treatment (treatment induced

senescence, TIS) (Ewald et al. 2010, Dörr et al. 2013). For this reason the organism attempts to clear senescent cells out of the tissue, which successfully happens after induction of cancer or liver fibrosis (Xue et al. 2007, Krizhanovsky et al., 2008, Lujambo, 2016).

5.5.1 Immunosurveillance of senescent cells

There is mounting evidence, that mainly natural killer (NK) cells, CD4-positive cells, T-cells and macrophages interact with and clear senescent cells (Xue et al. 2007, Kang et al. 2011, Krizhanovsky et al., 2008, Muñoz-Espín et al. 2013, Storer et al. 2013). This is the case for senescent stellate cells after liver damage, where an up regulation of the NK receptor natural killer-group 2, member D (NK2D) is crucial for immunosurveillance. In NK2D receptor deficient mice, senescent cells accumulate and become harmful later on. There is the possibility that senescent cardiac fibroblasts are cleared by macrophages or other immune cells, which have been shown to accumulate after TAC in fibrotic regions (Xia et al. 2009, Kuang et al. 2013, Weisheit et al. 2014). Interestingly, it has been shown that myofibroblasts disappear after scarring upon myocardial infarction and it is assumed that apoptosis is the underlying cause. However, a clearance of senescent myofibroblasts might also contribute to the disappearance. In support of this theory, a recent finding pointed out that particularly senescent cells attract mainly macrophages *in vivo* (Hall et al. 2016). If senescent cells are cleared out of the heart after TAC, or if they remain and damage cardiac organ structure and function over time, has to be investigated (ideally with a transient cardiac insult model system).

5.6 Outlook

5.6.1 Why does CF senescence occur during cardiac fibrosis?

Similar to the findings in the skin, liver and kidney, senescence seems to be a basic mechanism during cardiac damage. Senescent cells (as judged by SA-ß-gal) can be observed almost immediately after TAC, which makes it infeasible that senescent fibroblasts per se are anti-fibrotic. More likely, early senescent fibroblasts display pro-remodeling features, although they do not exhibit the full senescence phenotype, i.e. in terms of proliferation arrest and probably gene expression profile. In the skin, senescent fibroblasts occur early after insult and secrete a panel of pro-remodeling molecules in order to accelerate wound closure (Demaria et al. 2014, Campisi, unpublished data.) However, the

presence of senescent cells finally limits skin and liver fibrosis, and importantly also cardiac fibrosis. Since SA-ß-gal positive cells are shown to be present shortly after TAC, but increase fibrosis when absent, a phenotypic switch of early to late senescent CF may exist. Importantly, in other organs when a short-term insult is applied, senescent cells develop anti-fibrotic properties and are transiently expressed (Krizhanovsky et al., 2008, J. Il Jun & Lau 2010a, Jun & Lau 2010b, 2010, Kim et al. 2013, Lujambio et al. 2013, Demaria et al. 2014). Conversely, TAC is a consistent insult, so that there might be a persistent mixture of pro- and anti-remodeling senescent cells. Ideally, a transient cardiac insult can give insight into physiological senescence kinetics and fate of senescent fibroblasts in the heart. With the recently generated mouse models of Demaria et al. (2014) or Baker et al. (2016), it is possible to detect, isolate and *in vivo* visualize senescent cells. The usage of these models can help to understand the different phenotypes of senescent cells during cardiac insult. There is evidence that, depending on the senescence stage, there are different secretion patterns (Campisis, unpublished data), which might explain the different contributions of early and late stage senescent cells in terms of remodeling and fibrogenesis. Senescence is initially protective, acting as a fail-safe mechanism after DNA damage or DNA damage independent stressors (Muñoz-Espín & Serrano 2014, Campisi 2013). In the course of cardiac fibrogenesis, senescent cells accumulate early after insult and may first promote the remodeling and thereby the wound healing process by producing e.g. TGF-ß, Il-1 and TNF-α. Later on, they stop to proliferate and express and secrete ECM degrading molecules such as MMP3 and 9 and decrease fibronectin and collagen expression in order to limit fibrogenesis.

5.6.2 Can senescence induction be a therapeutic tool in general and for limiting or resolving cardiac fibrosis in particular?

Senescence has been manifested as one of the most important tumor suppressive mechanisms in *vivo* (Braig et al. 2005, Braig & Schmitt 2006, Serrano 2007, Reddy & Li 2011, Ohtani et al. 2009, Muñoz-Espín & Serrano 2014). Intriguingly, senescent cells can be detected in many premalignant lesions for example in prostate, lung and skin in mice and humans and disappear during cancer development (Collado et al. 2005, Collado & Serrano 2010, Saab 2011). Most of the common anticancer therapies are chemotherapy and radiation, causing DNA damage and are therefore able to induce senescence. Thus, many partially retrospective, clinical and experimental studies have shown not only apoptosis, but also senescence involvement in limiting tumor growth upon cancer treatment (Roninson 2002, Berns 2002, Schmitt et al. 2002, Roberson et al. 2005, Collado & Serrano 2006b,

Gewirtz et al. 2008, Suzuki & Boothman 2008, Varna et al. 2009, Byun et al. 2009, J.-J. Lee et al. 2011, Ablain et al. 2014, Pérez-Mancera et al. 2014). Additionally, there is evidence for senescence susceptibility of tumors as a predictive tool for treatment outcome (Schmitt et al. 2002, Haugstetter et al. 2010, Althubiti et al. 2014). Therefore, therapy induced senescence (TIS) was developed to directly target senescence for improving cancer treatment (Ewald et al. 2010, Nardella et al. 2011). There is a large number of ongoing clinical trials for TIS, targeting telomerase, CDKIs and p53 (Suzuki & Matsubara 2011, Cheok et al. 2011, Flaherty et al. 2012, Senzer et al. 2013, Finn et al. 2015, DeMichele et al., 2015, Mita et al. 2014, Gopalan et al. 2014, DeMichele et al. 2015, Jafri et al. 2016). Importantly, the p16 mimetic and senescence inducing drug palbociclib has been approved for the treatment of breast cancer in 2015 and is involved in many advanced clinical trials for other cancer types (DeMichele et al.) Despite the fact that the SASP is a key feature of senescent cells, its targeting in treatment remains difficult, since the complexity of composition and context dependent outcome (beneficial and detrimental) has not yet been fully understood (Zhang & Yang 2011, Gordon & Nelson 2012, Campisi, 2013). Plenty of TIS clinical trials have shown an improved outcome after treatment, confirming numerous studies of senescence induced cancer restriction in basic research. Nonetheless, previous *in vitro* and *in vivo* findings strongly support the detrimental outcome of long-term senescence induction during cancer treatment (most likely due to consistent inflammation) (Dörr et al. 2013, Velarde et al. 2013, Tchkonia et al. 2013, van Deursen, 2014, Lujambio 2016, Childs et al. 2014, Lujambio et al., 2016). In summary, senescence induction is a very useful tool in limiting cancer. However, a better understanding of physiological senescence elimination and the SASP is crucial for developing long-term beneficial drugs. The full beneficial effects of cellular senescence may require subsequent elimination of senescent cells by the immune system.

In terms of fibrosis, it has been shown for the liver that CCN1 induced senescence can prevent remodeling after CCL_4 treatment and is even able to resolve fibrosis in treatment based experiments (Kim et al. 2013). In the skin, application of CCN1 and PDGFa was shown to accelerate wound closure by inducing senescence (Demaria et al. 2014). It is obvious, that similar therapeutic approaches are possible for the treatment of cardiac fibrosis although fully beneficial treatment might be dependent on physiological elimination. Further investigations, concentrating on senescence induction, kinetics and the SASP have to uncover how to develop TIS to treat cardiac fibrosis.

5.6.3 Follow-up experiments

In order to modulate cardiac fibroblast senescence, the identification of senescence inducing cells and mediating factors is crucial. It is feasible that there is a prominent CM-CF interaction upon cardiac challenging, which is inducing senescence. To test this hypothesis initially, *in vitro* experiments via co-culture and conditioned medium with primary CM and CF with and without hypertrophy induction can be performed. To further investigate if senescent CF can induce senescence of non-senescent CF, similar co-culture and conditioned medium approaches can be conducted. Moreover, it should be clarified, if secreted factors (conditioned medium) of either CM or CF are able to induce senescence or if direct cell-cell contacts (co-culture) are necessary. However, it is possible that secreted factors may be sufficient to induce senescence as this was shown for other cells, i.e. human fibroblasts (Acosta et al. 2013). To identify molecules secreted by CM or CF, proteome analysis of the conditioned medium of hypertrophied CM versus non-hypertrophied CM and senescent versus non-senescent cells has to be performed. Knock-down or neutralizing experiments can point out the necessity of each of the molecules as well as the described CCN1 to induce senescence. Senescent fibroblasts can be analyzed i.e. via deep sequencing figuring out the ECM associated gene regulation. Most likely, senescence kinetics have to be involved, since early and late stage senescent cells might have different expression profiles. *In vivo*, the 3MR mouse (Demaria et al. 2014) or the INK-ATTAC mouse model (Baker et al. 2011) can be used to identify ECM regulation by senescent fibroblasts, since senescent cells can specifically be killed, *in vivo* visualized and isolated. With similar approaches, it is possible to rule out the cell fate of senescent (myo)fibroblasts and supposable interactions with immune cells.

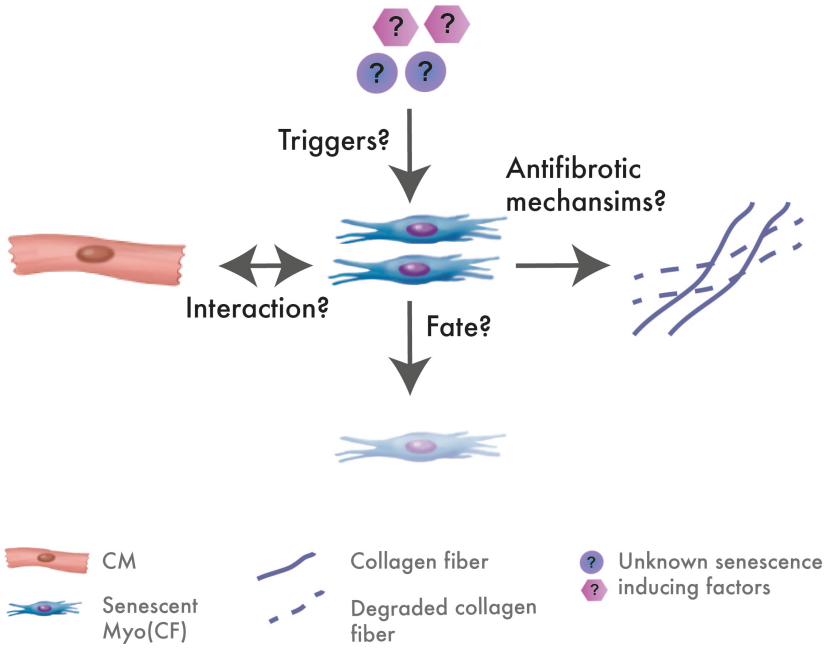

Figure 20: Potential Follow-up questions. Detailed explanations of experimental approaches are described in the text.

6 Summary

In this study, comprehensive evidence for an essential role of premature cellular senescence as a mechanism to restrain cardiac fibrosis was presented. It was demonstrated that senescent cells accumulate in fibrotic myocardial tissue and identified myofibroblasts as predominant cardiac cell population undergoing senescence. Mechanistically, evidence that the cellular senescence program of CF is dependent on both p53/p21 $^{CIP1/WAF1}$ and p16 $^{INK4a/Rb}$ pathways was provided, and it was shown that genetic ablation of *Trp53/Cdkn2a* results in diminished senescence that is associated with aggravated fibrosis and functional impairment of the heart after TAC. Conversely, induction of the cellular senescence program in CF by cardio tropic expression of the matricellular protein CCN1 had cardio protective effects and led to reduced fibrosis and improved cardiac function after TAC. Collectively, our results

reveal senescent fibroblasts as critical regulators of cardiac fibrogenesis, and establish the cellular senescence program as potential target for anti-fibrotic therapies (**Fig. 19**).

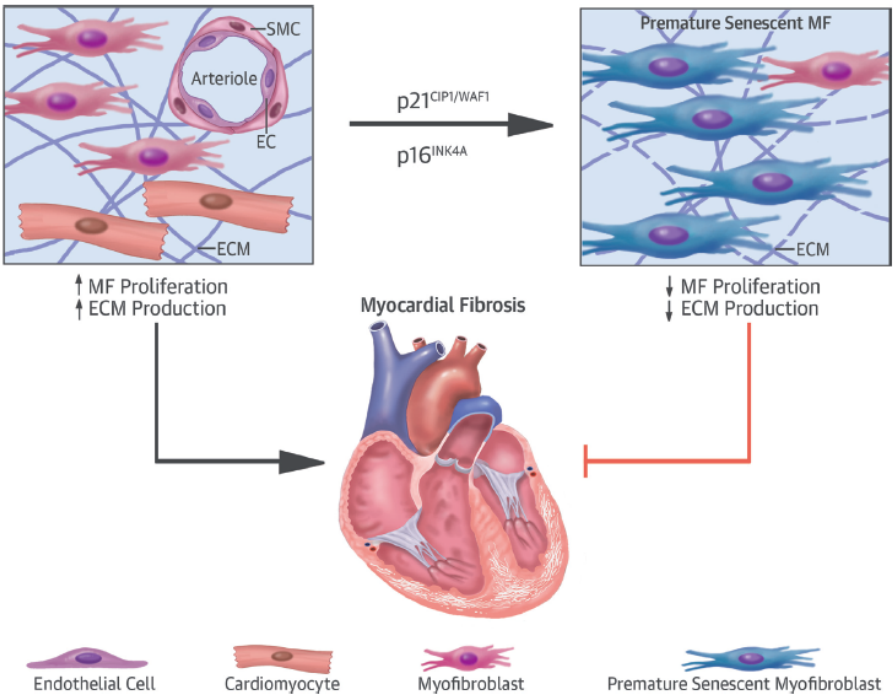

Figure 19: Fibrosis is marked by excessive deposition of extracellular matrix (ECM) by cardiac (myo)fibroblasts (MF), leading to morphologic changes that impair heart function. This study provided evidence that (myo)fibroblasts undergo a state of non–age-dependent premature senescence that restrains myocardial fibrosis. Cellular senescence is mediated by cell cycle inhibitors $p16^{INK4a}$/$p21^{CIP1/WAF1}$ and characterized by an irreversible cell-cycle arrest, enlarged cell morphology, and up-regulation of senescence-associated ß-galactosidase. Several mechanisms may contribute to the anti-fibrotic features of premature senescence in the heart including proliferation arrest of myofibroblasts, thereby reducing the number of ECM-producing cells, curtailing of ECM production,or enhancing degradation of ECM components. EC. endothelial cells; SMC . smooth muscle cells.

7 References

Ablain, J. et al., 2014. Activation of a promyelocytic leukemia-tumor protein 53 axis underlies acute promyelocytic leukemia cure. *Nature medicine*, 20(2), pp.167–74.

Acosta, J.C. et al., 2013. A complex secretory program orchestrated by the inflammasome controls paracrine senescence. *Nature cell biology*, 15(8), pp.978–90.

Acosta, J.C. et al., 2008. Chemokine Signaling via the CXCR2 Receptor Reinforces Senescence. *Cell*, 133(6), pp.1006–1018.

Althubiti, M. et al., 2014. Characterization of novel markers of senescence and their prognostic potential in cancer. *Cell death & disease*, 5(11), p.e1528.

Aoyagi, T. & Matsui, T., 2012. The Cardiomyocyte as a Source of Cytokines in Cardiac Injury. *Journal of Cell Science & Therapy*, 01(S5), pp.3–5.

Baker, D.J. et al., 2011. Clearance of p16Ink4a-positive senescent cells delays ageing-associated disorders. *Nature*, 479(7372), pp.232–6.

Baker, D.J. et al., 2016. Naturally occurring p16 Ink4a -positive cells shorten healthy lifespan. *Nature*, pp.1–5.

Bartkova, J. et al., 2006. Oncogene-induced senescence is part of the tumorigenesis barrier imposed by DNA damage checkpoints. *Nature*, 444(7119), pp.633–637.

Baum, J. & Duffy, H.S., 2011. Fibroblasts and myofibroblasts: what are we talking about? *Journal of cardiovascular pharmacology*, 57(4), pp.376–9.

Beausejour, C.M., 2003. A. Krtolica, . "Reversal of human cellular senescence: roles of the p53 and p16 pathways. *Embo J*, 22(16), pp.4212–4222.

Berns, A., 2002. Senescence: A companion in chemotherapy? *Cancer Cell*, 1(4), pp.309–311.

Besson, A., Dowdy, S.F. & Roberts, J.M., 2008. CDK Inhibitors: Cell Cycle Regulators and Beyond. *Developmental Cell*, 14(2), pp.159–169.

Beyne-Rauzy, O. et al., 2004. Tumor necrosis factor alpha induces senescence and chromosomal instability in human leukemic cells. *Oncogene*, 23(45), pp.7507–16.

Biran, A. et al., 2014. Senescent cells communicate via intercellular protein transfer. *Genes and Development*, 29(8), pp.791–802.

Blasco, M. et al., 1998. Essential role of mouse telomerase in highly proliferative organs.

Nature, 392(6676), pp.569–74.

Bonda, T.A. et al., 2015. Transcriptional and post-transcriptional regulation of CCN genes in failing heart. *Pharmacological Reports*, 67(2), pp.204–208.

Borkham-Kamphorst, E. et al., 2014. The anti-fibrotic effects of CCN1/CYR61 in primary portal myofibroblasts are mediated through induction of reactive oxygen species resulting in cellular senescence, apoptosis and attenuated TGF-?? signaling. *Biochimica et Biophysica Acta - Molecular Cell Research*, 1843(5), pp.902–914.

van den Borne, S.W.M. et al., 2010. Myocardial remodeling after infarction: the role of myofibroblasts. *Nature reviews. Cardiology*, 7(1), pp.30–37.

Bornstein, P. & Sage, E.H., 2002. Matricellular proteins: Extracellular modulators of cell function. *Current Opinion in Cell Biology*, 14(5), pp.608–616.

Boström, H. et al., 1996. PDGF-A signaling is a critical event in lung alveolar myofibroblast development and alveogenesis. *Cell*, 85(6), pp.863–873.

Bracken, A.P. et al., 2007. The Polycomb group proteins bind throughout the INK4A-ARF locus and are disassociated in senescent cells. *Genes and Development*, 21(5), pp.525–530.

Braig, M. et al., 2005. Oncogene-induced senescence as an initial barrier in lymphoma development. *Nature*, 436(7051), pp.660–665.

Braig, M. & Schmitt, C.A., 2006. Oncogene-induced senescence: Putting the brakes on tumor development. *Cancer Research*, 66(6), pp.2881–2884.

Braun, H. et al., 2012. Cellular Senescence Limits Regenerative Capacity and Allograft Survival. *Journal of the American Society of Nephrology*, 23(9), pp.1467–1473.

Brigstock, D.R. et al., 2003. Proposal for a unified CCN nomenclature. *Molecular pathology : MP*, 56, pp.127–128.

Camelliti, P., Borg, T.K. & Kohl, P., 2005. Structural and functional characterisation of cardiac fibroblasts. *Cardiovascular Research*, 65(1), pp.40–51.

Campisi, J. et al., 2011. Cellular senescence: A link between cancer and age-related degenerative disease? *Seminars in Cancer Biology*, 21(6), pp.354–359.

Campisi, J., 2005. Senescent cells, tumor suppression, and organismal aging: Good citizens, bad neighbors. *Cell*, 120(4), pp.513–522.

Campisi, J., 2013. The beginning of the end. *Nature*, 505, pp.35–36.

Campisi, J. & d'Adda di Fagagna, F., 2007. Cellular senescence: when bad things happen to good cells. *Nature reviews. Molecular cell biology*, 8(9), pp.729–740.

Chen, C.-C. et al., 2007. Cytotoxicity of TNFalpha is regulated by integrin-mediated matrix signaling. *The EMBO journal*, 26(5), pp.1257–67.

Chen, C.-C., Kim, K.-H. & Lau, L.F., 2015. The matricellular protein CCN1 suppresses hepatocarcinogenesis by inhibiting compensatory proliferation. *Oncogene*, 35(April), pp.1–10.

Chen, C.-C. & Lau, L.F., 2009. Functions and mechanisms of action of CCN matricellular proteins. *The international journal of biochemistry & cell biology*, 41(4), pp.771–83.

Chen, J.H., Hales, C.N. & Ozanne, S.E., 2007. DNA damage, cellular senescence and organismal ageing: Causal or correlative? *Nucleic Acids Research*, 35(22), pp.7417–7428.

Chen, N. et al., 2004. Identification of a novel integrin αvβ3 binding site in CCN1 (CYR61) critical for pro-angiogenic activities in vascular endothelial cells. *Journal of Biological Chemistry*, 279(42), pp.44166–44176.

Chen, Z. et al., 2005. Crucial role of p53-dependent cellular senescence in suppression of Pten-deficient tumorigenesis. *Nature*, 436(7051), pp.725–730.

Cheok, C.F. et al., 2011. Translating p53 into the clinic. *Nature Reviews. Clinical Oncology*, 8(January 2011), pp.25–37.

Childs, B.G. et al., 2014. Senescence and apoptosis: dueling or complementary cell fates? *EMBO reports*, 15(11), pp.1139–53.

Christophorou, M. a et al., 2006. The pathological response to DNA damage does not contribute to p53-mediated tumour suppression. *Nature*, 443(7108), pp.214–217.

Clements, M.E. et al., 2013. Increased Cellular Senescence and Vascular Rarefaction Exacerbate the Progression of Kidney Fibrosis in Aged Mice Following Transient Ischemic Injury. *PLoS ONE*, 8(8).

Collado, M. et al., 2005. Tumour biology: senescence in premalignant tumours. *Nature*, 436(7051), p.642.

Collado, M., Blasco, M.A. & Serrano, M., 2007. Cellular senescence in cancer and aging. *Cell*, 130(2), pp.223–33.

Collado, M. & Serrano, M., 2010a. Senescence in tumours: evidence from mice and humans. *Nature reviews. Cancer*, 10(1), pp.51–57.

Collado, M. & Serrano, M., 2010b. Senescence in tumours: evidence from mice and humans. *Nature reviews. Cancer*, 10(1), pp.51–57.

Collado, M. & Serrano, M., 2006a. The power and the promise of oncogene-induced senescence markers. *Nature reviews. Cancer*, 6(6), pp.472–6.

Cooke, M.S. et al., 2003. Oxidative DNA damage: mechanisms, mutation, and disease. *FASEB journal*, 17(10), pp.1195–214.

Coppé, J.-P. et al., 2008. Senescence-associated secretory phenotypes reveal cell-nonautonomous functions of oncogenic RAS and the p53 tumor suppressor. *PLoS biology*, 6(12), pp.2853–68.

Coppé, J.-P. et al., 2010. The senescence-associated secretory phenotype: the dark side of tumor suppression. *Annual review of pathology*, 5, pp.99–118.

Courtois-Cox, S. et al., 2006. A negative feedback signaling network underlies oncogene-induced senescence. *Cancer Cell*, 10(6), pp.459–472.

d'Adda di Fagagna, F., 2008. Living on a break: cellular senescence as a DNA-damage response. *Nature reviews. Cancer*, 8(7), pp.512–522.

Davis, J. & Molkentin, J.D., 2014. Myofibroblasts: Trust your heart and let fate decide. *Journal of Molecular and Cellular Cardiology*, 70, pp.9–18.

Demaria, M. et al., 2014. An essential role for senescent cells in optimal wound healing through secretion of PDGF-AA. *Developmental Cell*, 31(6), pp.722–733.

DeMichele, A. et al., 2015. CDK 4/6 Inhibitor palbociclib (PD0332991) in Rb^+ advanced breast cancer: Phase II activity, safety, and predictive biomarker assessment. *Clinical Cancer Research*, 21(5), pp.995–1001.

van Deursen, J.M., 2014. The role of senescent cells in ageing. *Nature*, 509(7501), pp.439–446.

Díez, J. et al., 2001. Clinical aspects of hypertensive myocardial fibrosis. *Current opinion in cardiology*, 16(6), pp.328–335.

Dimri, G.P. et al., 1995. A biomarker that identifies senescent human cells in culture and in aging skin in vivo. *Proceedings of the National Academy of Sciences*, 92(20), pp.9363–9367.

DiRocco, D.P. et al., 2014. CDK4/6 inhibition induces epithelial cell cycle arrest and ameliorates acute kidney injury. *American journal of physiology. Renal physiology*, 306(4), pp.F379–88.

Dörr, J.R. et al., 2013. Synthetic lethal metabolic targeting of cellular senescence in cancer therapy. *Nature*, 501(7467), pp.421–425.

Du, J. et al., 2014. Aging increases CCN1 expression leading to muscle senescence. *American journal of physiology. Cell physiology*, 306(1), pp.C28–36.

Engelhardt, S. et al., 1999. Progressive hypertrophy and heart failure in beta1-adrenergic receptor transgenic mice. *Proceedings of the National Academy of Sciences of the United States of America*, 96(12), pp.7059–64.

Ewald, J.A. et al., 2010. Therapy-induced senescence in cancer. *Journal of the National Cancer Institute*, 102(20), pp.1536–1546.

di Fagagna, F. d'Adda et al., 2003. A DNA damage checkpoint response in telomere-initiated senescence. *Nature*, 426(6963), pp.194–198.

Falke, L.L. et al., 2015. Diverse origins of the myofibroblast—implications for kidney fibrosis. *Nature reviews. Nephrology*, 11(4), pp.233–44.

Fataccioli, V. et al., 2002. Stimulation of angiogenesis by cyr61 gene: a new therapeutic candidate. *Hum.Gene Ther.*, 13(12), pp.1461–1470.

Finn, R.S. et al., 2015. The cyclin-dependent kinase 4/6 inhibitor palbociclib in combination with letrozole versus letrozole alone as first-line treatment of oestrogen receptor-positive, HER2-negative, advanced breast cancer (PALOMA-1/TRIO-18): A randomised phase 2 study. *The Lancet Oncology*, 16(1), pp.25–35.

Flaherty, K.T. et al., 2012. Phase I, dose-escalation trial of the oral cyclin-dependent kinase 4/6 inhibitor PD 0332991, administered using a 21-day schedule in patients with advanced cancer. *Clinical Cancer Research*, 18(2), pp.568–576.

Franzen, C.A. et al., 2009. Matrix protein CCN1 is critical for prostate carcinoma cell proliferation and TRAIL-induced apoptosis. *Molecular cancer research : MCR*, 7(7), pp.1045–55.

Freund, A. et al., 2010. Inflammatory networks during cellular senescence: causes and consequences. *Trends in Molecular Medicine*, 16(5), pp.238–246.

Freund, A. et al., 2012. Lamin B1 loss is a senescence-associated biomarker. *Molecular biology of the cell*, 23(11), pp.2066–75.

Gabbiani, G., 2003. The myofibroblast in wound healing and fibrocontractive diseases. *Journal of Pathology*, 200(4), pp.500–503.

Gewirtz, D.A., Holt, S.E. & Elmore, L.W., 2008. Accelerated senescence: An emerging role in

tumor cell response to chemotherapy and radiation. *Biochemical Pharmacology*, 76(8), pp.947–957.

Girgis, N.M. et al., 2014. Ly6Chigh Monocytes Become Alternatively Activated Macrophages in Schistosome Granulomas with Help from CD4+ Cells. *PLoS Pathogens*, 10(6).

Gogiraju, R. et al., 2015. Endothelial p53 Deletion Improves Angiogenesis and Prevents Cardiac Fibrosis and Heart Failure Induced by Pressure Overload in Mice. *Journal of the American Heart Association*, 4(2), pp.1–22.

Gopalan, P.K. et al., 2014. A phase II clinical trial of the CDK 4/6 inhibitor palbociclib (PD 0332991) in previously treated, advanced non-small cell lung cancer (NSCLC) patients with inactivated CDKN2A. *Journal of Clinical Oncology*, 32(15), p.1291017.

Gordon, R.R. & Nelson, P.S., 2012. Cellular senescence and cancer chemotherapy resistance. *Drug resistance updates : reviews and commentaries in antimicrobial and anticancer chemotherapy*, 15(1-2), pp.123–31.

Grote, K. et al., 2007. The angiogenic factor CCN1 promotes adhesion and migration of circulating CD34+ progenitor cells: Potential role in angiogenesis and endothelial regeneration. *Blood*, 110(3), pp.877–885.

Guachalla, L.M. & Rudolph, K.L., 2010. ROS induced DNA damage and checkpoint responses: Influences on aging? *Cell Cycle*, 9(20), pp.4058–4060.

Guevara, N. V et al., 1999. The absence of p53 accelerates atherosclerosis by increasing cell proliferation in vivo. *Nat. Med.*, 5(3), pp.335–339.

Hall, B.M. et al., 2016. Aging of mice is associated with p16 (Ink4a) ‐ and β ‐ galactosidase ‐ positive macrophage accumulation that can be induced in young mice by senescent cells. , 8(7), pp.1–22.

Han, J.S. et al., 2003. Regulation of Cyr61/CCN1 gene expression through RhoA GTPase and p38MAPK signaling pathways: Role of CREB and AP-1 transcription factors. *European Journal of Biochemistry*, 270(16), pp.3408–3421.

Harley, C.B., Futcher, A.B. & Greider, C.W., 1990. Telomeres shorten during ageing of human fibroblasts. *Nature*, 345(6274), pp.458–60.

Haseley, A. et al., 2012. Extracellular matrix protein CCN1 limits oncolytic efficacy in glioma. *Cancer Research*, 72(6), pp.1353–1362.

Haugstetter, a M. et al., 2010. Cellular senescence predicts treatment outcome in

metastasised colorectal cancer. *British journal of cancer*, 103, pp.505–509.

Hayflick, L. & Moorhead, P.S., 1961. the Serial Cultivation of Human Diploid Cell Strains. *Experimental cell research*, 1.

Henley, S.A. & Dick, F.A., 2012. The retinoblastoma family of proteins and their regulatory functions in the mammalian cell division cycle. *Cell division*, 7(1), p.10.

Herbig, U. et al., 2004. Telomere shortening triggers senescence of human cells through a pathway involving ATM, p53, and p21CIP1, but not p16INK4a. *Molecular Cell*, 14(4), pp.501–513.

Herbig, U. & Sedivy, J.M., 2006. Regulation of growth arrest in senescence: Telomere damage is not the end of the story. *Mechanisms of Ageing and Development*, 127(1), pp.16–24.

Hilfiker-Kleiner, D. et al., 2004. Regulation of Proangiogenic Factor CCN1 in Cardiac Muscle: Impact of Ischemia, Pressure Overload, an Neurohumoral Activation. *Circulation*, 109(18), pp.2227–2233.

Hilfiker, A. et al., 2002. Expression of CYR61, an angiogenic immediate early gene, in arteriosclerosis and its regulation by angiotensin II. *Circulation*, 106(2), pp.254–260.

Hinkel, R. et al., 2014. MRTF-A controls vessel growth and maturation by increasing the expression of CCN1 and CCN2. *Nature communications*, 5, p.3970.

Hoare, M. & Narita, M., 2013. Transmitting senescence to the cell neighbourhood. *Nature cell biology*, 15(8), pp.887–889.

Hsu, P.L. et al., 2013. Extracellular matrix protein CCN1 regulates cardiomyocyte apoptosis in mice with stress-induced cardiac injury. *Cardiovascular Research*, 98(1), pp.64–72.

Hulot, J.-S. et al., 2011. Critical role for stromal interaction molecule 1 in cardiac hypertrophy. *Circulation*, 124(7), pp.796–805.

Humphreys, B.D. et al., 2010. Fate tracing reveals the pericyte and not epithelial origin of myofibroblasts in kidney fibrosis. *The American journal of pathology*, 176(1), pp.85–97.

Hung, C. et al., 2013. Role of lung Pericytes and resident fibroblasts in the pathogenesis of pulmonary fibrosis. *American Journal of Respiratory and Critical Care Medicine*, 188(7), pp.820–830.

Jafri, M.A. et al., 2016. Roles of telomeres and telomerase in cancer, and advances in telomerase-targeted therapies. *Genome Medicine*, 8(1), p.69.

Jay, P. et al., 1997. The human growth factor-inducible immediate early gene, CYR61, maps to chromosome 1p. *Oncogene*, 14(14), pp.1753–1757.

Jim Leu, S.J. et al., 2013. The matricellular protein CCN1 suppresses lung cancer cell growth by inducing senescence via the p53/p21 pathway. *Journal of Cellular Biochemistry*, 114(9), pp.2082–2093.

Jones, S.L. & Cichowski, K., 2008. Many roads lead to oncogene-induced senescence. *Oncogene*, 27, pp.2801–2809.

Jun, J. Il & Lau, L.F., 2010. Cellular senescence controls fibrosis in wound healing. *Aging*, 2(9), pp.627–631.

Jun, J.-I. & Lau, L.F., 2011. Taking aim at the extracellular matrix: CCN proteins as emerging therapeutic targets. *Nature reviews. Drug discovery*, 10(12), pp.945–63.

Jun, J.-I. & Lau, L.F., 2010. The matricellular protein CCN1 induces fibroblast senescence and restricts fibrosis in cutaneous wound healing. *Nature cell biology*, 12(7), pp.676–85.

Juric, V., Chen, C.-C. & Lau, L.F., 2009. Fas-mediated apoptosis is regulated by the extracellular matrix protein CCN1 (CYR61) in vitro and in vivo. *Molecular and cellular biology*, 29(12), pp.3266–3279.

Kang, T.-W. et al., 2011. Senescence surveillance of pre-malignant hepatocytes limits liver cancer development. *Nature*, 479(7374), pp.547–551.

Khanna, A.K., 2009. Enhanced susceptibility of cyclin kinase inhibitor p21 knockout mice to high fat diet induced atherosclerosis. *Journal of biomedical science*, 16(1), p.66.

Kilic Eren, M. & Tabor, V., 2014. The role of hypoxia inducible factor-1 alpha in bypassing oncogene-induced senescence. *PloS one*, 9(7), p.e101064.

Kim, K.-H. et al., 2013. Matricellular protein CCN1 promotes regression of liver fibrosis through induction of cellular senescence in hepatic myofibroblasts. *Molecular and cellular biology*, 33(10), pp.2078–90.

Kim, K.S. et al., 2007. Induction of cellular senescence by insulin-like growth factor binding protein-5 through a p53-dependent mechanism. *Molecular biology of the cell*, 18(11), pp.4543–52.

Kim, W.Y. & Sharpless, N.E., 2006. The Regulation of INK4/ARF in Cancer and Aging. *Cell*, 127(2), pp.265–275.

Kipling, D. & Cooke, H.J., 1990. Hypervariable ultra-long telomeres in mice. *Letters To Nature*, 347, pp.400–402.

Kong, P., Christia, P. & Frangogiannis, N.G., 2014. The pathogenesis of cardiac fibrosis. *Cellular and Molecular Life Sciences*, 71(4), pp.549–574.

Kong, X. et al., 2012. Interleukin-22 induces hepatic stellate cell senescence and restricts liver fibrosis in mice. *Hepatology*, 56(3), pp.1150–1159.

Krenning, G., Zeisberg, E.M. & Kalluri, R., 2010. The origin of fibroblast and mechanism of cardiac fibrosis. *Journal of cell physiology*, 225(3), pp.631–637.

Krizhanovsky, V. et al., 2008. Senescence of Activated Stellate Cells Limits Liver Fibrosis. *Cell*, 134(4), pp.657–667.

Kuang, S.Q. et al., 2013. Aortic remodeling after transverse aortic constriction in mice is attenuated with AT1 receptor blockade. *Arteriosclerosis, Thrombosis, and Vascular Biology*, 33(9), pp.2172–2179.

Kuilman, T. et al., 2008. Oncogene-Induced Senescence Relayed by an Interleukin-Dependent Inflammatory Network. *Cell*, 133(6), pp.1019–1031.

Kuilman, T. et al., 2010. The essence of senescence. *Genes and Development*, 24(22), pp.2463–2479.

Kuilman, T. & Peeper, D.S., 2009. Senescence-messaging secretome: SMS-ing cellular stress. *Nature reviews. Cancer*, 9(2), pp.81–94.

Kurz, D.J. et al., 2000. Senescence-associated (beta)-galactosidase reflects an increase in lysosomal mass during replicative ageing of human endothelial cells. *Journal of cell science*, 113 (Pt 2, pp.3613–22.

Kurz, E.U. & Lees-Miller, S.P., 2004. DNA damage-induced activation of ATM and ATM-dependent signaling pathways. *DNA Repair*, 3(8-9), pp.889–900.

Laberge, R.-M. et al., 2015. MTOR regulates the pro-tumorigenic senescence-associated secretory phenotype by promoting IL1A translation. *Nature cell biology*, 17(8), pp.1049–1061.

LaPak, K.M. & Burd, C.E., 2014. The molecular balancing act of p16(INK4a) in cancer and aging. *Molecular cancer research : MCR*, 12(2), pp.167–83.

Lau, L.F., 2011a. CCN1/CYR61: The very model of a modern matricellular protein. *Cellular and Molecular Life Sciences*, 68(19), pp.3149–3163.

Lau, L.F., 2011b. CCN1/CYR61: The very model of a modern matricellular protein. *Cellular and Molecular Life Sciences*, 68(19), pp.3149–3163.

Lau, L.F., 2016. Cell surface receptors for CCN proteins. *Journal of Cell Communication and Signaling*, pp.1–7.

Leask, A., 2011. CCN1: A novel target for pancreatic cancer. *Journal of Cell Communication and Signaling*, 5(2), pp.123–124.

Leask, A., 2015. Getting to the heart of the matter: New insights into cardiac fibrosis. *Circulation Research*, 116(7), pp.1269–1276.

Leask, A., 2010. Potential therapeutic targets for cardiac fibrosis: TGF??, angiotensin, endothelin, CCN2, and PDGF, partners in fibroblast activation. *Circulation Research*, 106(11), pp.1675–1680.

Leask, A., 2007. TGF??, cardiac fibroblasts, and the fibrotic response. *Cardiovascular Research*, 74(2), pp.207–212.

Lee, B.Y. et al., 2006. Senescence-associated β-galactosidase is lysosomal β-galactosidase. *Aging Cell*, 5(2), pp.187–195.

Lee, S., Schmitt, C.A. & Reimann, M., 2011. The Myc/macrophage tango: Oncogene-induced senescence, Myc style. *Seminars in Cancer Biology*, 21(6), pp.377–384.

Lee, S.-J. et al., 2015. CCN1 suppresses pulmonary vascular smooth muscle contraction in response to hypoxia. *Pulmonary circulation*, 5(4), pp.716–722.

Lee, S.H. et al., 2013. Hypoxia inhibits cellular senescence to restore the therapeutic potential of old human endothelial progenitor cells via the hypoxia-inducible factor-1α-TWIST-p21 Axis. *Arteriosclerosis, Thrombosis, and Vascular Biology*, 33(10), pp.2407–2414.

Leu, S.-J., Lam, S.C.-T. & Lau, L.F., 2002. Pro-angiogenic activities of CYR61 (CCN1) mediated through integrins alphavbeta3 and alpha6beta1 in human umbilical vein endothelial cells. *The Journal of biological chemistry*, 277(48), pp.46248–55.

Lin, A.W. et al., 1998. Premature senescence involving p53 and p16 is activated in response to constitutive MEK/MAPK mitogenic signaling. *Genes and Development*, 12(19), pp.3008–3019.

Longo, D.L. et al., 2015. Fibrosis — A Common Pathway to Organ Injury and Failure. *New England Journal of Medicine*, 372(12), pp.1138–1149.

Lorell, B.H. & Carabello, B. a, 2000. Clinical Cardiology : New Frontiers Left Ventricular Hypertrophy. , pp.470–479.

Lujambio, A. et al., 2013. Non-cell-autonomous tumor suppression by p53. *Cell*, 153(2),

pp.449–460.

Lujambio, A., 2016. To clear, or not to clear (senescent cells)? That is the question. *Inside the Cell*, pp.1–9.

Macip, S. et al., 2002. Inhibition of p21-mediated ROS accumulation can rescue p21-induced senescence. *EMBO Journal*, 21(9), pp.2180–2188.

Martin, N. et al., 2013. Interplay between Homeobox proteins and Polycomb repressive complexes in p16INK4a regulation. *The EMBO Journal*, 32(7), pp.982–995.

Melk, A. et al., 2004. Expression of p16INK4a and other cell cycle regulator and senescence associated genes in aging human kidney. *Kidney International*, 65(2), pp.510–520.

Mercer, J. et al., 2005. Endogenous p53 protects vascular smooth muscle cells from apoptosis and reduces atherosclerosis in ApoE knockout mice. *Circulation Research*, 96(6), pp.667–674.

Di Micco, R. et al., 2006. Oncogene-induced senescence is a DNA damage response triggered by DNA hyper-replication. *Nature*, 444(7119), pp.638–642.

Mita, M.M. et al., 2014. Randomized phase II trial of the cyclin-dependent kinase inhibitor Dinaciclib (MK-7965) versus capecitabine in patients with advanced breast cancer. *Clinical Breast Cancer*, 14(3), pp.169–176.

Mizuno, S. et al., 2011. p53 Gene deficiency promotes hypoxia-induced pulmonary hypertension and vascular remodeling in mice. *American journal of physiology. Lung cellular and molecular physiology*, 300(5), pp.L753–61.

Mooi, W.J. & Peeper, D.S., 2006. Oncogene-induced cell senescence--halting on the road to cancer. *The New England journal of medicine*, 355(10), pp.1037–1046.

Moore-morris, T. et al., 2014. Resident fi broblast lineages mediate pressure overload – induced cardiac fi brosis. *The Journal of Clinical Investigation*, 124(7), pp.1–14.

Moore, C.S. & Crocker, S.J., 2012. An alternate perspective on the roles of TIMPs and MMPs in pathology. *American Journal of Pathology*, 180(1), pp.12–16.

Moore, L. et al., 2012. Tissue inhibitor of metalloproteinases (TIMPs) in heart failure. *Heart Failure Reviews*, 17(4), pp.693–706.

Morikawa, M., Derynck, R. & Miyazono, K., 2016. pendent TGF-β and the TGF-β Family: Context-DeRoles in Cell and Tissue Physiology. *Cold Spring Harbor perspectives in biology*, 8(5).

Morrison, C.J. et al., 2009. Matrix metalloproteinase proteomics: substrates, targets, and therapy. *Current Opinion in Cell Biology*, 21(5), pp.645–653.

Mouraret, N. et al., 2013. Activation of lung p53 by nutlin-3a prevents and reverses experimental pulmonary hypertension. *Circulation*, 127(16), pp.1664–1676.

Mozaffarian, D. et al., 2015. *Heart disease and stroke statistics-2015 update : A report from the American Heart Association*,

Muller, P.A.J. & Vousden, K.H., 2014. Mutant p53 in cancer: New functions and therapeutic opportunities. *Cancer Cell*, 25(3), pp.304–317.

Muñoz-Espín, D. et al., 2013. Programmed cell senescence during mammalian embryonic development. *Cell*, 155(5), pp.1104–18.

Muñoz-Espín, D. & Serrano, M., 2014. Cellular senescence: from physiology to pathology. *Nature reviews. Molecular cell biology*, 15(7), pp.482–96.

Naesens, M., 2011. Replicative senescence in kidney aging, renal disease, and renal transplantation. *Discovery medicine*, 11(56), pp.65–75.

Nakajima, H. et al., 2004. Expression of mutant p193 and p53 permits cardiomyocyte cell cycle reentry after myocardial infarction in transgenic mice. *Circulation Research*, 94(12), pp.1606–1614.

Nardella, C. et al., 2011. Pro-senescence therapy for cancer treatment. *Nature Reviews Cancer*, 11(7), pp.503–511.

Narita, M. et al., 2006. A Novel Role for High-Mobility Group A Proteins in Cellular Senescence and Heterochromatin Formation. *Cell*, 126(3), pp.503–514.

Narita, M. et al., 2003. Rb-mediated heterochromatin formation and silencing of E2F target genes during cellular senescence. *Cell*, 113(6), pp.703–716.

Nelson, G. et al., 2012. A senescent cell bystander effect: Senescence-induced senescence. *Aging Cell*, 11(2), pp.345–349.

Nozato, T. et al., 2001. Overexpression of cdk Inhibitor p16INK4a by adenovirus vector inhibits cardiac hypertrophy in vitro and in vivo: a novel strategy for the gene therapy of cardiac hypertrophy. *Journal of molecular and cellular cardiology*, 33(8), pp.1493–504.

Ohtani, N. et al., 2004. The p16INK4a-RB pathway: molecular link between cellular senescence and tumor suppression. *The journal of medical investigation : JMI*, 51(3-4), pp.146–53.

Ohtani, N., Mann, D.J. & Hara, E., 2009. Cellular senescence: Its role in tumor suppression and aging. *Cancer Science*, 100(5), pp.792–797.

Orjalo, A. V et al., 2009. Cell surface-bound IL-1alpha is an upstream regulator of the senescence-associated IL-6/IL-8 cytokine network. *Proceedings of the National Academy of Sciences of the United States of America*, 106(40), pp.17031–6.

Passos, J.F. et al., 2010. Feedback between p21 and reactive oxygen production is necessary for cell senescence. *Molecular systems biology*, 6(347), p.347.

Perbal, B., 2013. CCN proteins: A centralized communication network. In *Journal of Cell Communication and Signaling*. pp. 169–177.

Pérez-Mancera, P.A., Young, A.R.J. & Narita, M., 2014. Inside and out: the activities of senescence in cancer. *Nature reviews. Cancer*, 14(8), pp.547–558.

Pinto, A.R. et al., 2016. Revisiting cardiac cellular composition. *Circulation Research*, 118(3), pp.400–409.

Porter, K.E. & Turner, N.A., 2009a. Cardiac fibroblasts: At the heart of myocardial remodeling. *Pharmacology and Therapeutics*, 123(2), pp.255–278.

Porter, K.E. & Turner, N.A., 2009b. Cardiac fibroblasts: At the heart of myocardial remodeling. *Pharmacology and Therapeutics*, 123(2), pp.255–278.

Reddy, J.P. & Li, Y., 2011. Oncogene-induced senescence and its role in tumor suppression. *Journal of Mammary Gland Biology and Neoplasia*, 16(3), pp.247–256.

Reimann, M. et al., 2010. Tumor Stroma-Derived TGF-?? Limits Myc-Driven Lymphomagenesis via Suv39h1-Dependent Senescence. *Cancer Cell*, 17(3), pp.262–272.

Ressler, S. et al., 2006. p16INK4A is a robust in vivo biomarker of cellular aging in human skin. *Aging Cell*, 5(5), pp.379–389.

Roberson, R.S. et al., 2005. Escape from therapy-induced accelerated cellular senescence in p53-null lung cancer cells and in human lung cancers. *Cancer research*, 65(7), pp.2795–2803.

Rockman, H.A. et al., 1991. Segregation of atrial-specific and inducible expression of an atrial natriuretic factor transgene in an in vivo murine model of cardiac hypertrophy. *Proceedings of the National Academy of Sciences of the United States of America*, 88(18), pp.8277–81.

Rodier, F. et al., 2011. DNA-SCARS: distinct nuclear structures that sustain damage-induced

senescence growth arrest and inflammatory cytokine secretion. *Journal of cell science*, 124(Pt 1), pp.68–81.

Rodier, F. et al., 2009. Persistent DNA damage signalling triggers senescence-associated inflammatory cytokine secretion. *Nature cell biology*, 11(8), pp.973–9.

Rodier, F. & Campisi, J., 2011. Four faces of cellular senescence. *Journal of Cell Biology*, 192(4), pp.547–556.

Rodríguez, D., Morrison, C.J. & Overall, C.M., 2010. Matrix metalloproteinases: What do they not do? New substrates and biological roles identified by murine models and proteomics. *Biochimica et Biophysica Acta - Molecular Cell Research*, 1803(1), pp.39–54.

Roninson, I.B., 2002. Tumor senescence as a determinant of drug response in vivo. *Drug Resistance Updates*, 5(5), pp.204–208.

Rossiello, F. et al., 2014. Irreparable telomeric DNA damage and persistent DDR signalling as a shared causative mechanism of cellular senescence and ageing. *Current Opinion in Genetics and Development*, 26, pp.89–95.

Rother, M. et al., 2010. Matricellular signaling molecule CCN1 attenuates experimental autoimmune myocarditis by acting as a novel immune cell migration modulator. *Circulation*, 122(25), pp.2688–2698.

Saab, R., 2011. Senescence and pre-malignancy: How do tumors progress? *Seminars in Cancer Biology*, 21(6), pp.385–391.

Samani, N.J. & Schunkert, H., 2008. Chromosome 9p21 and cardiovascular disease: the story unfolds. *Circulation. Cardiovascular genetics*, 1(2), pp.81–4.

Sano, M. et al., 2007. p53-induced inhibition of Hif-1 causes cardiac dysfunction during pressure overload. *Nature*, 446(7134), pp.444–448.

Satyanarayana, A. & Rudolph, K.L., 2004. p16 and ARF: Activation of teenage proteins in old age. *Journal of Clinical Investigation*, 114(9), pp.1237–1240.

Schmitt, C.A. et al., 2002. A senescence program controlled by p53 and p16INK4a contributes to the outcome of cancer therapy. *Cell*, 109(3), pp.335–346.

Senzer, N. et al., 2013. Phase I study of a systemically delivered p53 nanoparticle in advanced solid tumors. *Molecular therapy : the journal of the American Society of Gene Therapy*, 21(5), pp.1096–103.

Serrano, M., 2007. Cancer regression by senescence. *The New England journal of medicine*,

356(19), pp.1996–1997.

Serrano, M. et al., 1997. Oncogenic ras provokes premature cell senescence associated with accumulation of p53 and p16INK4a. *Cell*, 88(5), pp.593–602.

Serrano, M. et al., 1996. Role of the INK4a locus in tumor suppression and cell mortality. *Cell*, 85(1), pp.27–37.

Serrano, M., 2014. Senescence helps regeneration. *Developmental Cell*, 31(6), pp.671–672.

Serrano, M., 2000. The INK4a/ARF locus in murine tumorigenesis. *Carcinogenesis*, 21(5), pp.865–869.

Serrano, M., 1997. The tumor suppressor protein p16(INK4a). *Exp Cell Res*, 237(1), pp.7–13.

Sharpless, N.E. & Sherr, C.J., 2015. Forging a signature of in vivo senescence. *Nature Reviews Cancer*, 15(7), pp.397–408.

Sherr, C.J., 2001. The INK4a/ARF network in tumour suppression. *Nature reviews. Molecular cell biology*, 2(10), pp.731–737.

Sherr, C.J. & McCormick, F., 2002. The RB and p53 pathways in cancer. *Cancer Cell*, 2(2), pp.103–112.

Sherr, C.J. & Roberts, J.M., 1999. CDK inhibitors: positive and negative regulators of G1-phase progression. *Genes & development*, 13(12), pp.1501–12.

Shimi, T. & Goldman, R.D., 2014. Nuclear lamins and oxidative stress in cell proliferation and longevity. *Advances in Experimental Medicine and Biology*, 773, pp.415–430.

Shimo, T. et al., 1999. Connective tissue growth factor induces the proliferation, migration, and tube formation of vascular endothelial cells in vitro, and angiogenesis in vivo. *Journal of biochemistry*, 126(1), pp.137–45.

Shivshankar, P. et al., 2012. Caveolin-1 deficiency protects from pulmonary fibrosis by modulating epithelial cell senescence in mice. *American Journal of Respiratory Cell and Molecular Biology*, 47(1), pp.28–36.

Snider, P. et al., 2010. NIH Public Access. , 105(10), pp.934–947.

Sperka, T., Wang, J. & Rudolph, K.L., 2012. DNA damage checkpoints in stem cells, ageing and cancer. *Nature reviews. Molecular cell biology*, 13(9), pp.579–90.

Spinale, F.G. & Wilbur, N.M., 2009. Matrix metalloproteinase therapy in heart failure. *Current Treatment Options in Cardiovascular Medicine*, 11(4), pp.339–346.

St, M.G., Sutton, J. & Sharpe, N., 2000. Clinical Cardiology : New Frontiers Left Ventricular Remodeling After Myocardial Infarction Pathophysiology and Therapy. , pp.2981–2988.

Stewart, S. a & Weinberg, R. a, 2002. Senescence: does it all happen at the ends? *Oncogene*, 21, pp.627–630.

Storer, M. et al., 2013. XSenescence is a developmental mechanism that contributes to embryonic growth and patterning. *Cell*, 155(5), pp.1119–1130.

Suckau, L. et al., 2009. Long-term cardiac-targeted RNA interference for the treatment of heart failure restores cardiac function and reduces pathological hypertrophy. *Circulation*, 119(9), pp.1241–52.

Suzuki, K. & Matsubara, H., 2011. Recent advances in p53 research and cancer treatment. *Journal of Biomedicine and Biotechnology*, 2011.

Takai, H., Smogorzewska, A. & De Lange, T., 2003. DNA damage foci at dysfunctional telomeres. *Current Biology*, 13(17), pp.1549–1556.

Tamamori-Adachi, M. et al., 2002. Expression of cyclin D1 and CDK4 causes hypertrophic growth of cardiomyocytes in culture: A possible implication for cardiac hypertrophy. *Biochemical and Biophysical Research Communications*, 296(2), pp.274–280.

Tchkonia, T. et al., 2013. Cellular senescence and the senescent secretory phenotype: Therapeutic opportunities. *Journal of Clinical Investigation*, 123(3), pp.966–972.

Tran, D. et al., 2014. Insulin-like growth factor-1 regulates the SIRT1-p53 pathway in cellular senescence. *Aging Cell*, 13(4), pp.669–678.

Travers, J.G. et al., 2016. Cardiac fibrosis: The fibroblast awakens. *Circulation Research*, 118(6), pp.1021–1040.

Tsukamoto, Y. et al., 2013. A novel heart failure mice model of hypertensive heart disease by angiotensin II infusion, nephrectomy, and salt loading. *American journal of physiology. Heart and circulatory physiology*, 305(11), pp.H1658–67.

Varna, M. et al., 2009. p53 dependent cell-cycle arrest triggered by chemotherapy in xenografted breast tumors. *International Journal of Cancer*, 124(4), pp.991–997.

Velarde, M.C., Demaria, M. & Campisi, J., 2013. Senescent cells and their secretory phenotype as targets for cancer therapy. *Cancer and Aging: From Bench to Clinics*, 38, pp.17–27.

Verzola, D. et al., 2008. Accelerated senescence in the kidneys of patients with type 2 diabetic nephropathy. *American journal of physiology. Renal physiology*, 295(5),

pp.F1563–F1573.

Visel, A. et al., 2010. Targeted deletion of the 9p21 non-coding coronary artery disease risk interval in mice. *Nature*, 464(7287), pp.409–12.

Visse, R. & Nagase, H., 2003. Matrix metalloproteinases and tissue inhibitors of metalloproteinases: Structure, function, and biochemistry. *Circulation Research*, 92(8), pp.827–839.

Vogelstein, B., Lane, D. & Levine, a J., 2000. Surfing the p53 network. *Nature*, 408(6810), pp.307–310.

Weber, K.T., 2000. Fibrosis and hypertensive heart disease. *Current opinion in cardiology*, 15(4), pp.264–272.

Weisheit, C. et al., 2014. Ly6Clow and not Ly6Chigh macrophages accumulate first in the heart in a model of murine pressure-overload. *PLoS ONE*, 9(11).

Welford, S.M. & Giaccia, A.J., 2011. Hypoxia and senescence: the impact of oxygenation on tumor suppression. *Molecular cancer research : MCR*, 9(5), pp.538–44.

Westhoff, J.H. et al., 2008. Hypertension induces somatic cellular senescence in rats and humans by induction of cell cycle inhibitor p16INK4a. *Hypertension*, 52(1), pp.123–129.

Wiemann, S.U. et al., 2002. Hepatocyte telomere shortening and senescence are general markers of human liver cirrhosis. *The FASEB journal : official publication of the Federation of American Societies for Experimental Biology*, 16(9), pp.935–942.

Wolstein, J.M. et al., 2010. INK4a knockout mice exhibit increased fibrosis under normal conditions and in response to unilateral ureteral obstruction. , (3), pp.1486–1495.

Xia, Y. et al., 2009. Characterization of the inflammatory and fibrotic response in a mouse model of cardiac pressure overload. *Histochemistry and Cell Biology*, 131(4), pp.471–481.

Xue, W. et al., 2007. Senescence and tumour clearance is triggered by p53 restoration in murine liver carcinomas. *Nature*, 445(7128), pp.656–60.

Yoshida, Y. et al., 2007. CCN1 protects cardiac myocytes from oxidative stress via β1 integrin-Akt pathway. *Biochemical and Biophysical Research Communications*, 355(3), pp.611–618.

Young, A.P. et al., 2008. VHL loss actuates a HIF-independent senescence programme mediated by Rb and p400. *Nature cell biology*, 10(3), pp.361–369.

Yu, L. et al., 2005. Cyclin-dependent kinase inhibitor p27Kip1, but not p21 WAF1/Cip1, is required for inhibition of hypoxia-induced pulmonary hypertension and remodeling by heparin in mice. *Circulation Research*, 97(9), pp.937–945.

Zeisberg, E.M. & Kalluri, R., 2010. Origins of cardiac fibroblasts. *Circ Res*, 107(11), pp.1304–1312.

Zerlanko, B.J. et al., 2012. Premature senescence and increased TGF?? signaling in the absence of Tgif1. *PLoS ONE*, 7(4).

Zhang, R. et al., 2005. Formation of macroH2A-containing senescence-associated heterochromatin foci and senescence driven by ASF1a and HIRA. *Developmental Cell*, 8(1), pp.19–30.

Zhang, Y. & Yang, J., 2011. The impact of cellular senescence in cancer therapy: is it true or not? *Acta Pharmacologica Sinica*, 32(10), pp.1199–1207.

Zhao, X. et al., 2014. Induction of the matricellular protein CCN1 through RhoA and MRTF-A contributes to ischemic cardioprotection. *Journal of Molecular and Cellular Cardiology*, 75, pp.152–161.

Zhu, F. et al., 2013. Senescent cardiac fibroblast is critical for cardiac fibrosis after myocardial infarction. *PloS one*, 8(9), p.e74535.

Zhu, W. et al., 2009. Acute doxorubicin cardiotoxicity is associated with p53-induced inhibition of the mammalian target of rapamycin pathway. *Circulation*, 119(1), pp.99–106.

Zhu, W. et al., 2014. P53 inhibition exacerbates late-stage anthracycline cardiotoxicity. *Cardiovascular Research*, 103(1), pp.81–89.